# A MODEL FOR THE VON KÁRMÁN VORTEX STREET

Thesis by

James Carl Schatzman

In Partial Fulfillment of the Requirements
for the Degree of
Doctor of Philosophy

Applied Mathematics
California Institute of Technology
Pasadena, California

1981
(Submitted May 4, 1981)

**Acknowledgement**

My primary thanks go to my advisor, Dr. Philip G. Saffman, for suggesting the topic of this thesis and for providing guidance throughout its progress as well as before and after. I am grateful to have had the opportunity to study at Caltech, and in particular, in the Applied Mathematics Option. I have benefitted from discussions with the students and faculty of Caltech, especially Dr. Bengt Fornberg, and also with a visitor from Imperial College, Dr. Derek W. Moore.

My work was supported by Caltech in the form of Graduate Research Assistantships, Graduate Teaching Assistantships, a Caltech Fellowship, and by the Department of Energy (Office of Basic Energy Sciences). I acknowledge with gratitude the granting of time by Control Data Corporation on the Cyber 203 Computer at the CDC Service Center, Arden Hills, Minnesota.

**Abstract**

In the wake of a two-dimensional bluff body placed in a uniform stream, for sufficiently large but not too large flow velocity a distinctive pattern of vorticity is observed. The pattern consists of "vortices" of high vorticity surrounded by nearly irrotational fluid. These vortices are organized in two nearly parallel staggered rows of vortices of opposite direction of rotation. This pattern is called the von Kármán vortex street.

This thesis is a report on the analysis of a model for the von Kármán vortex street. The model is inviscid, incompressible, two-dimensional, and consists of vortices of finite area and uniform vorticity. The first part of this thesis contains a brief survey of the work on this problem, and an explanation of the approach used in the present work; the second part describes calculations of steady solutions of the Euler equations of this kind, and the third part describes an analysis of the stability of these steady solutions to two-dimensional disturbances.

The calculations indicate that the vortex wake can be stabilized by sufficiently large area of the vortices. Data are given which (to some approximation) will permit relating the street to the flow past a body; this is proposed as a suitable study for further work.

**Table of Contents**

# I. Historical Overview and General Introduction

The Kármán vortex street is a complex fluid mechanical phenomenon which occurs in a remarkable variety of circumstances. The "singing" of power lines or kite strings in the wind is an every-day observable event. The sound is produced by a mechanism involving the alternating periodic shedding of vortices of opposite direction of rotation from opposite sides of the generating filament. Vortex streets are also observed in atmospheric flow about mountains and islands, in ocean flows about structural members and pipes, as well as in hydraulic and aeronautical systems.

The more general problem of the wakes in flow past bluff bodies has been the subject of experimental and theoretical work for more than a century. The phenomenon of periodic vortex shedding was apparently first studied experimentally by Strouhal (1878) in his work on "aeolian tones" produced by wires moving through air, and by Lord Rayleigh (1879). In 1911, von Kármán published the first theoretical study of vortex streets, at which time the subject became of widespread interest. Since then, roughly twenty relevant papers have appeared annually in the literature; a total of well over one thousand. It is not intended in this introduction to describe every aspect of every problem of this type which has been studied; rather, a brief overview of the field will be given.

Since the early work, interest has expanded to include very many facets of the phenomenon, as well as extensions to different but similar flow problems. Areas of research reported in the literature include:

1. Study of the unsteady street formation process; discharge of vorticity from the generating body.
2. Quantitative theoretical analysis giving characteristics of the street:
    a. shedding frequency

   b. width

   c. streamwise spacing

   d. vortex strength

   e. downstream evolution

3. Average forces on the body (eg. drag).
4. Oscillatory forces and interaction with aeroelastic bodies.
5. Non-uniqueness of the street as a function of the flow parameters.
6. Transitions between various flow regimes of fundamentally differing character.
7. Effects of accelerating (vibrating) bodies.
8. Effects of compressibility.
9. Effects of acceleration/deceleration of the background flow.
10. Effects of shear.
11. Effects of density stratification.
12. Effects of walls in the flow channel.
13. Effects of lift and unsymmetricality of the body.
14. Effects of changing two-dimensional body shape.
15. Effects of three-dimensional body orientation and shape:

   a. taper

   b. steps

   c. perpendicular barrier plates

   d. ends

16. Sound generation and absorption.
17. Interaction with shock waves.
18. Multiple-body configurations.
19. Fully three-dimensional wakes.

Papers reviewing much of the most fundamental work include Goldstein (1938), Rosenhead (1953), Krzywoblocki (1953), Wille (1960), Morkovin (1964), Berger and

Wille (1972), Ehrhardt (1979), Bearman and Graham (1980).

Some of the interest in the field has undoubtedly arisen due to the controversy over inconsistent experimental results obtained by different researchers. The experiments are difficult and are influenced by residual turbulence of the flow tunnel, roughness and shape of the body, wall effects (blocking of the channel), and measurement technique. The usual measurements performed do not measure the vorticity distribution or streamlines which would be best for theoretical analysis, but rather the velocity. To this day, the fundamental question of whether the spacing between vortex rows at first grows or decays has not been conclusively settled.

Similarly, there is controversy over the many theoretical attempts to study the problem. The exact problem is so intractable that quite severe approximations are generally made before analytical or computational methods are applied. The great variety of approximations which have been made, and the great variety of aspects of the problem which have been emphasized by different researchers, have resulted in much disagreement of results.

Viscosity of necessity is involved with the generation of the vortex layers by the body. A number of papers have appeared, describing attempts to simulate this shedding process by computer. For example, Gerrard (1963), Gerrard (1967), Sarpkaya (1968), Laird (1971), Chaplin (1973), Clements (1973), Takao (1973), Jain and Goel (1976), Kiya and Arie (1977a,b), Stansby (1977), Kuwahara (1978), Sarpkaya and Shoaff (1979) have used two-dimensional inviscid line vortex models with simulated vortex shedding, and Payne (1958), Jordan and Fromm (1972), Swanson and Spaulding (1978), and Hurlbut, Spaulding, and White (1978) have solved the two- or three-dimensional unsteady viscous flow equations for moderately low Reynolds number flow past a circular cylinder. However, it is apparent that viscosity is not essential to the formation of the vortex street once the vortex layers have been created; the first group of cited researchers were able to simulate the complete

process from shedding to street formation with purely inviscid models. Also, it has long been observed experimentally that there are considerable ranges of Reynolds number over which the Strouhal number (dimensionless shedding frequency) and drag coefficient remain essentially constant (eg. Roshko, (1961)). Also, Strouhal numbers have been formed using the distance between layers, the vortex shedding frequency, and the street velocity which are essentially independent of the (two-dimensional) body shape. Hence, it would appear that viscosity does not necessarily play a crucial role in the vortex wake development, and (except for the generation of the vortex layers) the body is not very important in the formation and evolution of the vortex street.

To test this hypothesis further, a number of authors have studied in the absence of viscosity the evolution of infinite parallel vortex layers with small periodic initial disturbances (Abernathy and Kronauer (1962), Christiansen (1973), Boldman, Brinich, and Goldstein (1976), Aref and Siggia (1981)). Despite the serious approximation involved with the line vortex method these researchers used, the Kármán vortex street seems to have been the generic result.

For this reason, it seems reasonable to restrict attention to the street proper, and to treat the body flow region as a "black box" which does not enter into the analysis in a fundamental way. This approach does not explain the initial vortex layer formation process. However, it seems reasonable that to good approximation, the latter problem could be studied separately. Areas of research interest for the street proper include:

1. Steady configurations for inviscid flow.
2. Stability of the steady configurations to two-dimensional disturbances.
3. Stability to three-dimensional disturbances.
4. Effects of viscosity which result in gradual evolution of the street and the pairing process whereby pairs of vortices amalgamate and produce a new street of

larger, more widely spaced, vortices.

5. The fully unsteady problem including a correct treatment of viscosity.

Most of the earlier analytical studies of the inviscid problem have dealt with the point vortex street. First studied by von Kármán (1911), this model has reappeared repeatedly since, despite its serious limitations (namely, its stability properties do not correlate with experimental observations and because of its unphysical infinite kinetic energy, it may not be connected with the body flow except through ad hoc assumptions). Two efforts to improve von Kármán's model are due to Domm (1955) and Ehrhardt (1979). Both researchers have produced stability diagrams similar in general character to the one discussed later in this thesis. However, this is probably fortuitous, as approximations of a very serious nature have been made in each case. Domm considered the stability to two-dimensional disturbances of Oseen-Hamel vortices (viscously diffusing line vortices) placed at positions specified by von Kármán's model. However, this configuration is not a solution of the equations of motion, and Domm's assumption that all vortices are of the same age is not reasonable. Ehrhardt considered the inviscid case, but with a particular cyclindrically symmetric vorticity distribution. Again, however, the assumed configuration (steady) is not a solution of the equations of motion. Furthermore, Ehrhardt considers the stability of motion of one vortex when all the others are held fixed; obviously irrelevant to the real problem. Rosenhead (1930) attempted to analyze the stability of viscous streets to three-dimensional disturbances, but, lacking quantitative information about the street itself, this work is not very satisfactory. These two serious errors: 1) considering via the equations of motion the "stability" of artificial configurations which are not solutions of the equations of motions; and 2) studying stability to perturbations which are irrelevant to the physical problem, have reappeared many times in the literature since von Kármán (1911). Stability of the street is a rather delicate question, and approximations of this severity have consistently resulted in conclusions which are either not useful or else highly

questionable.

Some recent researchers have attempted to study the question of stability of the fully developed vortex street by "solving" the initial value problem using the discrete vortex or cloud-in-cell method (Christiansen and Zabusky (1973), Aref and Siggia (1981)). Although there are computational difficulties associated with these methods (for example, artificial viscosity and anisotropy of interactions using the second), and the models become physically unreasonable after sufficiently long evolution time, the results are probably largely accurate for small times. However, the high cost of these methods prohibits a complete study of the problem, and interpretation of the results is sometimes difficult.

To avoid the limitation of low Reynolds number, and to avoid the difficulties outlined above, the present work deals only with the simplest case: a symmetrical (non-lifting), bluff, two-dimensional body in a uniform stream of a homogeneous, incompressible, perfect fluid. As von Kármán (1911) pointed out, it is sufficient to consider a parallel array of vortices extending to infinity in both upstream and downstream directions. A model is proposed wherein each vortex has finite area and uniform vorticity; this is probably the simplest possible extension of von Kármán's point vortex model. The model cannot be made to predict viscous effects accurately. It does have one advantage over most of the published viscous work (except the unsteady Navier-Stokes solutions) which is that it is a consistent model for which essentially exact (numerical) solutions may be obtained. Furthermore, it applies to the high Reynolds number case which cannot be studied (yet) by direct Navier-Stokes calculations. The fact that for large Reynolds number the wake rapidly becomes turbulent diminishes the importance of this model. However, it is believed that it is of value to have precise calculations for a mathematically consistent (although perhaps somewhat unphysical) model.

This thesis contains a study of the steady solutions of the flow equations of the

above-outlined type, and an analysis of stability to two-dimensional disturbances. Relating this highly idealized model to the flow past a body is a necessary task, and is proposed as a suitable study for further work.

# II. Steady States

## 1. Introduction

For a certain range of Reynolds number, a regular pattern of vortices is observed in the wake of a two-dimensional blunt body placed in a uniform stream. In his classical work, von Kármán modeled the problem with an infinite street of point vortices (see v. Kármán, (1911) and (1912); v. Kármán and Rubach, (1912)). This approximate approach has several limitations, among which are the infinite kinetic energy and difficulty in fitting the model to flow past a body.

To improve the model, the vortices are herein allowed to be of finite area, but uniform vorticity. An integro-differential equation is then solved to obtain the steady shapes of the vortices. This part of the thesis constitutes the first part of a study of the wake flow problem, and describes only properties of the steady solutions for the infinite vortex array.

## 2. Formulation

Consider an infinite array of uniform two-dimensional vortices, consisting of one row of identical vortices of area $A$ and strength $-\Gamma$ with centroids at positions $x=0, \pm l, \pm 2l, \pm 3l,\ldots, y=0$, and of a second row of identical vortices of area $A$ and strength $+\Gamma$ with centroids at $x=d, d\pm l, d\pm 2l, d\pm 3l,\ldots, y=-h$. The frame of reference is chosen with a uniform flow $U_s$ in the $x$ direction at infinity as in figure 1 so that the vortices are stationary. It is assumed that the flow is inviscid, incompressible, two-dimensional, and, outside the vortices, irrotational. This part of the thesis deals with the steady flows of this kind, principally with $d/l=0$ and 0.5 (for values other than 0 and 0.5 translating solutions exist but the street does not move parallel to itself; see Rosenhead, (1929)).

The complex potential outside the vortices can be written (with the notation $z=x+iy$, $z'=x'+iy'$):

$$w(z) = \frac{i\Gamma}{2\pi A}\left\{ \iint_{\Sigma_1} \log \sin\frac{\pi}{l}(z-z')\, dx'\, dy' - \iint_{\Sigma_2} \log \sin\frac{\pi}{l}(z-z')\, dx'\, dy' \right\} + U_s z, \qquad (2.1)$$

where $\Sigma_1$, $\Sigma_2$ refer to the cross-sections of one vortex in the upper and lower rows, respectively. By applying a Green's theorem, the complex velocity can be written as a line integral around the boundaries of the vortices:

$$u+iv = \frac{\Gamma}{2\pi A}\left\{ \int_{\Sigma_1} \log\left|\sin\frac{\pi}{l}(z-z')\right| dz' - \int_{\Sigma_2} \log\left|\sin\frac{\pi}{l}(z-z')\right| dz' \right\} + U_s. \qquad (2.2)$$

The requirement that the velocity field be tangent to the boundary of the vortices then determines the steady shapes of the vortices, apart from the scaling, as a function of the three dimensionless parameters $d/l \equiv \mu$, $h/l \equiv \kappa$, and $A/l^2 \equiv \alpha$.

To simplify the calculations, the vortices in the two rows are assumed to have identical shapes, differing only in position and orientation. There are two reasonable choices of symmetry; invariance to reflection about the line $y=-h/2$ (the streamwise axis centered between the two rows) and a suitable $x$ translation, and similarly with an *additional* reflection about $x=0$ (the vertical axis of one of the vortices). In both cases, it is sufficient to satisfy (2.2) along the boundary of a vortex in either row. For vortices of streamwise symmetry, these two cases are equivalent.

The second choice was picked, giving in place of (2.2):

$$u+iv = \frac{\Gamma}{2\pi A} \int_{\Sigma_1} \log\left|\sin\frac{\pi}{l}(z-z') \sin\frac{\pi}{l}(z+z'-\mu l+i\kappa l-2\overline{z})\right| dz' + U_s, \qquad (2.3)$$

where $\overline{z}$ denotes the centroid of $\Sigma_1$ and is for now assumed to be arbitrary. The first symmetry could also have been considered, but since only streamwise symmetric solutions were found using (2.3), this was not attempted.

Three quantities of interest are the propagation velocity $U_s$ of the array, the kinetic energy of the fluid, and the momentum transport. They are needed to relate this model to the wake flow problem. Specifically, the following quantities are defined:

$$T = \frac{1}{2l}\int_{-\infty}^{+\infty}\int_{-l/2}^{l/2}(u'^2+v^2)\,dx\,dy, \qquad D' = -\frac{1}{2}Im\int_{-i\infty}^{+i\infty}(u'-iv)^2\,dz. \tag{2.4}$$

where the contour integral in the expression for $D'$ is along any contour from $y=-\infty$ to $y=+\infty$ which does not pass through a vortex. Here $T$ is the kinetic energy of the fluid per unit length (streamwise), $D'$ is essentially the momentum flux of the fluid in the streamwise direction with the contribution from the vortices themselves omitted, and $u'=u-U_s$ is the $x$ velocity relative to the free stream. Dimensionless values of these quantities are defined as follows:

$$\hat{U}_s(\alpha,\kappa) = \frac{l}{\Gamma}U_s, \quad \hat{T}(\alpha,\kappa) = \frac{l}{\Gamma^2}T, \quad \hat{D}'(\alpha,\kappa) = \frac{l}{\Gamma^2}D'. \tag{2.5}$$

### 3. Circular Vortex Approximation

The vortices of small area for the exact problem are nearly circular, and for precisely circular vortices, the propagation velocity, momentum transport, and energy calculations can be done analytically. The former two calculations lead to the same result as for point vortices (Goldstein,(1938)) since the flow field outside a uniform circular vortex is identical to that of a point vortex of the same circulation. For $d=l/2$, $\mu=\frac{1}{2}$,

$$U_s = \frac{\Gamma}{2l}\tanh\frac{\pi h}{l}, \quad D' = \frac{\Gamma^2}{2\pi l} - \frac{\Gamma h}{l}U_s, \tag{3.1}$$

and the energy can be evaluated exactly by integration of the kinetic energy density:

$$T = \frac{\Gamma^2}{2\pi l}\left\{\log\left[\left(\frac{l^2}{\pi A}\right)^{\frac{1}{2}}\cosh\frac{\pi h}{l}\right] + \frac{1}{4}\right\}. \tag{3.2}$$

For $\mu$=0, *coth* replaces *tanh* in (3.1) and *sinh* replaces *cosh* in (3.2). Note that the circular vortex model loses physical validity when the vortices overlap, namely for $\alpha > \frac{\pi}{4}(\kappa^2 + \mu^2)$ or $\frac{\pi}{4}$.

**4. Asymptotic Analysis for Small Areas**

Perturbation expansions can be developed for small area A. A solution may be calculated with an expansion for the vortex shape of the form

$$z = (a_0 + a_2\cos 2\vartheta + a_3\sin 3\vartheta + a_4\cos 4\vartheta + a_5\sin 5\vartheta + \cdots)e^{i\vartheta} \tag{4.1}$$

where $\vartheta$ is the polar angle ($\vartheta$=0 corresponds to the positive $x$ direction) and where $a_2$, $a_3$,... are homogeneous polynomials in $a_0$. Substitution into the equations yields:

$$\left.\begin{aligned} z &= \left(\frac{A}{\pi}\right)^{\frac{1}{2}} e^{i\vartheta}\left[1 + \frac{\pi A}{l^2}\left(\tanh^2\pi\kappa - \frac{2}{3}\right)\cos 2\vartheta + \cdots\right] \qquad \mu = \frac{1}{2} \\ z &= \left(\frac{A}{\pi}\right)^{\frac{1}{2}} e^{i\vartheta}\left[1 + \frac{\pi A}{l^2}\left(\coth^2\pi\kappa - \frac{2}{3}\right)\cos 2\vartheta + \cdots\right] \qquad \mu = 0 \end{aligned}\right\}. \tag{4.2}$$

In principle, large numbers of terms may be calculated by computerized symbol manipulation and by using accelerated convergence techniques to approximate the solution for reasonably large areas. This was not attempted.

**5. Numerical Method**

Two successful numerical schemes were employed to calculate the steady vortex shapes; one using Newton's method in a straightforward manner and the other using an ad hoc iterative scheme (Pierrehumbert and Widnall, (1979)). Only solutions for vortices symmetric in the streamwise direction were computed. The first

numerical scheme allowed solutions lacking this symmetry, but none were found (although an exhaustive search was not conducted). For purposes of the calculations, $\Sigma_1$ was taken to be the vortex with centroid at the origin.

The condition that the vortex boundary be a streamline may be written:

$$Im\left\{\frac{\partial z^*}{\partial s}(u+iv)\right\}=0 \tag{5.1}$$

where the derivative is taken along the boundary. The boundary of $\Sigma_1$ is parameterized using polar coordinates:

$$\left.\begin{aligned} z &= R(\tilde{\vartheta})e^{i\vartheta(\tilde{\vartheta})} && 0\leq\tilde{\vartheta}\leq 2\pi \\ \vartheta(\tilde{\vartheta}) &= \vartheta_0+\tilde{\vartheta}-\delta\sin 2\tilde{\vartheta} && 0\leq\delta<\tfrac{1}{2} \\ R(\tilde{\vartheta}) &= \tfrac{1}{2}a_0+\sum_{j=1}^{N}(a_j\cos j\tilde{\vartheta}+b_j\sin j\tilde{\vartheta}) \end{aligned}\right\} \tag{5.2}$$

Here $\vartheta_0$, $\delta$ are parameters which permit limited adjustment of the scaling of $\vartheta$ in regions of high curvature of the boundary, so as to improve the rate of convergence of the Fourier series for R.

Equation (5.1) is evaluated at uniformly spaced values of $\tilde{\vartheta}$ :

$$\tilde{\vartheta}=\tilde{\vartheta}_j\equiv\frac{2\pi j}{2N+1}\qquad(j=0,\,1,\,2,\ldots,\,2N). \tag{5.3}$$

This gives $2N+1$ equations for the $2N+2$ unknowns $a_0,\ldots,\,a_N$, $b_1,\ldots,\,b_N$, $U_s$, and an additional equation comes from fixing the size of the vortex, eg.:

$$R(\varphi)=fixed, \tag{5.4}$$

where $\varphi$ is some fixed angle. However, the resulting system is singular, because (5.1) is invariant to a translation of z. The specification is completed by fixing the centroid of the vortex at the origin, ie.:

$$\overline{x} + i\overline{y} \equiv \frac{1}{3A}\int_{\Sigma_1} R^3 e^{i\vartheta}\, d\vartheta = 0. \tag{5.5}$$

The resulting $2N+4$ real equations for the $2N+2$ unknowns are not independent and the problem is handled by using the trick (Chen and Saffman, (1980)) of solving (5.4) combined with the $2N+1$ equations which arise from the discretization of:

$$Im\left\{\frac{\partial z^*}{\partial s}(u+iv)\right\} + f_1(\tilde{\vartheta})\overline{x} + f_2(\tilde{\vartheta})\overline{y} = 0, \tag{5.6}$$

where $f_1$ and $f_2$ are more or less arbitrary non-trivial functions chosen to ensure that the Jacobian of the system is non-zero for the solutions that satisfy (5.5). The choice of $\tilde{\vartheta}$ and $\tilde{\vartheta}^2$ respectively for $f_1$ and $f_2$ was found to be satisfactory. Also, the $\overline{z}$ appearing in (2.3) was dropped to simplify the equations slightly.

If $\delta$=0, then as the limiting case of touching vortices (in each row) is approached for the $\mu$=0.5 case, the curvature of $R$ with respect to $\vartheta$ becomes large near $\vartheta$=0 and $\vartheta$=$\pi$, and hence convergence of the series for R becomes slow. For large $\kappa$, $\vartheta_0$=0, $\delta$=0.4999 were used, which concentrates mesh points in these regions of large curvature, and hence smooths out $R$ as a function of $\tilde{\vartheta}$. This procedure works well for roughly $\kappa$> 0.36; below this point, large curvature appears for large area vortices away from $\vartheta$=0 and $\vartheta$=$\pi$, and the simple transformation to $\tilde{\vartheta}$ described by (5.2) is not useful. Probably, more complicated transformations could be found which would alleviate this difficulty, but this was not attempted. To speed up some computations, $\vartheta_0 = -\frac{\pi}{2}$, $\delta$=0 were used, and the vortices were assumed to be streamwise symmetric. In this case, the Fourier series for $R$ contains only the cosine terms, and hence the number of unknowns is reduced. Specifically, (5.6) is evaluated at the mesh points (5.3) for j=1,2,...,N, and the unknowns are $a_0$, $a_1$,..., $a_{N-1}$, $U_s$; the remaining Fourier coefficients are taken to be zero.

Integrals for velocity, centroid, and area were evaluated using the trapezoidal

rule, with care taken, in the former case, to preserve formal infinite order accuracy (see appendix A). Initial guesses for Newton's method were provided by using one Euler step to advance from the previous converged solution, starting with small vortices and gradually increasing the size by continuation in the parameter (5.4). However, convergence was observed to be insensitive to the initial guess. Accuracy was ensured by requiring that the highest order Fourier coefficients were sufficiently small, and by checking that increasing N had sufficiently small effect on the results. Values of N from 50 to 400 were found to be adequate for 5 digit precision in the final results. Each iteration required roughly from 1 to 25 seconds using a CDC Cyber 203 computer (64 bit floating point).

The second numerical scheme is essentially a scalar approximation to Newton's method. Consider the variation of the stream-function $\psi$ along the boundary of the vortex at some intermediary stage in the calculation. It is assumed that most of the change in $\psi$ on the boundary due to a perturbation of the boundary comes from the fact that it is computed at a different point, rather than the fact that the flow field is changed. Again, a polar coordinate representation for the boundary is employed:

$$\left.\begin{aligned} z(\tilde{\vartheta}) &= R(\tilde{\vartheta})e^{i\vartheta(\tilde{\vartheta})} \\ \vartheta(\tilde{\vartheta}) &= -\frac{\pi}{2}+\tilde{\vartheta}-\delta\sin 2\tilde{\vartheta} \end{aligned}\right\} \qquad (5.7)$$

but here streamwise symmetry of each vortex is assumed ab initio and the unknowns are taken to be $U_s$ and the values of R at:

$$\tilde{\vartheta} = \tilde{\vartheta}_j \equiv \frac{\pi j}{N} \qquad (j=0, 1, 2,\ldots,N) \qquad (5.8)$$

The iteration performed can be written:

$$R_j^{(n+1)} = R_j^{(n)} - \rho\frac{\psi_j^{(n)}-\psi_0^{(n)}}{\psi_{R,j}^{(n)}} \qquad (j=1, 2,\ldots,N)$$

(5.9)

The numerator of the quotient is obtained by integration of the velocity using the trapezoidal rule:

$$\psi_j^{(n)} - \psi_{j-1}^{(n)} \approx \tag{5.10}$$

$$\tfrac{1}{2}\frac{\pi}{N}\left\{\left(\frac{\partial\psi}{\partial R}\right)_j^{(n)}\left(\frac{\partial R}{\partial\tilde{\vartheta}}\right)_j^{(n)} + \left(\frac{\partial\psi}{\partial\vartheta}\right)_j^{(n)}\left(\frac{\partial\vartheta}{\partial\tilde{\vartheta}}\right)_j^{(n)} + \left(\frac{\partial\psi}{\partial R}\right)_{j-1}^{(n)}\left(\frac{\partial R}{\partial\tilde{\vartheta}}\right)_{j-1}^{(n)} + \left(\frac{\partial\psi}{\partial\vartheta}\right)_{j-1}^{(n)}\left(\frac{\partial\vartheta}{\partial\tilde{\vartheta}}\right)_{j-1}^{(n)}\right\}$$

and $\psi_R \equiv \partial\psi/\partial R$ is of course a velocity component. The relaxation factor $\rho$ is adjusted empirically for optimum convergence (typically $0.5 \leq \rho \leq 2$). Cycles of this iteration alternate with an update of $U_s$:

$$U_s^{(n+1)} = U_s^{(n)} - \rho\frac{\nabla\psi^{(n)}}{y_N - y_0} \tag{5.11}$$

where $\nabla\psi^{(n)}$ is obtained by integrating $d\psi$ around the half revolution from $\tilde{\vartheta}_0$ to $\tilde{\vartheta}_N$ . The velocity was calculated essentially as before (but see appendix A). As the final step of the iteration, the vortex is shifted in the $y$ direction to put the centroid at the origin, new values of $R_j$ being computed via interpolation.

This method has apparent advantages over Newton's method; namely, its simplicity and its speed per iteration (the cost is $O(N^2)$ per iteration versus $O(N^3)$ for Newton's method). However, highly unpredictable dependence on the initial guess and poor convergence rate in some cases are the penalties. Convergence is geometric with observed convergence factor ranging from about .15 for very small vortices to about .85 for large vortices. The method failed entirely to converge for very large vortices with small $\kappa$. Furthermore, more points are required for the same accuracy as compared with the previous method. Instability is controlled by limiting the maximum value of $\rho$ and was not a difficulty. Values of N ranging from 50 to 400 were found to be adequate. These calculations were performed using a

DEC VAX11/780 computer (64 bit floating point).

The energy can be obtained by a single contour integral over the vortex boundary requiring O(N) operations (see appendix B). The momentum integral was computed by applying the trapezoidal rule over a finite contour passing between two neighboring vortices, and extending to regions where the flow is essentially a uniform stream (the perturbation decays exponentially with $y$). Romberg integration was used to obtain sufficient accuracy for this calculation.

**6. Results of the Calculations**

Figures 2 to 5 show the calculated values of $\hat{U}_s$ , $\hat{T}$, and $\hat{D}'$ for the case $\mu$=0.5 for the exact problem, accompanied by the corresponding results for the circular vortex approximation. The curves were traced by using as continuation parameter the quantity $\alpha$ which is the ratio of the $x$ semi-axis of the vortices to $l$. As is evident in figure 5, a solution of simultaneous maximum area and minimum energy exists for each $\kappa$ in accordance with Kelvin's variational principle for the steady states (Saffman and Szeto, (1981)). This limit is a contour in the ($\kappa$,$\alpha$) plane, as depicted by curve 1 in figure 6. For roughly $\kappa > 0.36$, further increase in $\alpha$ results in a decrease in area and increase in energy, up to the point $\alpha$=0.5, where the vortices in each row touch. This limiting case is depicted by curve 2 in figure 6. Thus, between curves 1 and 2, there are two different configurations for a given ($\kappa$,$\alpha$). Presumably, the solution curves could be continued beyond $\alpha$=0.5 by considering two adjacent distorted vortex layers in place of discrete vortices, but this was not done. Similar behavior has been observed for the linear vortex array, which in fact corresponds to the limit $\kappa \to \infty$ (Saffman and Szeto, (1981)). Quite different behavior was observed for $\kappa$ smaller than about 0.36. In this case, the calculations indicate that the parameter $\alpha$ approaches a limiting value less than 0.5. To check that this phenomenon was not dependent on the choice of the horizontal semi-axis for continuation, the vertical semi-axes were also used as continuation parameters. In all

cases, the numerical evidence indicates that as the vortex size increases, vortices in each row protrude between vortices in the other row, and the solutions branches terminate when vortices in *opposite* rows approach and finally meet. Here there is no turn-around in area or energy, but maximum area and minimum energy occur at the limiting point of the solution branch. This behavior is similar to that observed for a pair of counter-rotating vortices as studied by Pierrehumbert (1980). The calculations for $\kappa < 0.36$ and for large area were costly, and an accurate calculation of the limiting case was not attempted. For this region, the corresponding segment of curve 1 in figure 6 should be regarded as a lower bound.

Presumably, there exists a critical value of $\kappa$ which divides the regions of the two types of limiting behavior. Due to cost limitations, it was not possible to determine accurately this critical value. However, it is believed to lie within the range from 0.35 to 0.365.

A geometric observation of relevance is that for small areas and for $\kappa > .36485$, the vortices are longer in the streamwise direction than in the transverse, and the converse for $\kappa$ less than this critical value. The exact dividing value for infinitesimal area is the solution to $\cosh^2 \pi\kappa = 3$, which is obvious from (4.2) and which may also be demonstrated using an elliptical vortex approximation (as has been applied to the linear vortex array; see Saffman and Szeto, (1981)). This is in good agreement with the numerically estimated large area critical value of $\kappa$ as discussed above, but there is no evidence to suggest that the large area critical value is precisely the infinitesimal area critical value.

Figures 7 to 43 are plots showing the vortex shapes and the velocity fields. The apparent good qualitative agreement with experimental observations (for example, Davies, (1976)) seems to provide some justification for the assumptions implicit in the proposed application of this model to the wake behind bluff bodies and its stability. However, this "apparent qualitative agreement" is not very significant, and

more meaningful comparison with experiment must wait for research beyond the scope of this thesis.

Figures 44 and 45 show the calculated values of $\hat{U}_s$ and $\hat{T}$ for the case $\mu$=0 as well as the corresponding results for the circular vortex approximation. The energy calculations are used in the next part of this thesis. The momentum flux was not calculated for these steady states.

# III. STABILITY

## 7. Introduction

The Kármán vortex street is a regular pattern of vortices consisting of two parallel staggered rows, which, for a certain range of Reynolds number, is observed in the wake of two-dimensional blunt bodies placed in a uniform stream. In the previous part of this thesis, an inviscid model for the wake flow was described which consists of two rows of staggered vortices of finite size, extending to infinity in both directions. Steady solutions (which propagate relative to the free stream) were found numerically, and their properties were calculated.

This part of the thesis discusses the stability of these steady solutions to two-dimensional disturbances. A normal mode analysis is carried out and the growth rates and frequencies of the modes are calculated for a range of values of the vortex size and separation/spacing ratio of the street. It is found that finite size can stabilize the street to infinitesimal disturbances. The results for superharmonic disturbances are in accord with those predicted by energy arguments based on Kelvin's variational principle. It will be pointed out that an attempt to use these energy arguments for subharmonic disturbances leads to fallacious conclusions.

## 8. Subharmonic Instabilities of the Point Vortex Array

The limiting case of point vortices ($\alpha$=0) was studied by von Kármán (1912); see also Lamb (1932, §156). It was shown that infinitesimal two-dimensional disturbances of wavelength $l/p$ grow like $e^{\sigma t}$, where

$$\frac{2l^2}{\pi\Gamma}\sigma = \pm B \pm (A^2-C^2)^{\frac{1}{2}} \tag{8.1}$$

and

$$A = 2p(1-p) - sech^2\pi\kappa, \tag{8.2}$$

$$B = i\left[\frac{2p\sinh\pi\kappa(1-2p)}{\cosh\pi\kappa} + \frac{\sinh 2\pi\kappa p}{\cosh^2\pi\kappa}\right], \tag{8.3}$$

$$C = \frac{\cosh 2\pi\kappa p}{\cosh^2\pi\kappa} - \frac{2p\cosh\pi\kappa(1-2p)}{\cosh\pi\kappa}. \tag{8.4}$$

Note that $p$ need not be an integer or rational. Since the steady flow has wavelength $l$, it follows from Floquet or Bloch wave theory that the normal modes of the system (for finite as well as point vortices) are of the form

$$e^{\sigma t}\, e^{2\pi i x p/l} P(x,y) \tag{8.5}$$

where $P(x+l,y) \equiv P(x,y)$. Disturbances with $p$ equal to an integer or zero will be called *superharmonic*; they always have wavelength $l$. If $p$ is not equal to an integer, there is clearly no loss of generality in supposing that $0 < p < 1$, and such disturbances will in general have components with wavelengths greater than $l$ and will be called *subharmonic*.

Figure 46 shows the regions of stable ($\mathrm{Re}\,\sigma = 0$) and unstable ($\mathrm{Re}\,\sigma > 0$) eigenfunctions in the $(\kappa,p)$ plane for point vortices. It should be noted that not all eigenfunctions are linearly unstable but for $\kappa \neq \kappa_c$ there always exist unstable disturbances. For $\kappa = \kappa_c$ (where $\cosh^2\pi\kappa_c = 2$) all the disturbances are linearly stable, and this case was identified by von Kármán as the stable configuration of the street. However, it was discovered by Kochin (1939) that this "stable" configuration is in fact unstable at second order approximation in the disturbance amplitude (for an elegant demonstration, see Domm (1956).) These higher order studies have dealt only with the case $p = 0.5$, and it is not known whether approximation of the evolution equations to order higher than first would lead to growing disturbances for other values of $p$. The disturbances for the $p = 0.5$, $\kappa = \kappa_c$ case grow in time as $e^{\varepsilon t}$ where $\varepsilon > 0$ is proportional to the initial disturbance, as opposed to the $e^{\sigma_R t}$ behavior ($\sigma_R$

independent of initial conditions) which occurs in the unstable region away from the stability/instability boundary.

Initially, it was hoped that an energy criterion could be used to answer this question of finite amplitude stability away from the stability boundary. The Kirchhoff-Routh path function $W(x_1,y_1,x_2,y_2,\cdots)$ (which is a measure of the "interaction energy", see Lin (1943)) determines the motion of the vortices $(x_i,y_i)$ through the relations:

$$\left.\begin{aligned}\frac{dx_i}{dt} &= -\frac{1}{\Gamma_i}\frac{\partial W}{\partial y_i}\\ \frac{dy_i}{dt} &= \frac{1}{\Gamma_i}\frac{\partial W}{\partial x_i}\end{aligned}\right\} \qquad (8.6)$$

By a trivial change of variables, say $x_i \rightarrow -x_i$ for vortices with $\Gamma_i=-\Gamma$, this becomes a Hamiltonian system with Hamiltonian $W$. The right-hand sides of the (Hamilton's) equations may be expanded in Taylor series about the steady solutions $x_i$, $y_i$. The linearized equations reproduce figure 46. The second and higher order terms are, for sufficiently small deviation from the steady state, a small correction to the linear (and integrable) system. There exists a body of theory for such "nearly integrable" Hamiltonian systems in the literature (see, for example, Chirikov (1979)). In general, such systems exhibit the slow instability phenomenon known as "Arnol'd diffusion". Fairly general bounds exist for the average growth rate of this instability (eg. Nekhoroshev (1971)) but these do not appear to provide useful conclusions for the present problem.

The stability boundaries of figure 46 will obviously be perturbed by the effect of finite size of the vortices, and the degenerate saddle will separate into one of the possibilities marked by the dashed lines in the figure. If case 1 is the situation, then there will be stability to infinitesimal disturbances for a finite range of $\kappa$ in the vicinity of $\kappa=\kappa_c$. If case 2 obtains, then finite vortex size makes the array unstable for all $\kappa$.

In principle, the problem of deciding between case 1 and case 2 can be treated by perturbation theory by expanding in powers of the area of the vortices, i.e. $\alpha$. However, for reasons to be given below, it appears that the algebraic complexity is great, and direct numerical methods were employed instead. These, of course, have the advantage that they give results for finite areas not accessible to perturbation methods. It clearly suffices to consider only the subharmonic (pairing) disturbances with $p$=0.5, and we therefore restrict attention henceforth to disturbances which are periodic with period $2l$ in the $x$-direction. Note that the superharmonic disturbances are then automatically included, as these are trivially of period $2l$.

**9. Analysis of the Stability**

It is appropriate for disturbances with period $2l$ to consider four independent perturbed vortex shapes (and positions), corresponding to the four vortices in one period $2l$, and extended periodically to infinity along the street, as in figure 47. The approach is to calculate the first variation of the velocity field due to a perturbation in vortex shape and position, and then to require that the linearized kinematic condition be satisfied on the boundaries of the vortices. In particular, solutions are looked for that are normal modes proportional to $e^{\sigma t}$; an eigenvalue problem is the result.

A convenient parameterization for the vortex boundaries is a polar coordinate representation:

$$\left.\begin{aligned} z(\vartheta) &= z_0(\vartheta) + z'(\vartheta) \\ z'(\vartheta) &= [\tfrac{1}{2}a_0 + \sum_{n=1}^{N}(a_n \cos n\vartheta + b_n \sin n\vartheta)]e^{i\vartheta} \end{aligned}\right\} \qquad (9.1)$$

Here $z_0(\vartheta)$ describes the steady boundary in question and $z'(\vartheta)$ describes the added disturbances.

As was shown in the previous part of the thesis, the complex velocity field produced by a single row of vortices (of spacing $2l$) can be calculated by integration

around the boundary of a single vortex in the row as follows:

$$u+iv = \frac{\Gamma}{2\pi A}\int \log\left|\sin\frac{\pi}{l}(z-Z)\right| \, dZ \tag{9.2}$$

where $z \equiv x+iy$ is the complex coordinate, lower case variables refer to the point of evaluation of the flow field and upper case variables refer to the path of integration. When evaluated on a vortex boundary, this will give the velocity contribution on the vortex boundaries of each vortex in the corresponding $2l$-periodic row due to disturbances of the other three $2l$-periodic vortex rows, added to the unperturbed value. Substituting $z=z_0+z'$, $Z=Z_0+Z'$, and assuming constant area $A$, the corresponding first variation of the velocity contribution is:

$$u'+iv' = \frac{\Gamma}{2\pi A}\int\left[\log\left|\sin\frac{\pi}{2l}(z_0-Z_0)\right|\frac{dZ'}{d\Theta} + Re\left\{\frac{\pi}{2l}\cot\frac{\pi}{2l}(z_0-Z_0)\,(z'-Z')\right\}\frac{dZ_0}{d\Theta}\right]d\Theta \tag{9.3}$$

As was remarked in the previous part of the thesis, the "self-induced" velocity for one row of vortices may be written:

$$u+iv = \int\left[\left\{\log\left|\frac{\sin\frac{\pi}{2l}(z-Z)}{\frac{\pi}{2l}(z-Z)}\right| - i[arg(z-Z)-\tfrac{1}{2}\Theta]\right\}\frac{dZ}{d\Theta} + \tfrac{1}{2}iZ\right]d\Theta - i\pi z \tag{9.4}$$

where the arg function is taken so as to make the integrand periodic. The corresponding first variation is then:

$$u'+iv' = \frac{\Gamma}{2\pi A}\int\left\{\left[Re\left\{\left[\frac{\pi}{2l}\cot\frac{\pi}{2l}(z_0-Z_0) - \frac{1}{z_0-Z_0}\right](z'-Z')\right\} - Im\left\{\frac{z'-Z'}{z_0-Z_0}\right\}\frac{dZ_0}{d\Theta}\right]\right. \tag{9.5}$$

$$\left. + \left\{\log\left|\frac{\sin\frac{\pi}{2l}(z_0-Z_0)}{\frac{\pi}{2l}(z_0-Z_0)}\right| - i\,[arg(z_0-Z_0) - \tfrac{1}{2}\Theta]\right\}\frac{dZ'}{d\Theta} + \tfrac{1}{2}iZ'\right\}d\Theta - i\pi z'$$

Note that all singularities of the integrand have been removed. To calculate the change in flow field due to the complete disturbance, three terms of the form (9.3)

and one of the form (9.5) are summed with appropriate choice for the sign of $\Gamma$ and the vortex coordinate parameters in each case.

The kinematic condition that the vortex boundaries move with the fluid may be written:

$$\frac{D}{Dt}\left[r - R(\vartheta,t)\right] = 0 \tag{9.6}$$

Here:

$$\left.\begin{aligned} R(\vartheta,t) &\equiv R_0(\vartheta) + R'(\vartheta,t) \\ \frac{D}{Dt} &\equiv \frac{\partial}{\partial t} + u_r\frac{\partial}{\partial r} + \frac{1}{r}u_\vartheta\frac{\partial}{\partial\vartheta} \end{aligned}\right\} \tag{9.7}$$

where, as before, the subscript nought refers to the unperturbed quantity and the superscript prime refers to added perturbations. Also, $u_r$ and $u_\vartheta$ are the polar velocity components. The solutions of interest are normal modes with perturbations proportional to $e^{\sigma t}$, so that:

$$\left.\begin{aligned} R'(\vartheta,t) &= e^{\sigma t}R'(\vartheta) \\ u(r,\vartheta,t) &= u_0(r,\vartheta) + e^{\sigma t}u'(r,\vartheta) \end{aligned}\right\} \tag{9.8}$$

where the latter holds for each velocity component. To leading order:

$$u(r,\vartheta) = \left[u_0 + e^{\sigma t}R'\frac{\partial u_0}{\partial r} + u'\right](R_0,\vartheta) \tag{9.9}$$

for each velocity component. Equations (9.7), (9.8), and (9.9) may be substituted into (9.6) and terms of second and higher order in the perturbation omitted, giving:

$$u_r' + \frac{\partial u_{r0}}{\partial r}R' - \frac{1}{R_0}\frac{dR_0}{d\vartheta}u_\vartheta' + \frac{\partial u_{\vartheta 0}}{\partial r}R' = \tag{9.10}$$

$$\sigma R' - \frac{1}{R_0^2}\frac{dR_0}{d\vartheta}u_{\vartheta 0}R' + \frac{u_{\vartheta 0}}{R_0}\frac{dR'}{d\vartheta}$$

where now all quantities are evaluated on $r=R_0(\vartheta)$, and use has been made of the

fact that:

$$u_{r0} - \frac{1}{R_0}\frac{dR_0}{d\vartheta}u_{\vartheta 0} = 0 \quad on \quad r=R_0. \tag{9.11}$$

The left hand side of (9.10) is the perturbation in normal velocity component $\delta u_n$ divided by the geometric factor:

$$\cos\eta \equiv \left[1+(\frac{1}{R_0}\frac{dR_0}{d\vartheta})^2\right]^{-\frac{1}{2}} \tag{9.12}$$

where the effect of the change in normal direction due to the perturbation has been omitted. Also, $u_{\vartheta 0}$ and the unperturbed tangential velocity component $u_{t0}$ are related by:

$$u_{\vartheta 0} = u_{t0}\cos\eta \tag{9.13}$$

so that (9.10) may be written:

$$\delta u_n = \sigma\cos\eta\, R' - \cos^2\eta\,\frac{1}{R_0^2}\frac{dR_0}{d\vartheta}u_{t0}R' + \cos^2\eta\,\frac{u_{t0}}{R_0}\frac{dR'}{d\vartheta}. \tag{9.14}$$

This may be equated to the corresponding quantity calculated by the integration above (ie. by (9.3) and (9.5)) and using:

$$\left.\begin{aligned} \delta u_\eta &= \cos\eta\ \ u_r' - \frac{1}{R_0}\frac{dR_0}{d\vartheta}u_\vartheta' \\ u_r' &= u'\cos\vartheta + v'\sin\vartheta \\ u_\vartheta' &= -u'\sin\vartheta + v'\cos\vartheta \end{aligned}\right\} \tag{9.15}$$

After substituting (9.1) and evaluating at the $2N+1$ points

$$\vartheta = \vartheta_j \equiv \frac{2\pi j}{2N+1} \qquad (j=0,\,1,\ldots,\,2N) \tag{9.16}$$

the result is a generalized eigenvalue problem of the form:

$$\mathbf{A}\mathbf{w} = \sigma\mathbf{B}\mathbf{w} \tag{9.17}$$

where **A** and **B** are $8N+4$ by $8N+4$ matrices and **w** is a vector containing the four sets of $2N+1$ Fourier coefficients from (9.1). The real parts of the eigenvalues of this system then give the growth rates of the corresponding normal modes. Inspection leads to the conclusion that if $\sigma$ is an eigenvalue, then so are $-\sigma$, $\sigma^*$, and $-\sigma^*$. Thus, it is evident that at best, a steady state may have only normal modes with zero linear growth rate, and otherwise, the state is linearly unstable.

For numerical purposes, the system (9.17) may be simplified somewhat, by recognizing the symmetry of the problem. It is sufficient to consider disturbances where the vortex shape perturbations $z'$ are negatives for vortices of rows 1 and 2 above, and similarly for rows 3 and 4. This simplification reduces the size of the system to $4N+2$ equations in two sets of Fourier coefficients. Values of $N$ from 10 to 25 were used, depending on the size of the vortices.

Computations of the eigensystem were performed with standard library routines using an IBM 3033 computer (64 bit floating point). Some computational difficulties were encountered; an explanation follows: Note that for isolated circular vortices of area $A$ and circulation $\Gamma$, normal mode perturbations exist of the form (see Lamb, (1932,pp.230-1)):

$$\left.\begin{aligned} R' &= \varepsilon \cos m\vartheta\, e^{\sigma t} \\ \sigma &= \tfrac{1}{2}i\frac{\Gamma}{2\pi A}(m-1) \\ &\quad (m=2,\ 3,\ 4,\ldots). \end{aligned}\right\} \tag{9.18}$$

Since the corresponding flow field perturbations fall off in distance $r$ as $r^{-m-1}$, and since small area vortices for the street are nearly circular, it is evident that for small $A$ and large $m$, there will exist such solutions for the street. These in fact are the superharmonic disturbances. For small area $A$, these eigenvalues are much larger in modulus than the subharmonic ($p$=0.5) modes which are bounded as $A$

decreases. In fact, although this behavior is most severe for small areas, for all states that were computed, these "nearly isolated" modes had eigenvalues with dominating moduli. This characteristic showed itself in a great sensitivity of the calculated small eigenvalues to errors in the steady calculations (hence the matrices **A** and **B**). Typically, an error of roughly 0.1% in radius or tangential velocity completely destroyed the small eigenvalue computation. A second computational problem was failure of convergence of the iterative procedure for eigenvalue and eigenvector computation. This difficulty usually manifested itself near the stability/instability interface, and the explanation is not clear.

The results of the stability calculations are plotted in figures 48 to 68 and summarized in figure 69. As described in Chapter 6, curve 1 denotes the approximate maximum area for a given spacing ratio, and between curves 1 and 2 there are two solutions for a given $(\kappa,\alpha)$ pair. Outside of the nearly enclosed central v-shaped region indicated in the $(\kappa,\alpha)$ plane, there are modes with positive growth rates, and hence these outlying states are linearly unstable. Inside this region, there are no such modes (with $x$ period $2l$). With the exception of the smaller energy state in the non-unique region (between curves 1 and 2 in figure 69), all eigenvalues corresponding to superharmonic disturbances were found to be purely imaginary. The exceptional cases were found to be difficult to calculate, but the growing superharmonic modes appear to have real eigenvalues (see figure 68). Aside from the trivial modes (uniform displacements) the non-growing modes were found to be approximately given by (9.18), at least for $m$ greater than 3 or 4, with best matching for large $m$. There is agreement with the unsteady initial-value calculations of Christiansen and Zabusky (1973), as indicated in figure 69.

The observed change of subharmonic stability as $\alpha$ crosses some critical value $\alpha_c$ occurs when an imaginary eigenvalue splits to become a growing/decaying pair. This may be explained as follows. Since the eigenvalues $\sigma$ are given (to arbitrary approximation) by the roots of a polynomial whose coefficients presumably are

smooth functions of $\alpha$, non-analytic behavior of $\sigma(\alpha)$ is limited to the existence of branch points (Bender and Orszag, (1978, pp.350)). Thus, the observed splitting as $\alpha$ is decreased below $\alpha_c$ (say), may be described locally by

$$\sigma_{\pm} \approx \pm\sqrt{\alpha_c-\alpha} + i\omega \tag{9.19}$$

Hence, transition from stable to unstable conditions is accompanied by the degeneration of two imaginary eigenvalues. This phenomenon was clearly observed both for the stabilization at smaller area and the subsequent destabilization at larger area, and is apparent in many of figures 49 to 65. The superharmonic instabilities seem to have more complicated behavior, and due to the difficulty of these calculations, this matter remains obscure.

For small areas, the width in $\kappa$ of the stability region decreases and a plot of calculations in the vicinity (figure 70) indicates that the critical value of area $\alpha$ at which stabilization occurs, asymptotically for small area, is approximately:

$$\left.\begin{aligned} \alpha &\approx 1.31(\kappa_c-\kappa)^{\frac{1}{2}} \qquad \kappa<\kappa_c \\ \alpha &\approx 0.78(\kappa-\kappa_c)^{\frac{1}{2}} \qquad \kappa>\kappa_c \end{aligned}\right\} \tag{9.20}$$

This approximate result indicates for the following reason that its exact calculation by perturbation analysis may be a laborious task: When $\alpha$=0 and $p$=0.5, the eigenvalues are the roots of the quartic

$$\sigma^4 + 2(B^2-A^2)\sigma^2 + (B^2+A^2)^2 = 0. \tag{9.21}$$

It is expected that the coefficients of the equation for the eigenvalues are analytic functions of $\kappa$ and $\alpha$. Hence, for $\alpha << 1$, the perturbed eigenvalues are roots of the quartic

$$\sigma^4 + [(2(B^2-A^2)+\alpha^2 f_2(\kappa)+\alpha^4 f_4(\kappa)\cdots]\sigma^2 + [(B^2+A^{2)^2}+\alpha^2 g_2(\kappa)+\alpha^4 g_4(\kappa)\cdots] = 0.$$

(9.22)

(Invariance to changes in the sign of the vorticity requires the coefficients to be even functions of $\alpha$). The roots will, as functions of $\alpha$, have branch point singularities, corresponding to a change in stability of the system, where the roots of the quartic are not distinct, i.e. when

$$-16A^2B^2 + [4(B^2-A^2)f_2-4g_2]\alpha^2 + [4(B^2-A^2)f_4+f_2^2-4g_4]\alpha^4 + \cdots = 0. \tag{9.23}$$

The results shown in figure 70 indicate that when expanded in $(\kappa-\kappa_c)$ as well as $\alpha$, this equation takes the approximate form

$$1.04(\kappa-\kappa_c)^2 - 2.32\alpha^2(\kappa-\kappa_c) + \alpha^4 = 0. \tag{9.24}$$

The principal point, however, is that it is necessary to go to fourth order in $\alpha$ in order to determine the behavior of the eigenvalues for small area.

**10. The Energy Criterion for Stability**

It was pointed out by Kelvin (1910,pp.116) (see also Arnol'd (1980,pp.335)) that for given vorticity and momentum, steady states correspond to stationary points of the kinetic energy with respect to kinematically allowable isovorticial perturbations. The steady state is then stable if it is a local maximum or miminum in energy.

For this problem, assuming perturbations periodic in the streamwise direction (say with period $Nl$, $N$ an integer), it is sufficient to apply the above criterion to one period of the flow field. Holding the vorticity constant, and assuming that vortices of opposite sense do not amalgamate, the requirement of kinematically allowable perturbations forces the total area of the vortices of each sense to remain unchanged. The condition of momentum invariance requires that the components of hydrodynamic impulse per unit length,

$$I_x = -\frac{1}{Nl}\int_0^{Nl}\int_{-\infty}^{+\infty} \omega y \, dx \, dy = \frac{\Gamma h}{l}, \tag{10.1}$$

$$I_y = -\frac{1}{Nl}\int_0^{Nl}\int_{-\infty}^{+\infty} \omega x \, dx \, dy = 0, \tag{10.2}$$

stay constant. This is ensured by keeping the distance between the centroids of the two rows constant. In the following discussion it shall be assumed that $N$=2.

Now consider a system with period $2l_0$ and consider the following four configurations (see figure 71):

(1) $l=2l_0,\ d=l_0,\ h=h_0,\ A=2A_0$

(2) $l=2l_0,\ d=0,\ h=h_0,\ A=2A_0$ (10.3)

(3) $l=l_0,\ d=\frac{1}{2}l_0,\ h=h_0,\ A=A_0$

(4) $l=l_0,\ d=0,\ h=h_0,\ A=A_0$

These states are apparently unique for small values of $\alpha$ (below curve 2 in figure 69 for states (1) and (3)). It is clear that these four states satisfy the above conditions (10.1) and (10.2). Presumably, there are other steady states that do so, such as finer splittings and multiple vortex layers, but the existence of such configurations is not crucial to this argument, as their energy is (believed to be) less than that of configuration (4). We are concerned with the stability of configuration (3) to superharmonic disturbances of period $l_0$ in which all vortices in a row are disturbed in the same way, and to subharmonic disturbances of period $2l_0$.

Calculations based on the circular vortex approximation (see Chapter 3) indicate that the energies of the four steady states can be ranked as follows when $\alpha=A_0/l_0^2$ is small:

$$E_1 > E_2 > E_3 > E_4 \tag{10.4}$$

Since $E$ is clearly bounded above, $E_1$ is an absolute maximum and configuration (1) is stable; it follows from the similarity of (1) and (3) that configuration (3) is stable to all *superharmonic* disturbances, and this will remain true for all $\alpha$ below curve 2 in figure 69. (When there are two states, the one with less energy will be unstable.) This confirms our calculations of *superharmonic* instability but state (3) is not stable to *subharmonic* disturbances for $\kappa$ outside the range shown in figure 69 and will therefore be in this range a minimax of energy.

Now it can be shown from calculations of the system with $d$=0 that when $\alpha$ is large it is possible for $E_2 < E_3$ to occur. When this problem was first studied, it was speculated that a mechanism for the stabilization of configuration (3) against subharmonic infinitesimal and finite amplitude disturbances is that the drop in $E_2$ below $E_3$ for sufficiently large area results in a change in the topology of the energy surface in the infinite dimensional configuration space (for this configuration) so that it becomes a local maximum in energy. Non-dimensionalization leads to $T = \frac{\Gamma^2}{l}\hat{T}(\alpha, \kappa, \mu)$ for the energy per unit length of a given steady state (assuming it exists). The condition that $E_2$=$E_3$ then leads to:

$$2\,\hat{T}(\tfrac{1}{2}\alpha, \tfrac{1}{2}\kappa, 0) = \hat{T}(\alpha, \kappa, \tfrac{1}{2}) \qquad (10.5)$$

where $\alpha$ and $\kappa$ are the parameters associated with configuration three. The result of applying this criterion is shown by curve 3 of figure 69. It was observed that for the $\mu$=0 cases (configurations (2) and (4)), solutions exist only for vortices up to a limiting area. As the vortex area approaches this limit adjacent vortices in opposite rows near each other. It is believed that this behavior is qualitatively similar to that observed for a pair of counter-rotating vortices by Pierrehumbert (1980). For small $\kappa$, the limit occurs at small area, and since interactions between neighboring pairs are then small, the counter-rotating vortex pair should indeed be a good approximation. Curve 4 of figure 69 represents this approximation. Some calcula-

tions for the exact problem were attempted and are in reasonable agreement with curve 4 (the approximate calculated limiting areas were always less than curve 4 and within about 25%). However, accurate calculation of the limiting area is prohibitively expensive, and was not undertaken. According to this argument, the region of stability lies between curves 3 and 4 in figure 69 and is moreover a region of stability to finite amplitude disturbances which are not too large. The results of the linear stability analysis shows that this argument is fallacious. Incidentally, there is no evidence to suggest that the symmetrical configuration ($d$=0) can be stabilized by finite size, but Taneda (1965) reported that oscillation of the body produced streets of symmetrical vortices. At present no explanation of this phenomenon can be offered.

**11. Conclusion**

Von Kármán's analysis of the linear stability of the point vortex street has been generalized to vortices of finite size and it has been demonstrated that finite size can stabilize the array. The boundary of the linear stability region for subharmonic disturbances of period twice the separation is shown in figure 69. The open questions deal with non-linear stability and with stability to more general disturbances. At present, there seems to be no way to study the former question other than by direct numerical calculation of an initial value problem. This was carried out to some approximation by Christiansen and Zabusky (1973), as commented earlier, and their results indicate that linear stability implies non-linear stability, or at least, very slow growth. The possibility of unstable disturbances of more general character than those considered here could also be investigated in this way.

For point vortices, the equations of motion amount to a Hamiltonian system of a finite number of degrees of freedom (depending on the assumed periodicity) and the theory of nearly integrable systems (eg. see Chirikov (1979)) suggests that this system is subject to slow instability ("Arnol'd diffusion"). However, it may be that the

instability is so slow that streets of physical interest are in a practical sense stable. This question has not been resolved. Intuitively, one can perhaps expect this behavior to persist to the finite area case, but it would be worthwhile to investigate this matter further.

# IV. Directions for Future Research

As was pointed out previously, there are unresolved questions pertaining to the stability of the inviscid model described herein. A conclusive resolution of the questions of neutral versus true stability and stability to three-dimensional disturbances would be highly desirable in order to complete the theoretical understanding of this idealized model. These are rather subtle but generic problems, and a solution might provide some general understanding of the class of inviscid but rotational flows. However, it is possibly true that these questions are of more theoretical than practical interest. Another unresolved question is whether or not there are two-dimensional disturbances of more general character than considered here which result in greater instability. In principle, disturbances of longer wavelength could by studied by allowing more than the four independent vortex perturbations allowed in the present work. This approach would not resolve the possibility of the existence of a continuous spectrum.

An interesting and useful extension of this work would deal with the cases of vortex streets with rows of vortices of unequal strength (and/or area and shape) and uncentered stagger, which might be produced in the wake of lifting and vibrating bodies or bodies with unequal free-stream velocities above and below. These extensions require only minor modifications to the methods used for the model problem considered here. A more difficult extension of the model would deal with nonuniform vorticity, although still in the context of inviscid flow. If the vorticity is taken to be piecewise constant with each vortex consisting of several concentric "layers", each of uniform vorticity, the present numerical schemes could also be used with minor changes. A more general distribution of vorticity probably would require a different approach. It is not known what effect on the results a nonuniform distribution of vorticity would have, but it is conjectured that the changes would be of an unessential nature.

From the point of view of the experimentalist and applied fluid dynamicist, probably the most unsatisfactory aspect of the present work is the neglect of viscosity. While it is of interest to observe how well the physically observed phenomena may be predicted by an inviscid model (the author plans to investigate this matter further), it is probably true that comparison with experiment must remain doubtful. Viscous effects are fundamentally important in real physical systems producing Kármán vortex streets, but their presence greatly complicates the theoretical analysis, and a fully satisfactory treatment of the viscous problem has not yet been achieved.

**Appendix A - Calculation of the Velocity**

To evaluate the integrals in (2.2) it is useful to write:

$$\int_{\Sigma_1} \log\left|\sin\frac{\pi}{l}(z-z')\right| dz' = \int_0^{2\pi} \log\left|\sin\frac{\pi}{l}(z-Z)\right| \frac{dZ}{d\Theta}\, d\Theta, \tag{A.1}$$

where $Z \equiv z\,|_{\vartheta=\Theta}$ and $dZ/d\Theta$ can be determined from (5.2) as finite Fourier series in $\Theta$. Hence, the integrand is $2\pi$-periodic, and the trapezoidal rule gives formally infinite order accuracy - provided that the integrand has infinitely many derivatives, ie. that z is not on the boundary of the vortex. Unfortunately, z *is* on the boundary for one of the integrals when (5.6) is solved to obtain the vortex shapes.

To preserve accuracy in this case, the following trick is used (suggested by Dr. B. Fornberg):

$$\int \log\left|\sin\frac{\pi}{l}(z-z')\right| dz' = \int \log\left|\frac{\sin\frac{\pi}{l}(z-z')}{\frac{\pi}{l}(z-z')}\right| dz' + \int \log\left|\frac{\pi}{l}(z-z')\right| dz' \tag{A.2}$$

The first integral presents no difficulties, and the second can be calculated as follows:

$$\int \log\left|\frac{\pi}{l}(z-z')\right| dz' = \int \log\frac{\pi}{l}(z-z')\, dz' - \int \log\frac{z-z'}{|z-z'|}\, dz' \tag{A.3}$$

$$= -i \int arg\,(z-z')\, dz'$$

$$= -i \int_{\vartheta}^{\vartheta+2\pi} arg\,(z-Z)\, \frac{dZ}{d\Theta}\, d\Theta$$

$$= -i \int_{\vartheta}^{\vartheta+2\pi} \left[arg\,(z-Z) - \tfrac{1}{2}\Theta\right] \frac{dZ}{d\Theta}\, d\Theta - \tfrac{1}{2}i \int_{\vartheta}^{\vartheta+2\pi} \Theta\, \frac{dZ}{d\Theta}\, d\Theta$$

$$= -i \int_{\vartheta}^{\vartheta+2\pi} \left\{\left[arg\,(z-Z) - \tfrac{1}{2}\Theta\right] \frac{dZ}{d\Theta} - \tfrac{1}{2}Z\right\} d\Theta - i\pi z(\vartheta)$$

where the arg function is taken so that the integrand is $2\pi$-periodic.

For the second numerical scheme, $R_\vartheta$ was approximated by a fourth order centered finite difference formula, and $z_\vartheta$ then obtained from this. Hence, the integrals were approximated to third order.

**Appendix B - Energy Calculation**

The calculation of the kinetic energy for the infinite vortex street proceeds nearly identically as for the infinite linear array (Saffman and Szeto, (1981)). The result (with unit density) may be written:

$$T = \frac{1}{4}\frac{\Gamma}{A}\int_{\Sigma_1} R^2 \frac{\partial \psi}{\partial n}\, ds - \frac{\Gamma}{2\pi}\int_{\Sigma_1} \chi \frac{\partial \psi}{\partial n}\, ds - \frac{1}{16}\frac{\Gamma^2}{A^2}\int_0^{2\pi} R^4\, d\vartheta \tag{B.1}$$

where $(R,\vartheta)$ are polar coordinates with origin at the centroid of the prime vortex, and $\chi$ is the integrand in (2.1) that gives the value of the stream function at the origin, after combining the integrals. Ie.:

$$\psi(0,0) = \frac{\Gamma}{2\pi A}\int\int_{\Sigma_1} \chi\, dA \tag{B.2}$$

The functional form of $\chi$ depends on the symmetry presumed to exist between the two rows of the street. Corresponding to (2.3), the actual function that was used in these calculations is:

$$\chi(z) = \log\left|\frac{\sin\frac{\pi}{l}z}{\sin\frac{\pi}{l}(z-d+ih)}\right| \tag{B.3}$$

**References**

[1] F.H. Abernathy and R.E. Kronauer, *The Formation of Vortex Streets*, J. Fluid Mech., 13(1962), pp.1-20.

[2] H. Aref and E.D. Siggia, *Evolution and Breakdown of a Vortex Street in Two Dimensions*, J. Fluid Mech., (to be published), (1981).

[3] V.I. Arnol'd, *Mathematical Methods of Classical Mechanics*, Springer-Verlag, New York, 1980, pp.332-337.

[4] P.W. Bearman and J.M.R. Graham, *Vortex Shedding from Bluff Bodies in Oscillatory Flow: A Report on Euromech 119*, J. Fluid Mech., 99(1980), pp.225-245.

[5] C.M. Bender and S.A. Orszag, *Advanced Mathematical Methods for Scientists and Engineers*, McGraw-Hill, New York, 1978.

[6] E. Berger and R. Wille, *Periodic Flow Phenomena*, Ann. Rev. Fluid Mech., 4(1972), pp.313-340.

[7] D.R. Boldman, P.F. Brinich, and M.E. Goldstein, *Vortex Shedding from a Blunt Trailing Edge with Equal and Unequal External Mean Velocities*, J. Fluid Mech., 75(1976), pp.721-735.

[8] J.R. Chaplin, *Computer Model of Vortex Shedding from a Cylinder*, ASCE Proc., Hydraulics Division, 99(1973), pp.155-165.

[9] B. Chen and P.G. Saffman, *Numerical Evidence for the Existence of New Types of Gravity Waves of Permanent Form on Deep Water*, Studies in Appl. Math., 62(1980), pp. 1-21.

[10] B.V. Chirikov, *A Universal Instability of Many-Dimensional Oscillator Systems*, Physics Reports, 52(1979), pp.263-379.

[11] A.J. Chorin, *Numerical Study of Slightly Viscous Flow*, J. Fluid Mech., 57(1973), pp.785-796.

[12] J.P. Christiansen, *Numerical Simulation of Hydrodynamics by the Method of Point Vortices*, J. Comp. Phys., 13(1973), pp.363-379.

[13] J.P. Christiansen and N.J. Zabusky, *Instability, Coalescence and Fission of Finite-Area Vortex Structures*, J. Fluid Mech., 61 (1973), pp. 219-243.

[14] R.R. Clements, *An Inviscid Model of Two-Dimensional Vortex Shedding*, J. Fluid Mech., 57(1973), pp.321-336.

[15] M.E. Davies, *A Comparison of the Wake Structure of a Stationary and Oscillating Bluff Body, Using a Conditional Averaging Technique*, J. Fluid Mech., 75(1976), pp. 209-231.

[16] U. Domm, *The Stability of Vortex Streets with Consideration of the Spread of Vorticity of the Individual Vortices*, J. Aeronaut. Sci., 22(1955), pp.750-754.

[17] U. Domm, *Über die Wirbelstraßen von geringster Instabilität*, Zeitschrift Fur Angewandte Mathematik Und Mechanik,30(1956), pp.367-371.

[18] G. Ehrhardt, *Stabilität Zweireihiger Straßen geradlinger und Kreisförmiger Wirbel*, Fortschritt-Berichteder VDI-Zeitschriften, 7(1979), no. 49, pp.1-52.

[19] J.H. Gerrard, *The Calculation of the Fluctuating Lift on a Circular Cylinder and its Application to the Determination of Aeolian Tone Density*, A.G.A.R.D. Report 463 (1963).

[20] J.H. Gerrard, *Numerical Computation of the Magnitude and Frequency of the Lift on a Circular Cylinder*, Phil. Trans. Roy. Soc. A, 261(1967), pp.137-162.

[21] S. Goldstein, ed., *Modern Developments in Fluid Dynamics*, Vol II, Clarendon Press, Oxford, 1938, pp. 556-565.

[22] S.E. Hurlbut, M.L. Spaulding, and F.M. White, *Numerical Solution of the Time Dependent Navier-Stokes Equations in the Presence of an Oscillating Cylinder*, Nonsteady Fluid Dynamics: ASME Proc. Winter Annual Meeting, Dec. 10, New York (1978), pp.207-216.

[23] P.C. Jain and B.S. Goel, *Shedding of Vortices Behind a Circular Cylinder*, Computers and Fluids, 4(1976), pp.137-142.

[24] S.K. Jordan and J.E. Fromm, *Oscillatory Drag, Lift, and Torque on a Circular Cylinder in a Uniform Flow*, Physics of Fluids, 15(1972), pp.371-376.

[25] T. v.Kármán, *Über den Mechanismus des Widerstands, den ein bewegter Körper in einer Flüssigkeit erfährt*, Göttinger Nachrichten, Math. Phys. Kl., (1911), pp.509-517.

[26] T. v.Kármán, *Über den Mechanismus des Widerstands, den ein bewegter Körper in einer Flüssigkeit erfährt*, Göttinger Nachrichten, Math. Phys. Kl., (1912), pp.547-556.

[27] T. v.Kármán and H.L. Rubach, *Über den Mechanismus des Flüssigkeits- und Luftwiderstands*, Phys. Zeitschrift, 13(1912), pp. 49-59.

[28] Lord Kelvin, *Mathematical and Physical Papers*, Vol IV, Cambridge U.P., 1910.

[29] M. Kiya and M. Arie, *A Contribution to an Inviscid Vortex-Shedding Model for an Inclined Flat Plate in Uniform Flow*, J. Fluid Mech., 82(1977), pp.223-240.

[30] M. Kiya and M. Arie, *An Inviscid Numerical Simulation of Vortex Shedding from an Inclined Flat Plate in Shear Flow*, J. Fluid Mech., 82(1977), pp.241-253.

[31] N.J. Kochin, *On the Instability of Von Kármán's Vortex Street*, Comptes Rendus (Doklady) de l'Académie des Sciences de l'URSS, 24(1939),pp.19-23.

[32] M.Z. v.Krzywoblocki, *Vortex Streets in Incompressible Media*, Applied Mechanics Reviews, 6(1953), pp.393-397.

[33] K. Kuwahara, *Study of Flow Past a Circular Cylinder by an Inviscid Model*, J. Phys. Soc. Japan, 45(1978), pp.292-297.

[34] A.D.K. Laird, *Eddy Formation Behind Circular Cylinders*, ASCE Proc., Hydraul-

ics Division, 97(1971), pp.763-775.

[35] Sir Horace Lamb, *Hydrodynamics*, (Sixth Ed.), Cambridge U.P., 1932.

[36] C.C. Lin, *On the Motion of Vortices in Two Dimensions*, University of Toronto Studies, Applied Mathematics Series, 5(1943).

[37] M.V. Morkovin, *Flow Around Circular Cylinder - A Kaleidoscope of Challenging Fluid Phenomenon*, ASME Symp. Fully-Separated Flows, Philadelphia (1964), pp.102-118.

[38] N.N. Nekhoroshev, *The Behavior of Hamiltonian Systems that are Close to Integrable*, Functional Analysis and Its Applications, 5(1971),pp.338-339.

[39] R.B. Payne, *Calculation of Unsteady Viscous Flow Past a Circular Cylinder*, J. Fluid. Mech., 4(1958), pp.81-86.

[40] R.T. Pierrehumbert, *A Family of Steady, Translating Vortex Pairs With Distributed Vorticity*, J. Fluid Mech., 99(1980), pp. 129-144.

[41] R.T. Pierrehumbert and S.E. Widnall, *The Structure of Organized Vortices in a Shear Layer*, AIAA Paper 79-1560 (1979).

[42] Lord Rayleigh, *Acoustical Observation II*, Philosophical Magazine, 7(1879), pp.149-162.

[43] L. Rosenhead, *Double Row of Vortices with Arbitrary Stagger*, Proc. Camb. Phil. Soc., 25(1929), pp. 132-138.

[44] L. Rosenhead, *The Spread of Vorticity in the Wake Behind a Cylinder*, Proc. Roy. Soc. A, 127(1930), pp.590-612.

[45] L. Rosenhead, *Vortex Systems in Wakes*, Advances in App. Mech., 3(1953), pp.185-195.

[46] A. Roshko, *Experiments on the Flow Past a Circular Cylinder at Very High Reynolds Number*, J. Fluid Mech., 10(1961), pp.345-356.

[47] P.G. Saffman and R. Szeto, *Structure of a Linear Array of Uniform Vortices*, to be published, (1981).

[48] T. Sarpkaya, *An Analytical Study of Separated Flow About Circular Cylinders*, ASME Trans., Series D, Journal of Basic Engineering, (1968), pp.511-520.

[49] T. Sarpkaya and R.L. Shoaff, *An Inviscid Model of Two-Dimensional Vortex Shedding for Transient and Asymptotically-Stable Separated Flow Over a Cylinder*, AIAA Paper 79-0281 (1979), pp.1-9.

[50] P.K. Stansby, *An Inviscid Model of Vortex Shedding From a Circular Cylinder in Steady and Oscillatory Far Flows*, Proc. Inst. Civ. Eng., 63(1977), pp.865-880.

[51] V. Strouhal, *Uber eine besondere Art der Tonnerregung*, Annalen der Physik und Chemie, 5(1878), pp.216-251.

[52] J.C. Swanson and M.L. Spaulding, *Three-Dimensional Numerical Model of Vortex Shedding From a Circular Cylinder*, Nonsteady Fluid Dynamics: ASME Proc. Winter Annual Meeting, Dec. 10, New York (1978), pp.207-216.

[53] Y. Takao, IBM Japan Science Center Report G318-1909-0 (1973).

[54] S. Taneda, *Experimental Investigation of Vortex Streets*, J. Physical Society of Japan, 20(1965),pp.1714-1721.

[55] R. Wille, *Kármán Vortex Streets*, Advances in App. Mech., 6(1960), pp.273-287.

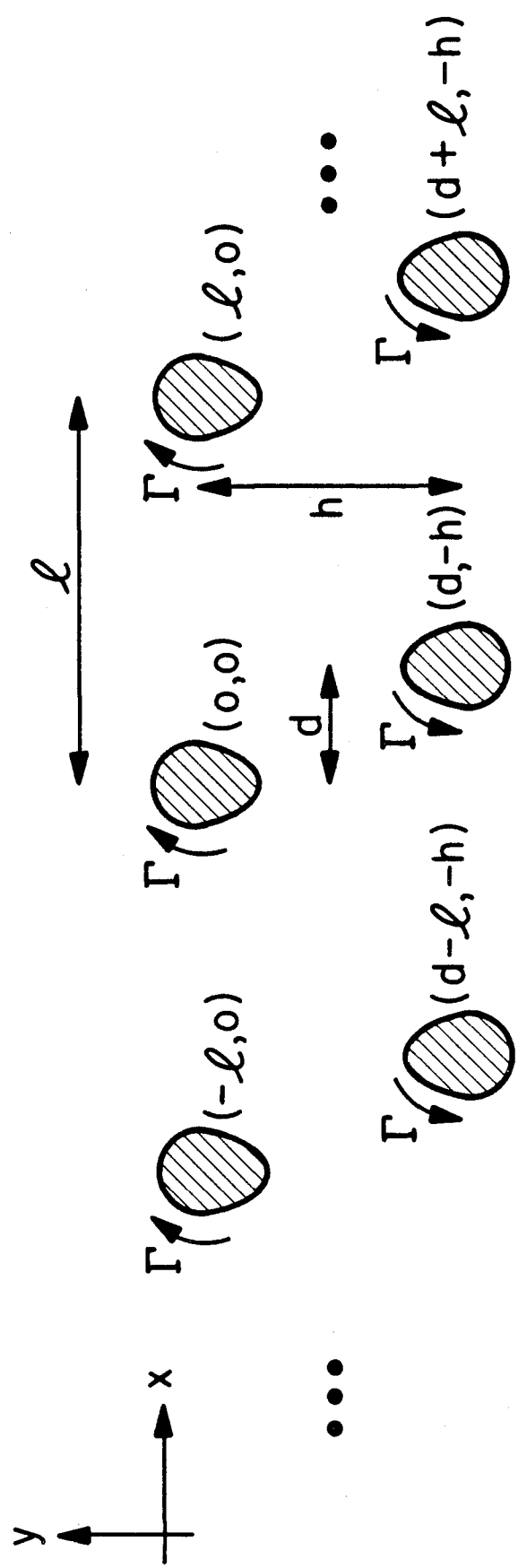


Figure 1. The configuration of the fully infinite vortex street with arbitrary stagger.

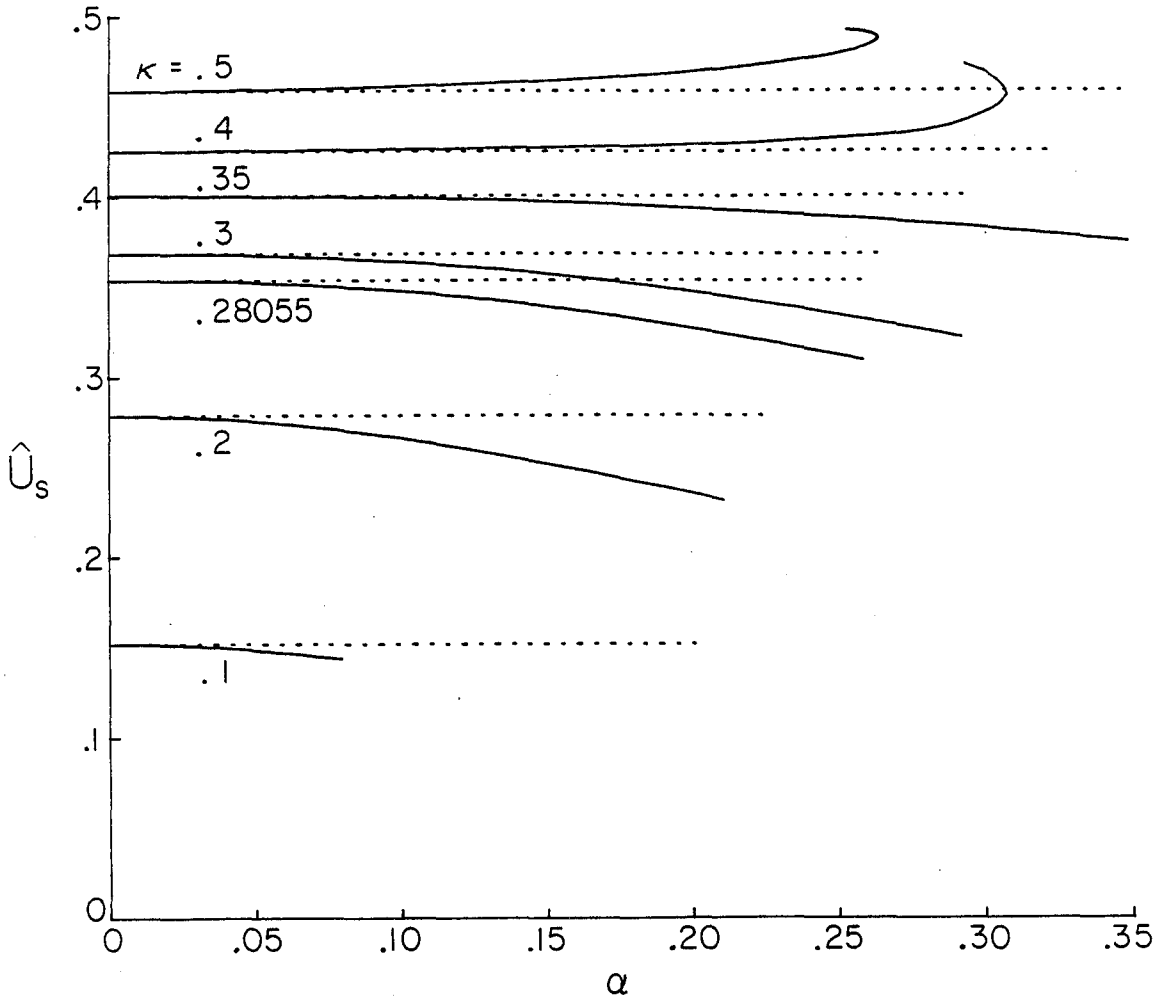


Figure 2. Values of the street propagation speed $\hat{U}_s$ for the staggered vortex array ($\mu=\frac{1}{2}$). Solid lines denote the calculated values for the exact problem and dashed lines denote the circular vortex approximation.

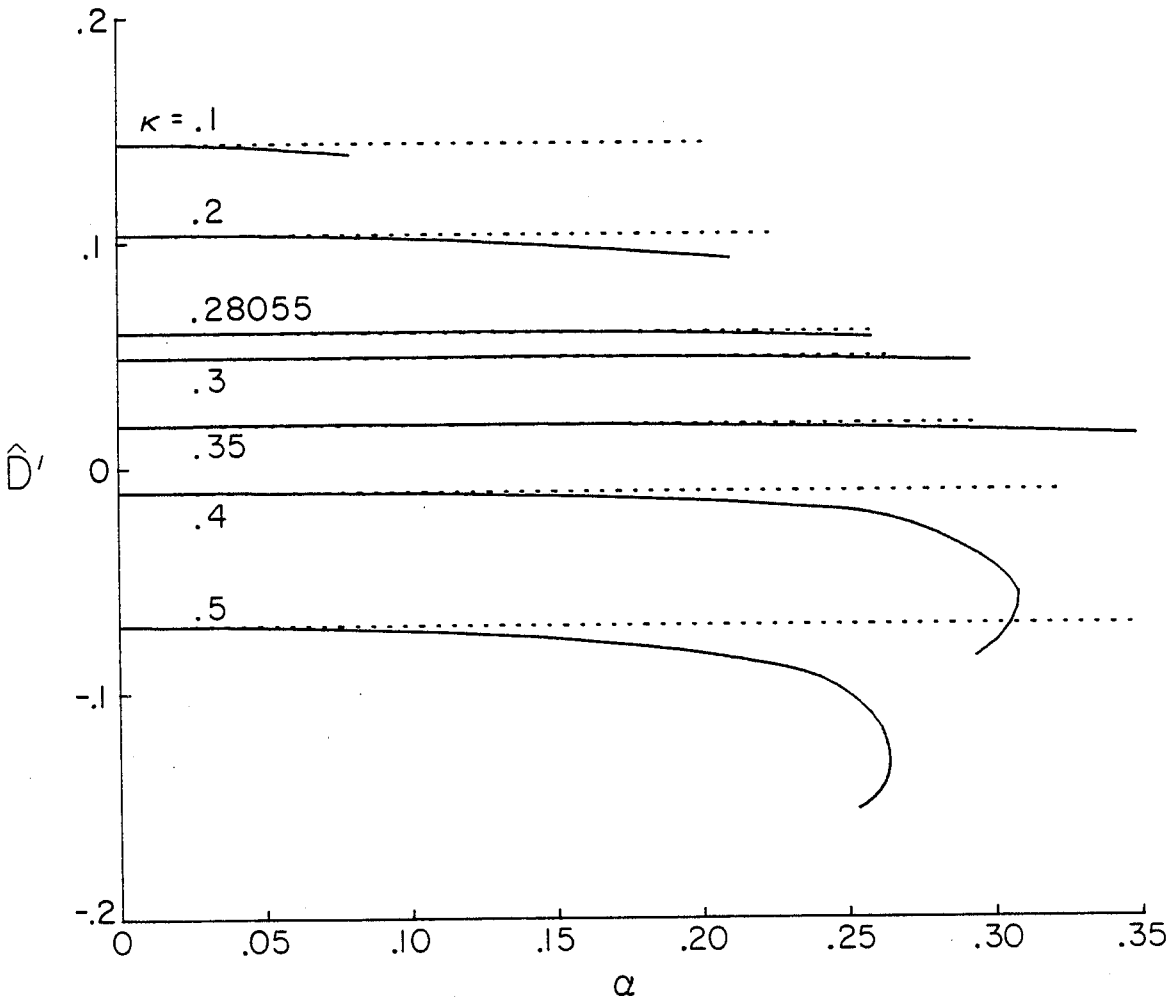


Figure 3. Values of the momentum flux $\hat{D}'$ for the staggered vortex array ($\mu=\frac{1}{2}$). Solid lines denote the calculated values for the exact problem and dashed lines denote the circular vortex approximation.

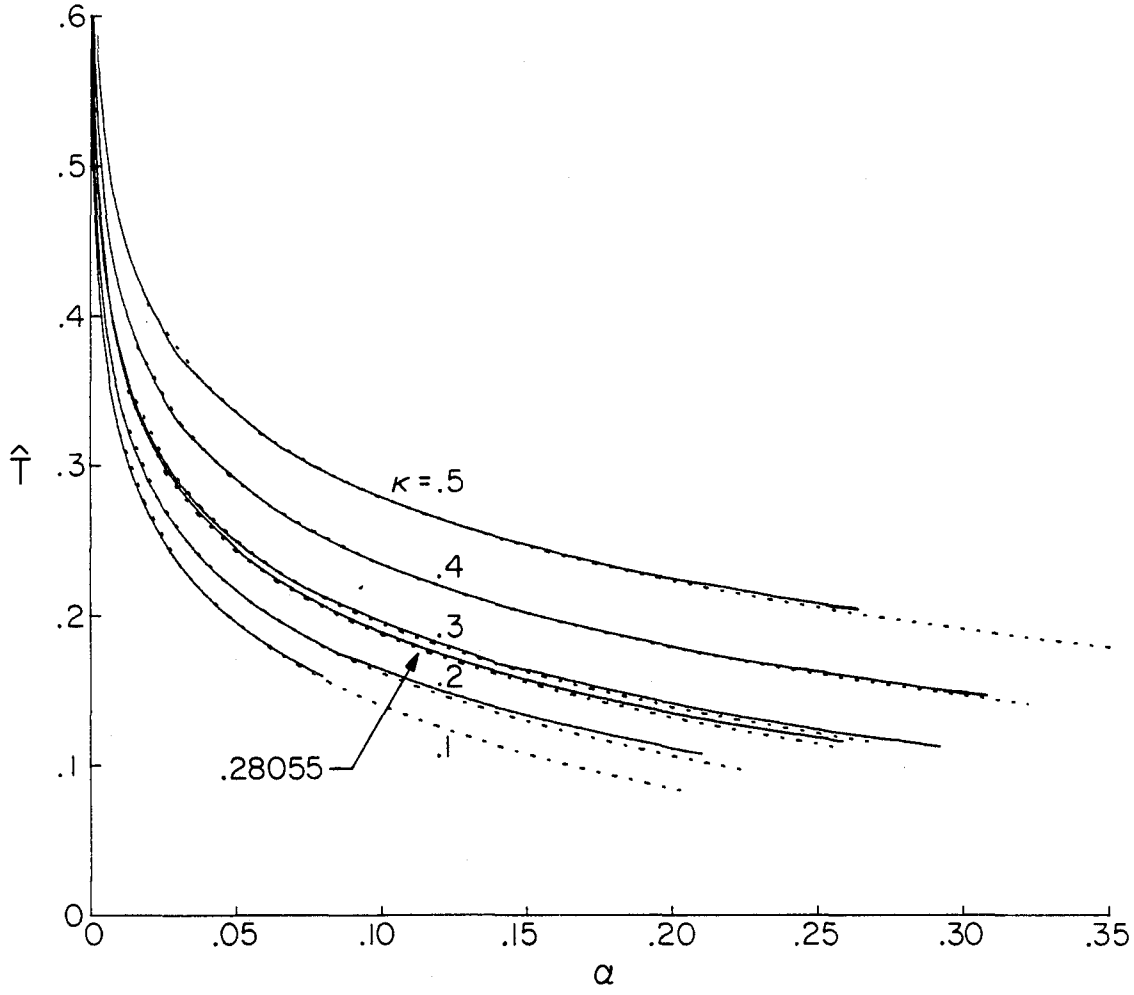


Figure 4. Values of the kinetic energy $\hat{T}$ for the staggered vortex array ($\mu=\frac{1}{2}$). Solid lines denote the calculated values for the exact problem and dashed lines denote the circular vortex approximation.

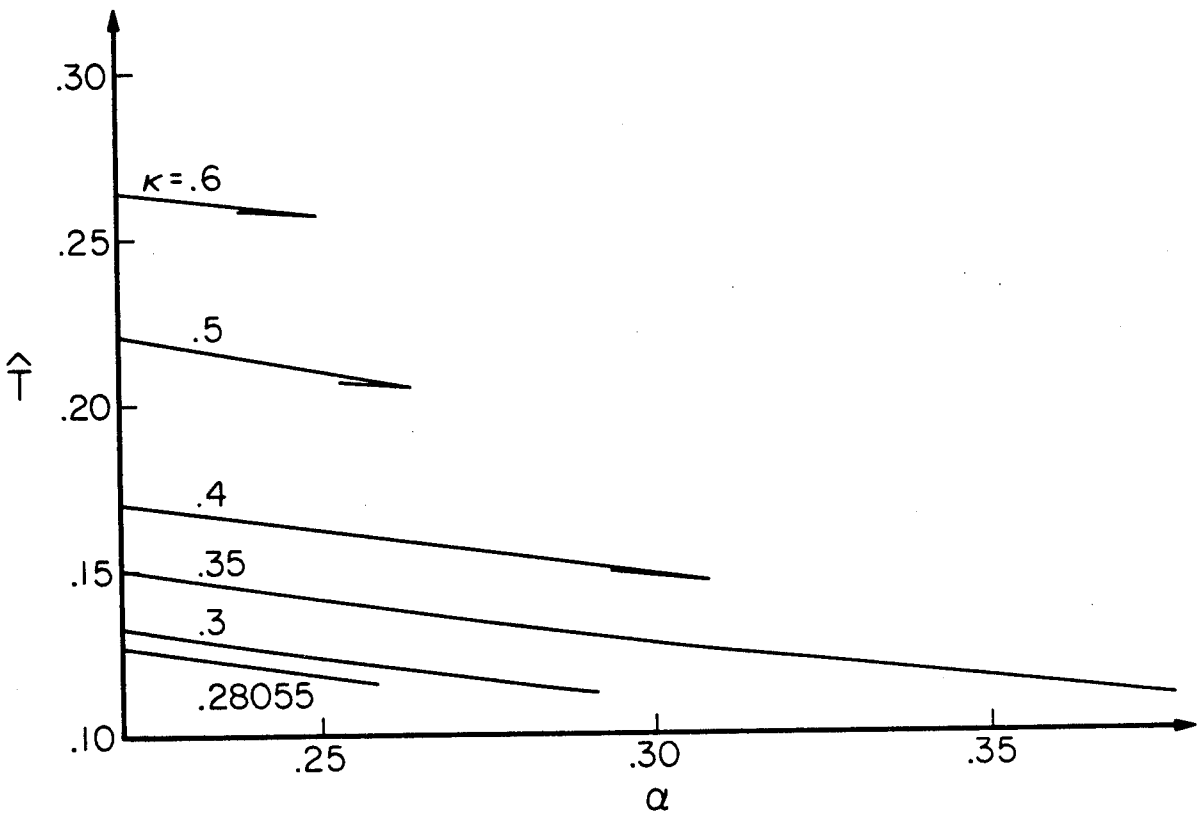


Figure 5. Expanded plot of kinetic energy $\hat{T}$ versus area $\alpha$, showing the non-uniqueness, maximum area, and minimum energy.

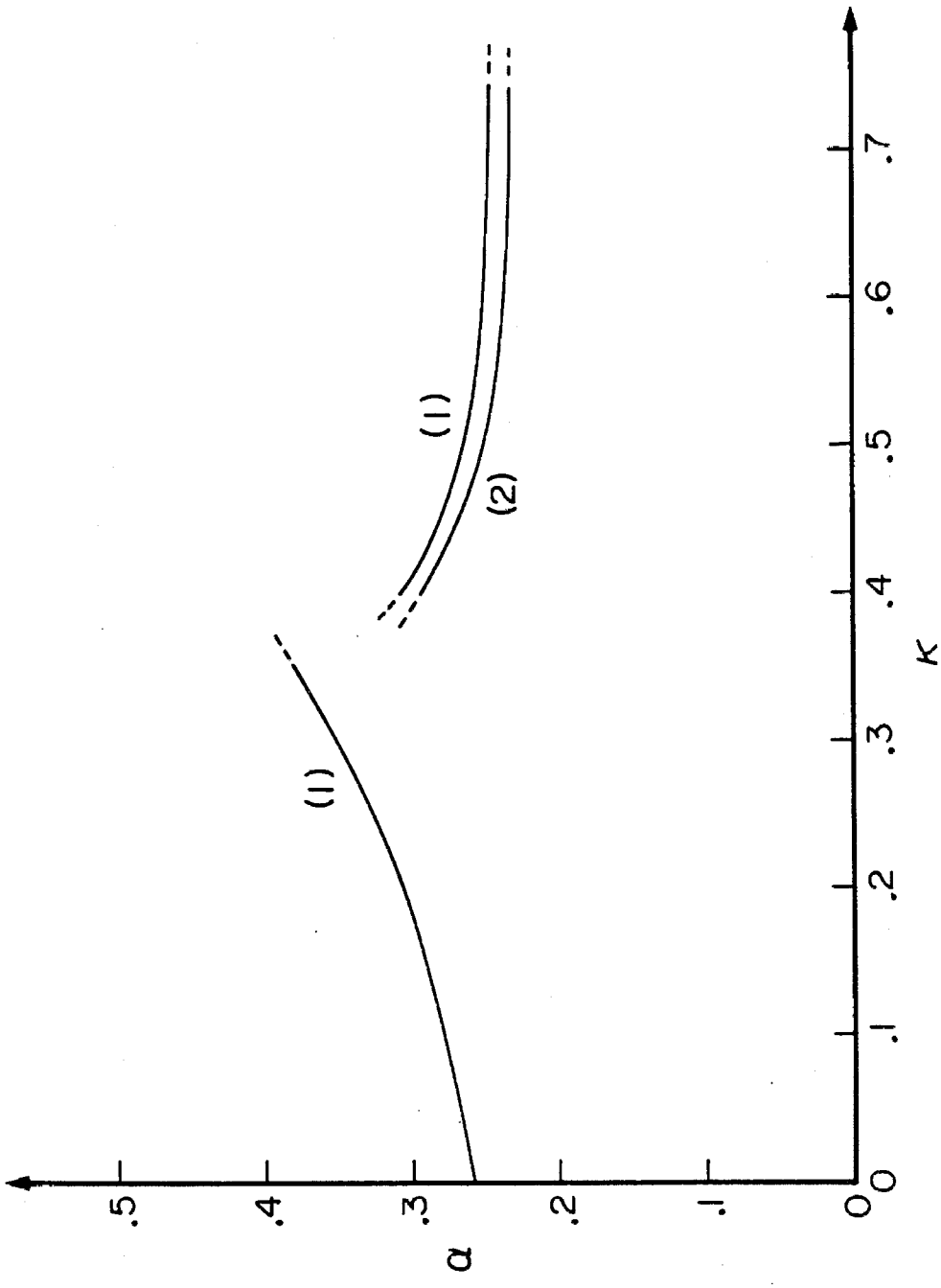


Figure 6. A plot of the area α versus spacing ratio κ plane. Curve 1 denotes the maximum area for a given spacing ratio. Between curves 1 and 2 there are two solutions for a given (κ,α).

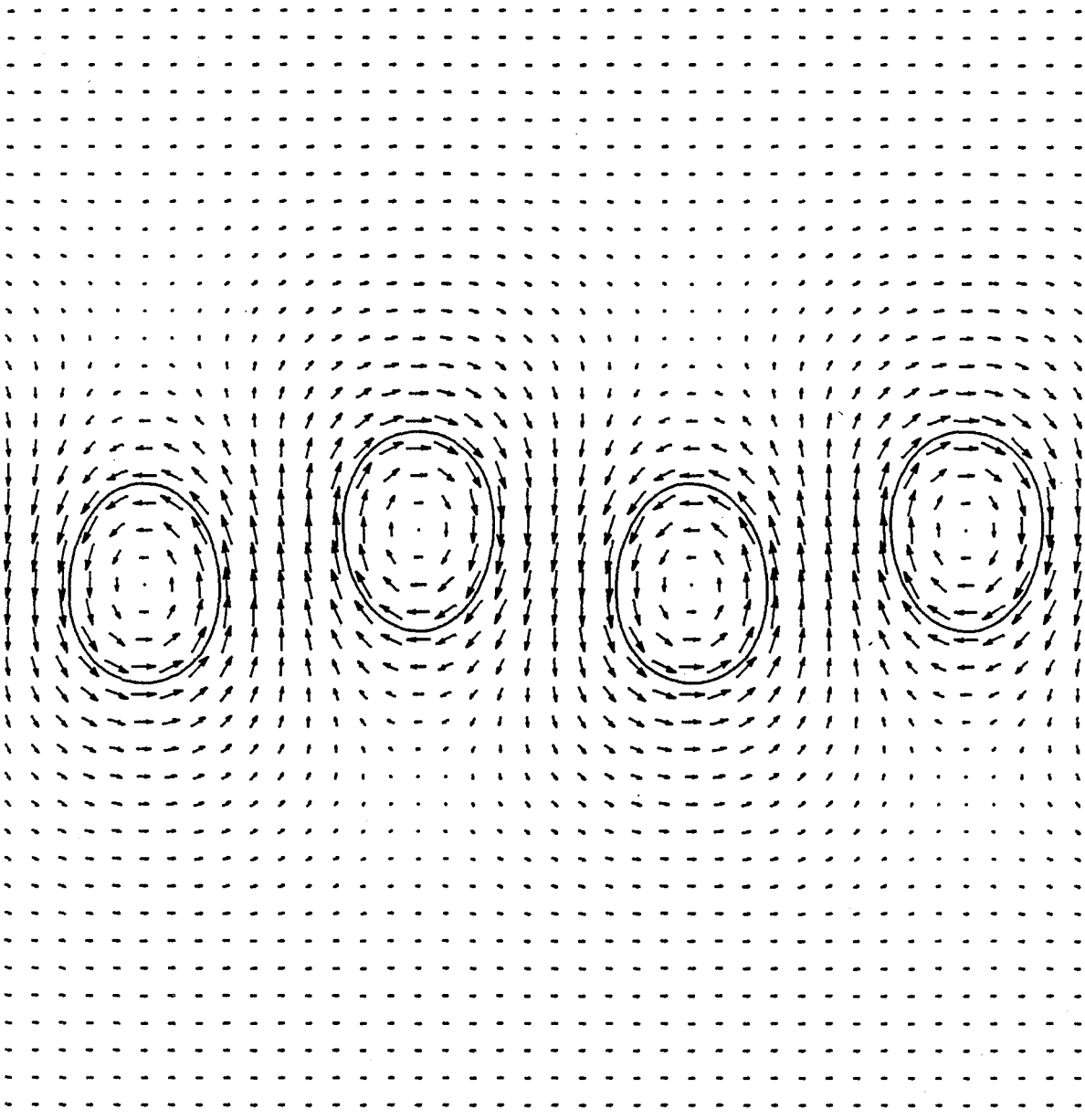

Figure 7. Plot of the vortex shapes and the velocity field for

$\kappa=.1$ $\alpha=.07948$

Arrow length is proportional to the speed of the fluid at midpoint.

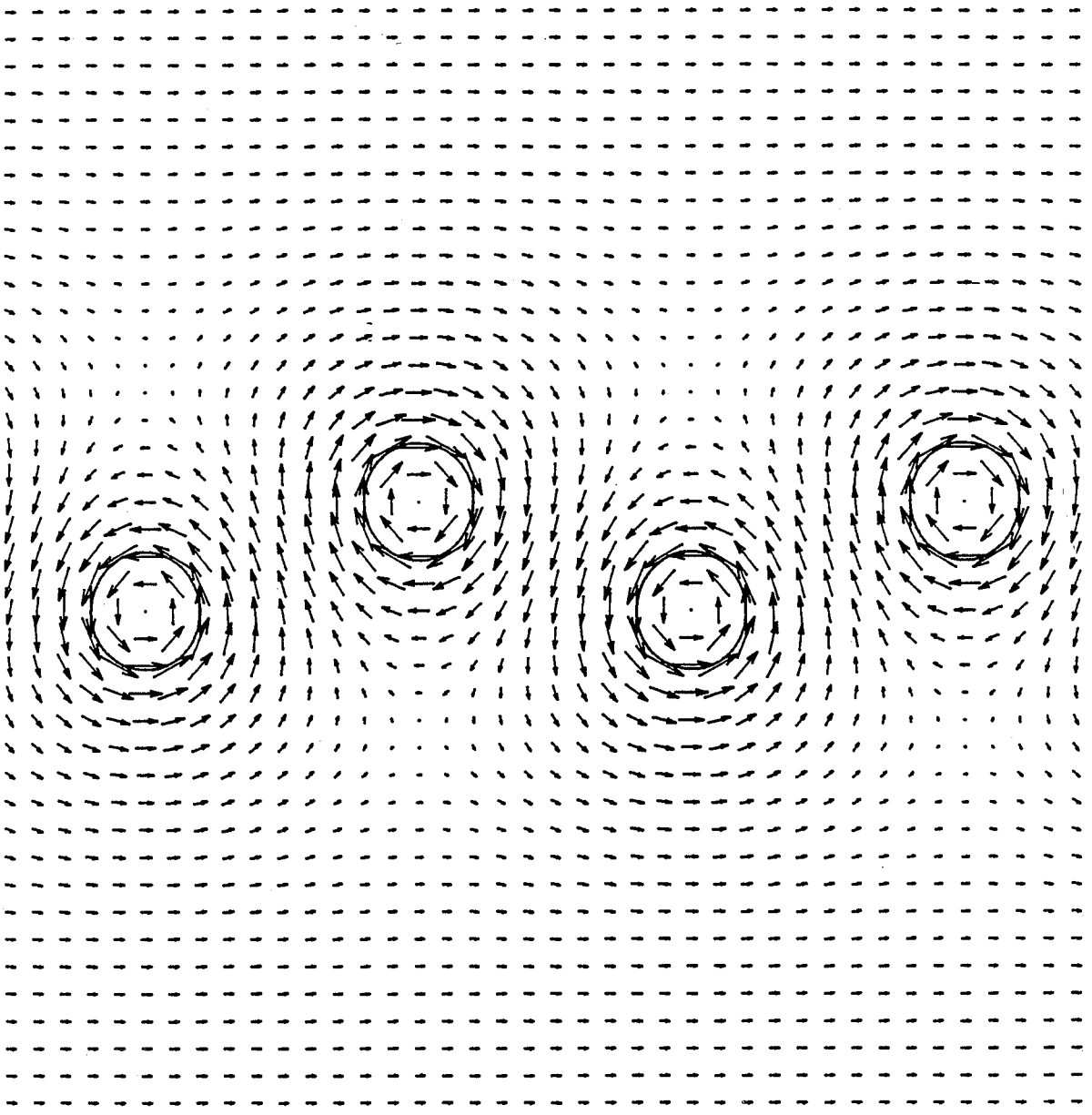

Figure 8. Plot of the vortex shapes and the velocity field for

$\kappa$=.2 $\alpha$=.03391

Arrow length is proportional to the speed of the fluid at midpoint.

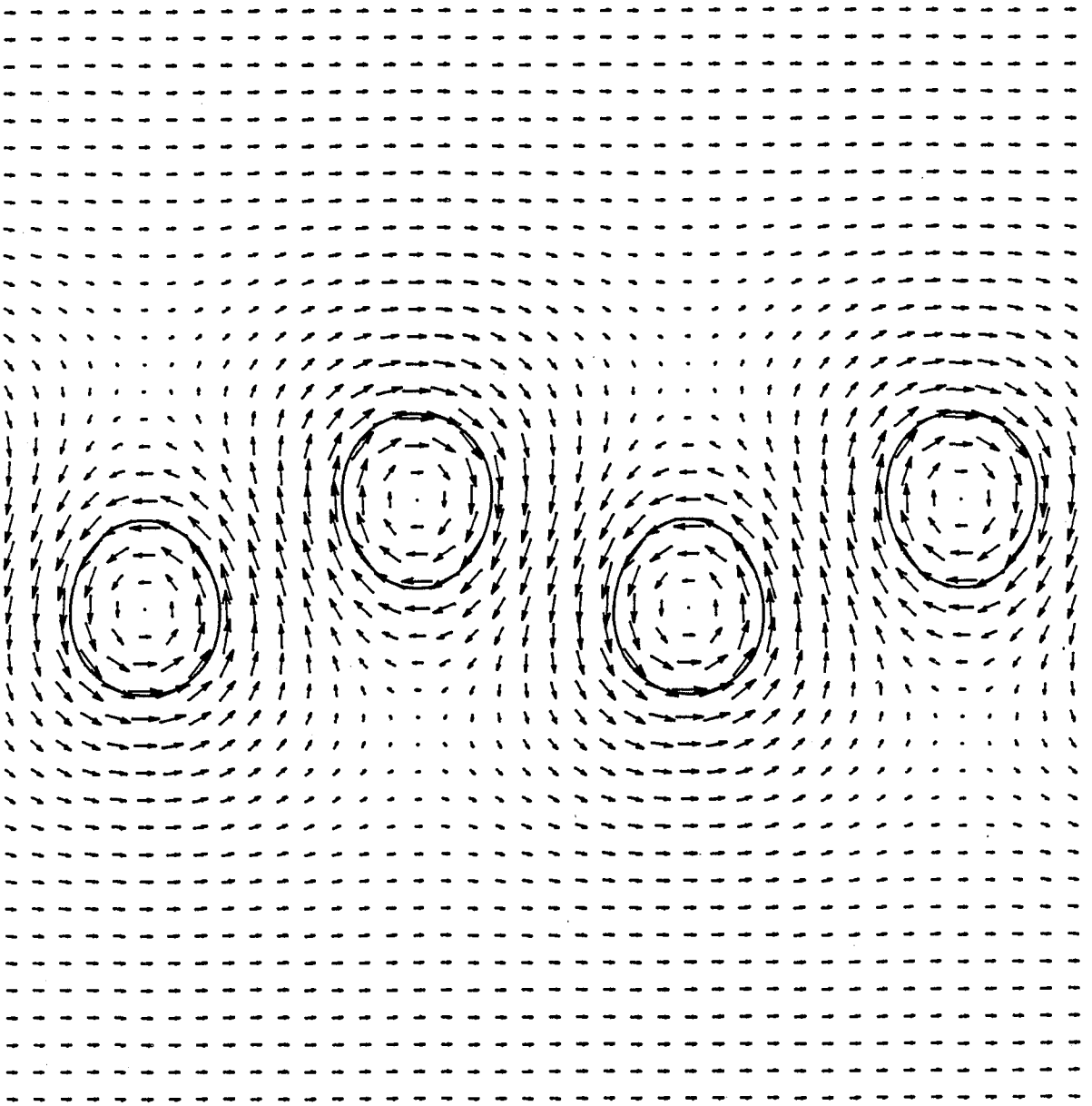

Figure 9. Plot of the vortex shapes and the velocity field for

$\kappa=.2$ $\alpha=.06963$

Arrow length is proportional to the speed of the fluid at midpoint.

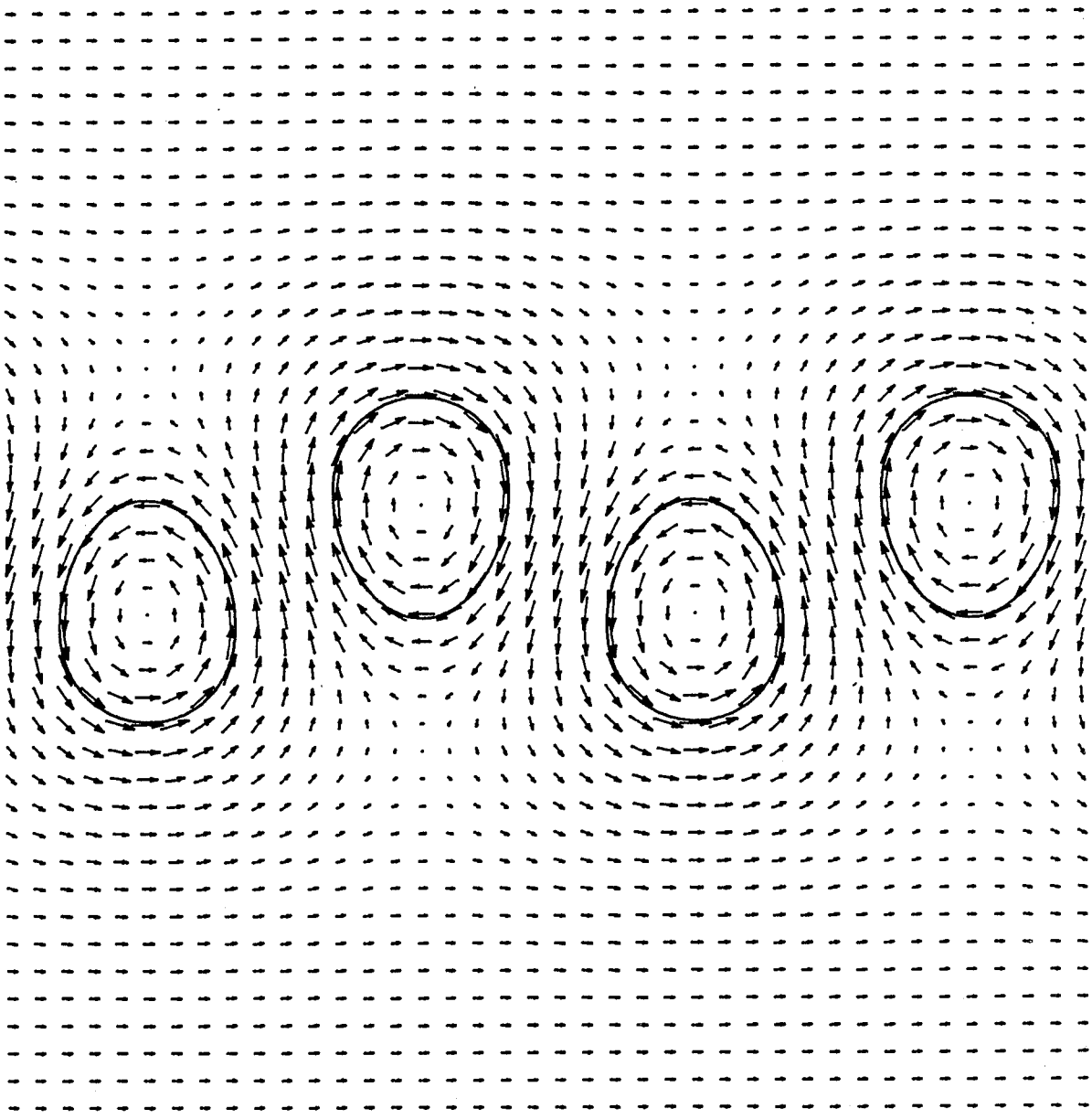

Figure 10. Plot of the vortex shapes and the velocity field for

$\kappa=.2$ $\alpha=.1019$

Arrow length is proportional to the speed of the fluid at midpoint.

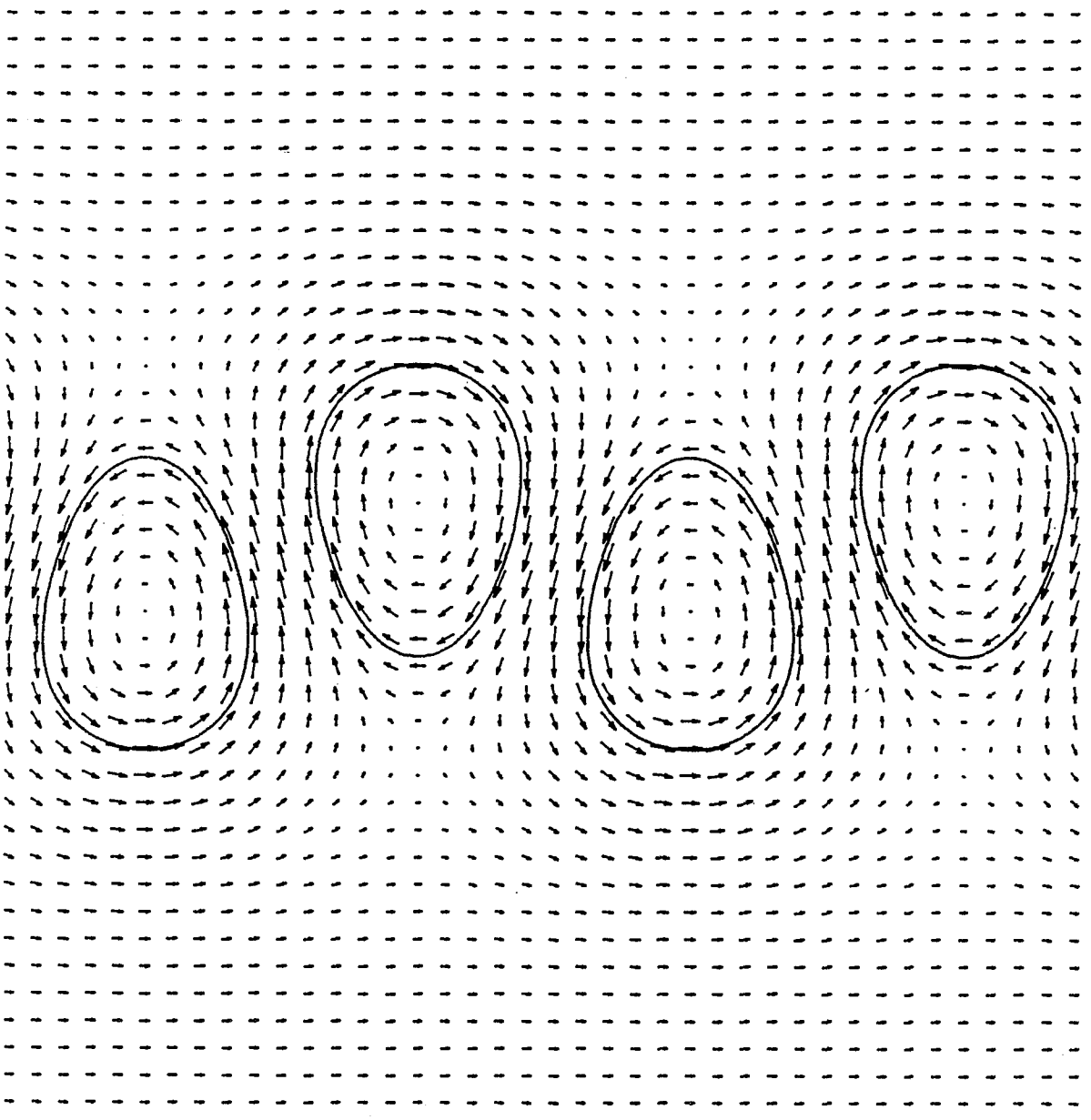

Figure 11. Plot of the vortex shapes and the velocity field for

$\kappa=.2$ $\alpha=.1566$

Arrow length is proportional to the speed of the fluid at midpoint.

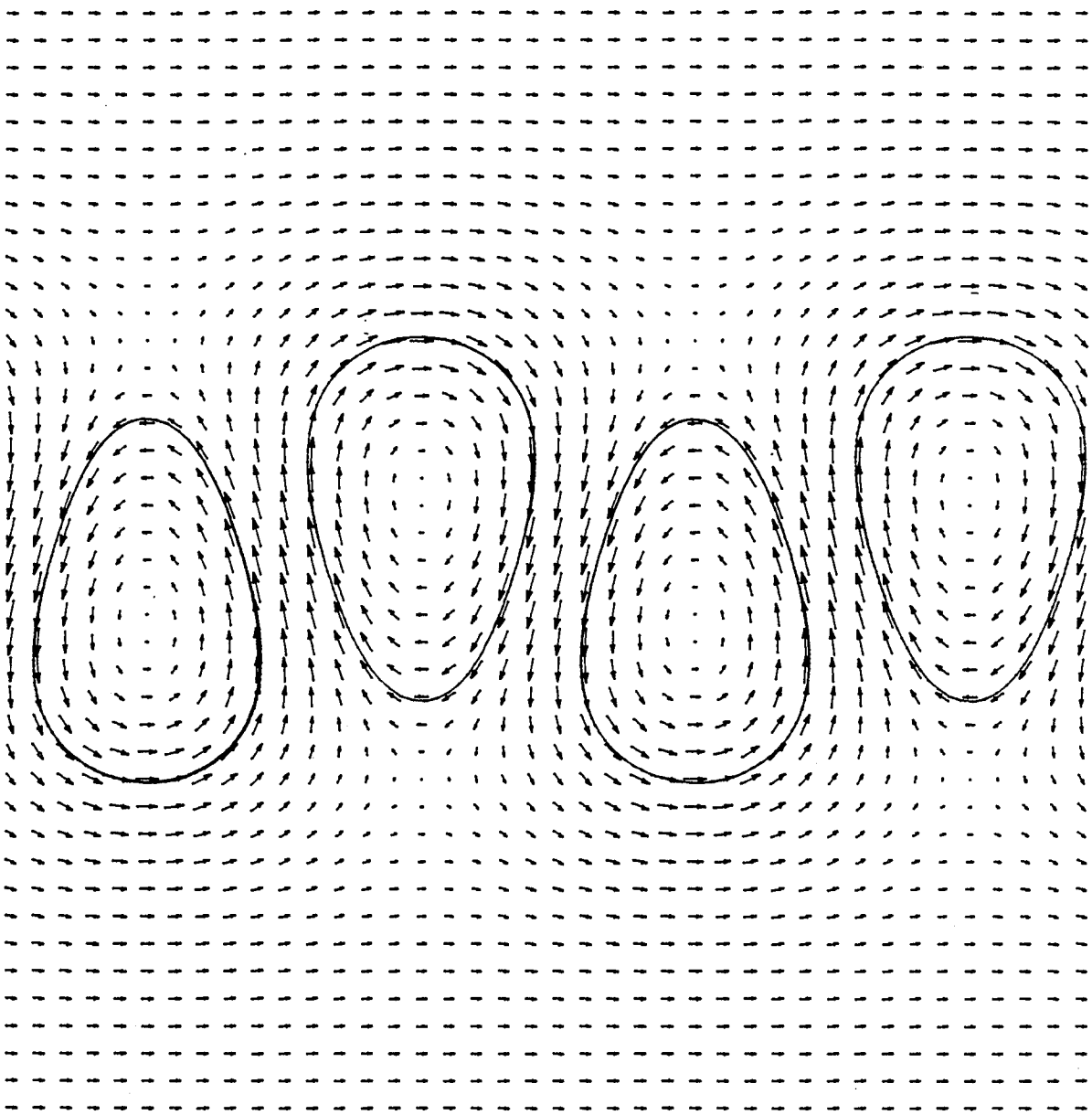

Figure 12. Plot of the vortex shapes and the velocity field for

$\kappa=.2$ $\alpha=.2102$

Arrow length is proportional to the speed of the fluid at midpoint.

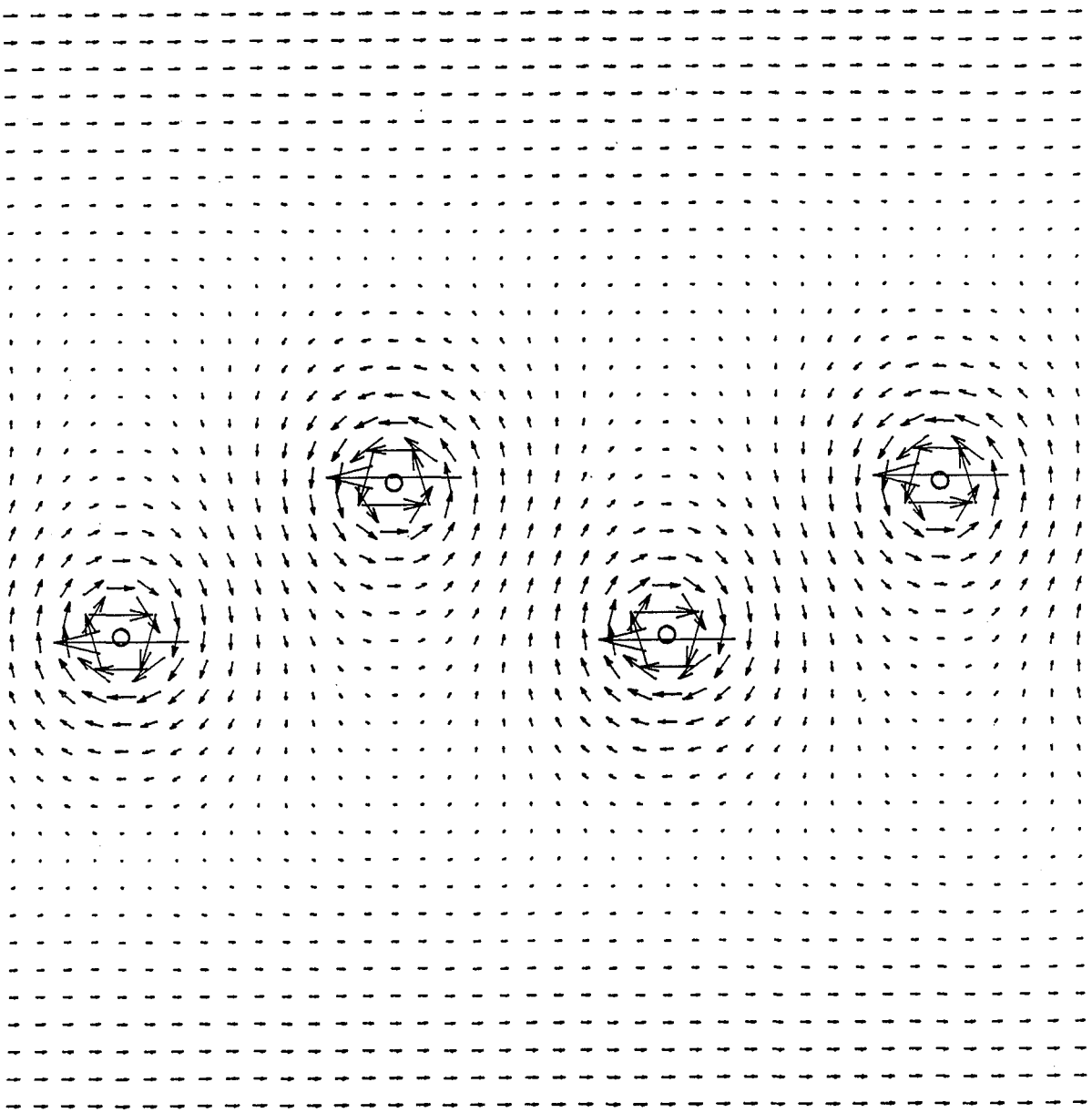

Figure 13. Plot of the vortex shapes and the velocity field for

$\kappa$=.28055 $\alpha$=.0007063

Arrow length is proportional to the speed of the fluid at midpoint.

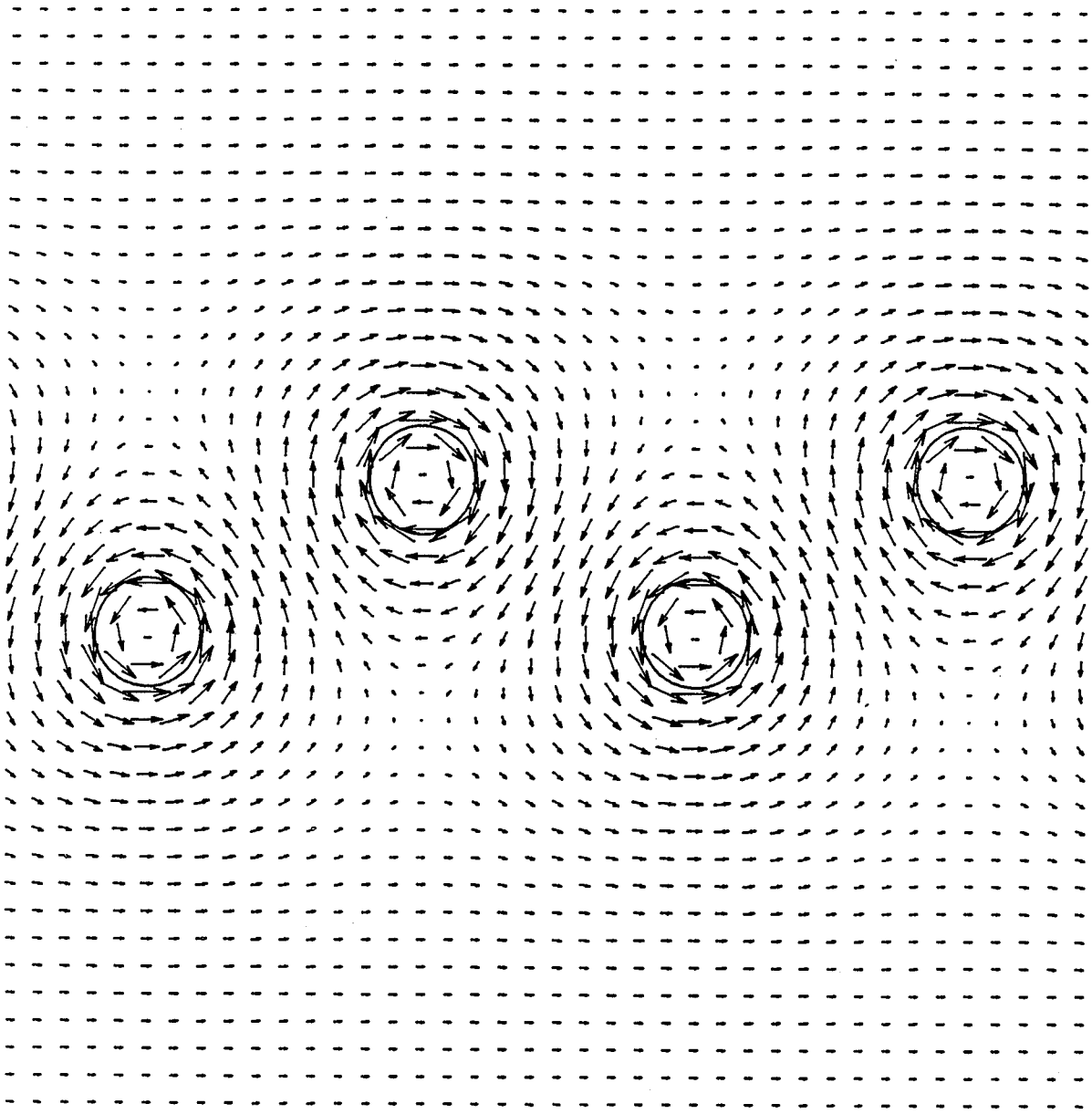

Figure 14. Plot of the vortex shapes and the velocity field for

$\kappa$=.28055 $\alpha$=.03011

Arrow length is proportional to the speed of the fluid at midpoint.

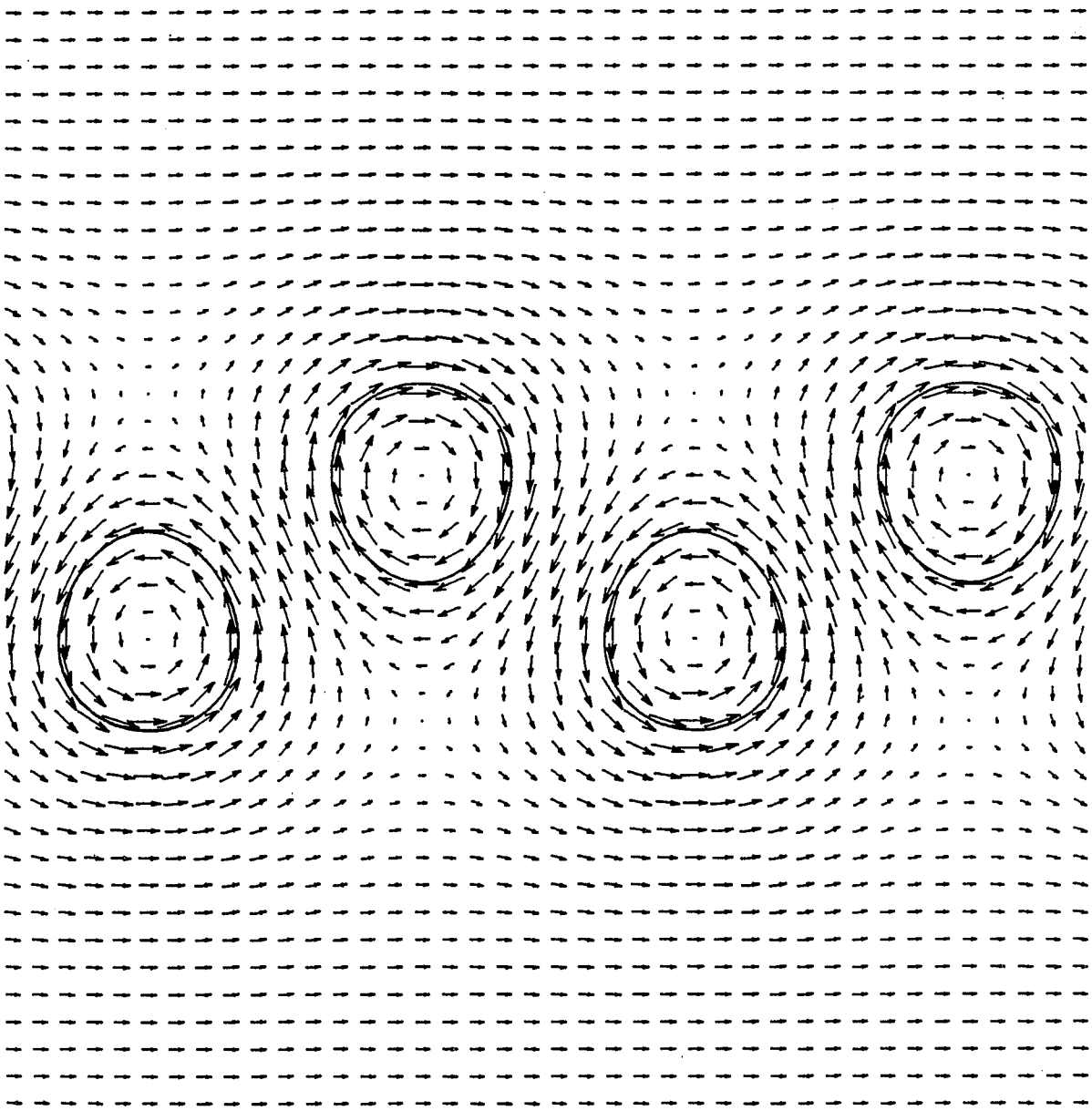

Figure 15. Plot of the vortex shapes and the velocity field for

$\kappa$=.28055 $\alpha$=.09382

Arrow length is proportional to the speed of the fluid at midpoint.

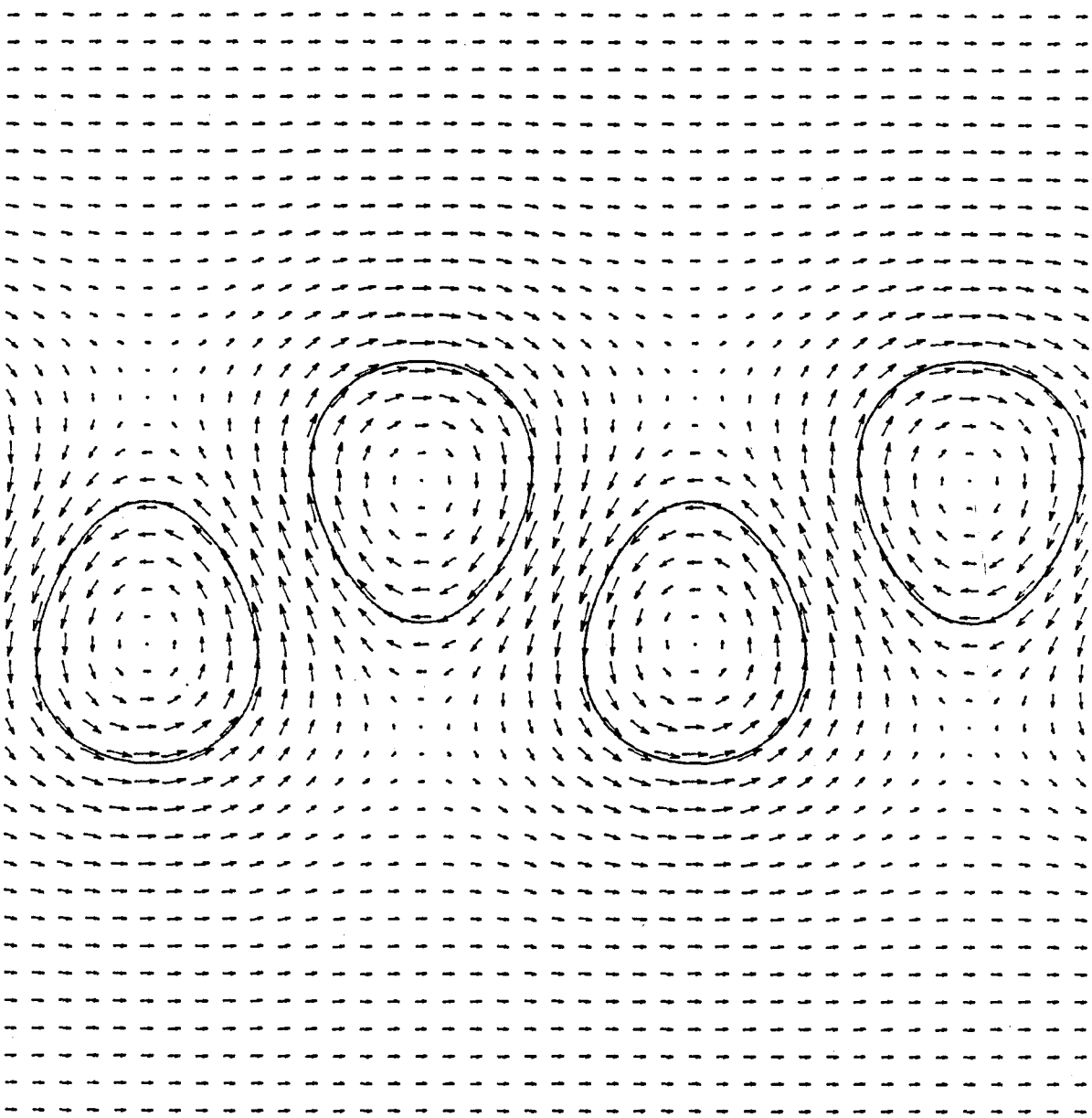

Figure 16. Plot of the vortex shapes and the velocity field for

$\kappa$=.28055 $\alpha$=.1485

Arrow length is proportional to the speed of the fluid at midpoint.

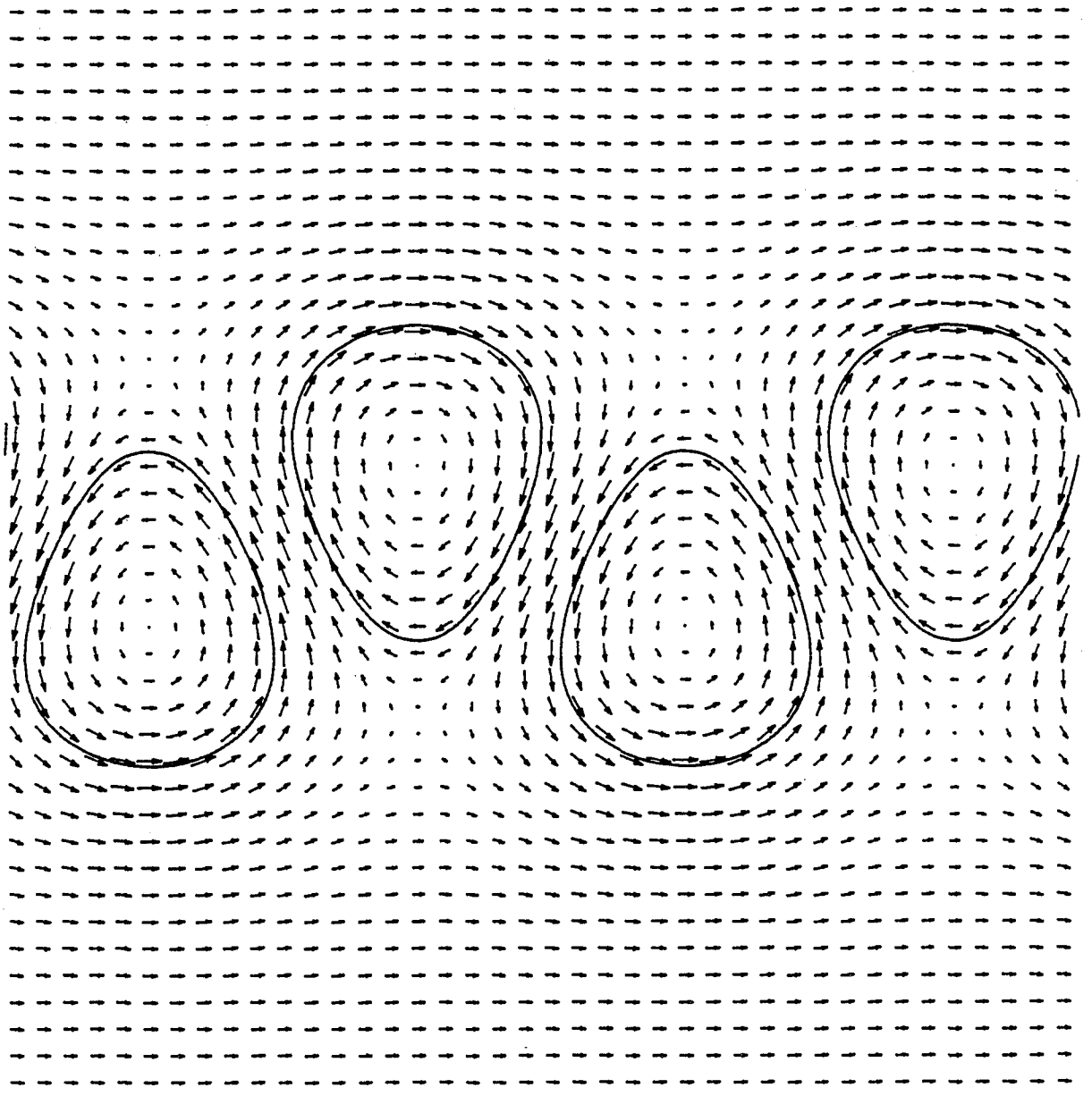

Figure 17. Plot of the vortex shapes and the velocity field for

$\kappa = .28055$ $\alpha = .2047$

Arrow length is proportional to the speed of the fluid at midpoint.

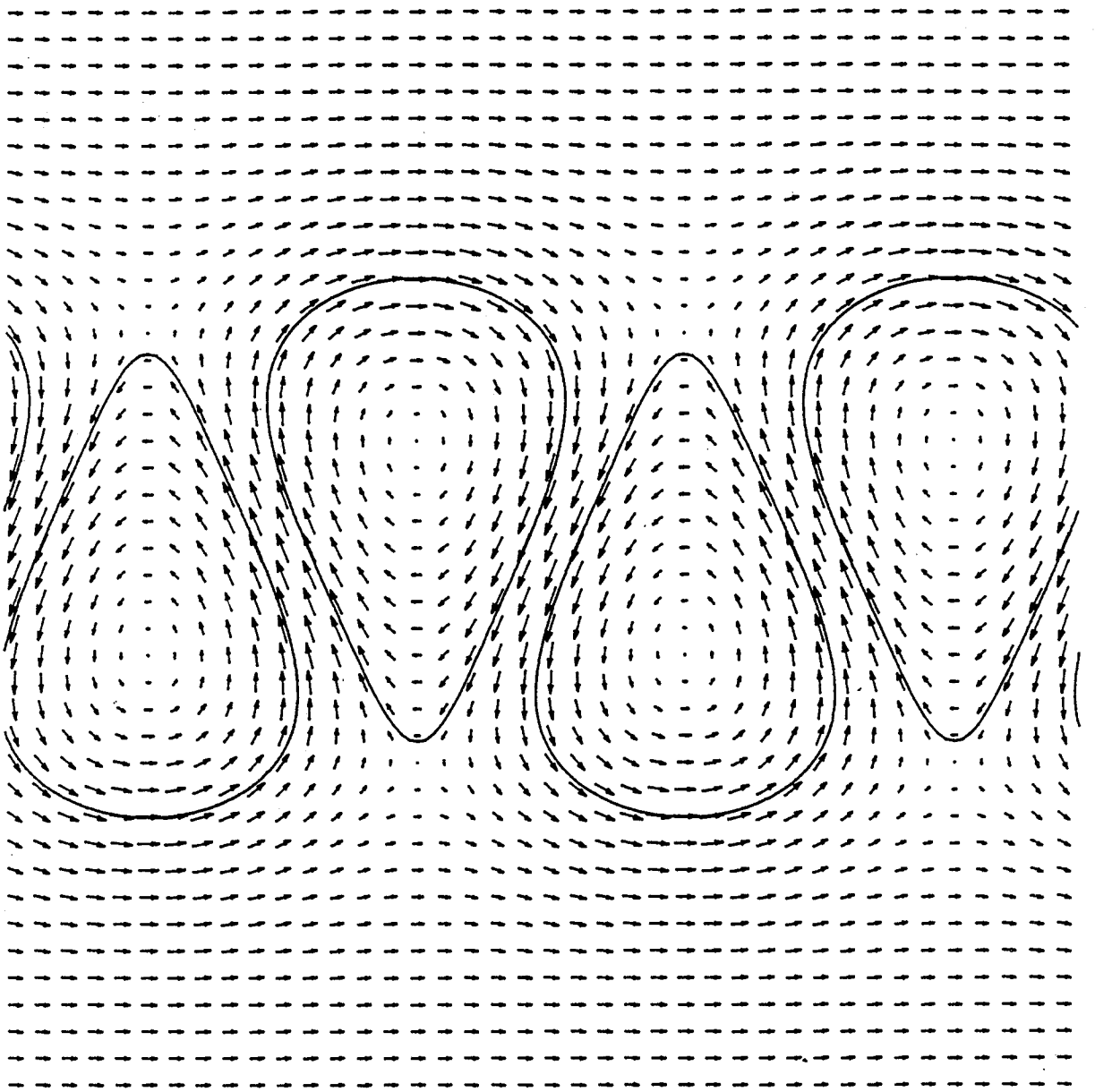

Figure 18. Plot of the vortex shapes and the velocity field for

$\kappa$=.28055 $\alpha$=.3247

Arrow length is proportional to the speed of the fluid at midpoint.

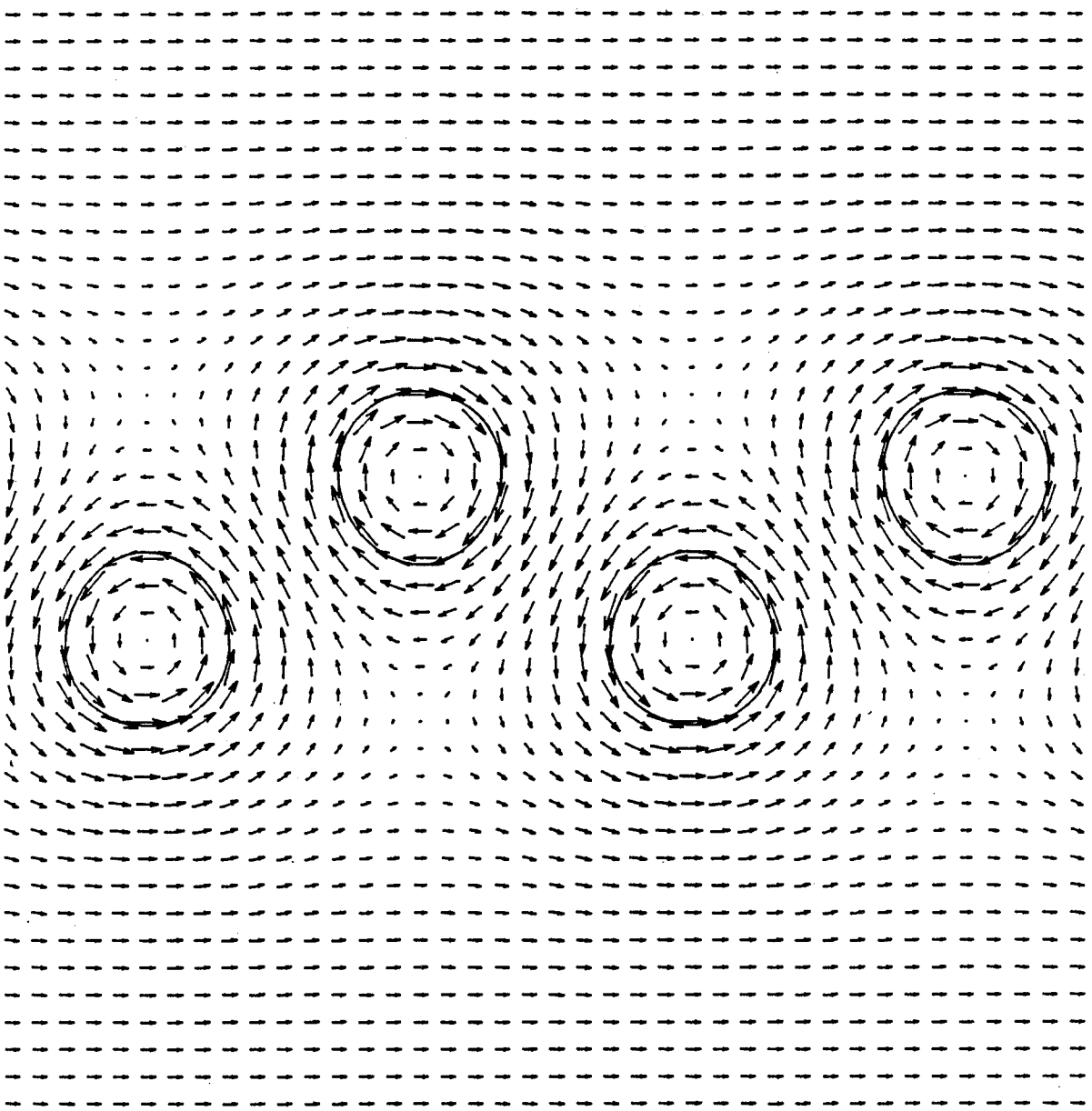

Figure 19. Plot of the vortex shapes and the velocity field for

$\kappa$=.3 $\alpha$=.07484

Arrow length is proportional to the speed of the fluid at midpoint.

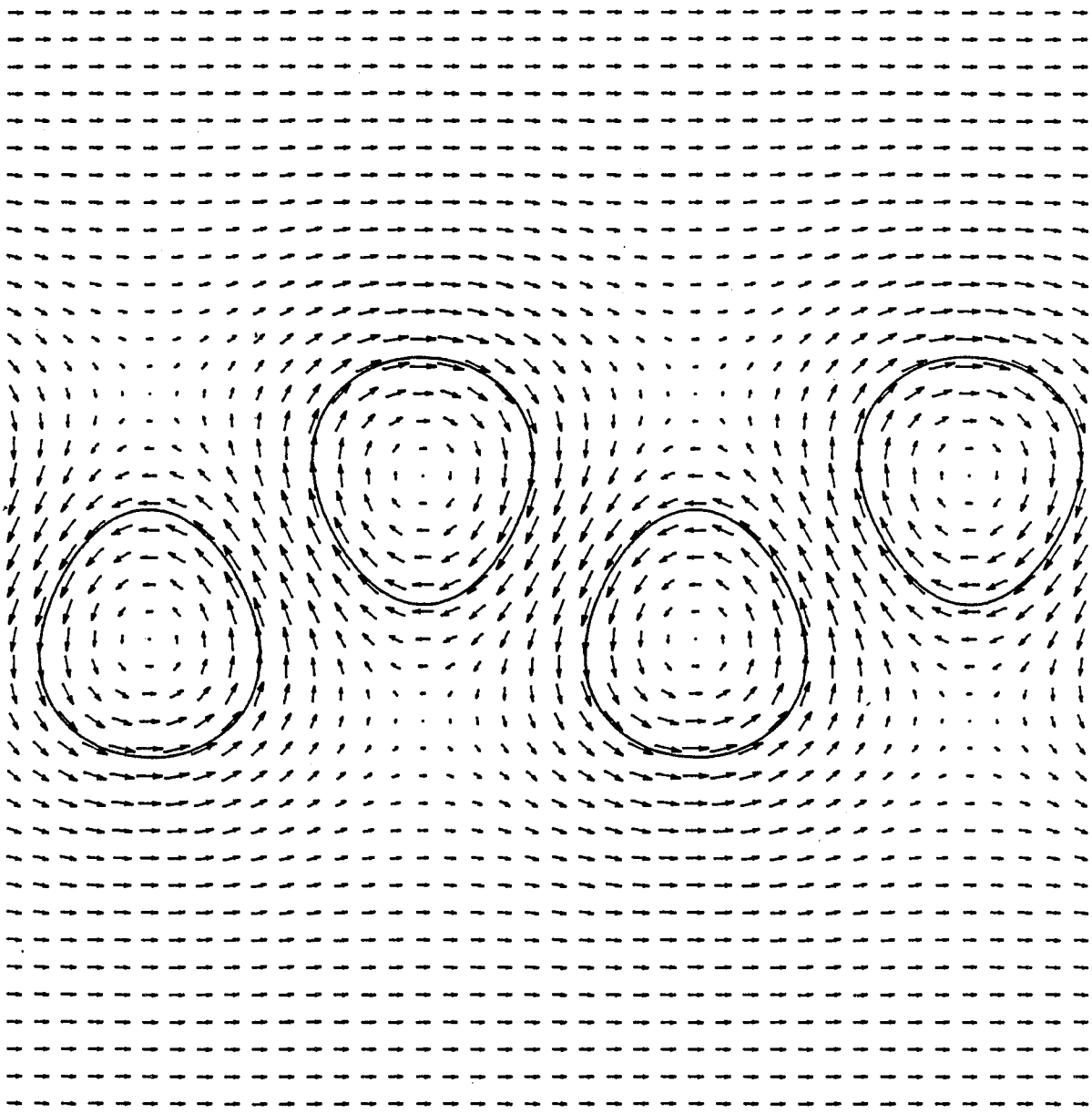

Figure 20. Plot of the vortex shapes and the velocity field for

$\kappa = .3$ $\alpha = .1409$

Arrow length is proportional to the speed of the fluid at midpoint.

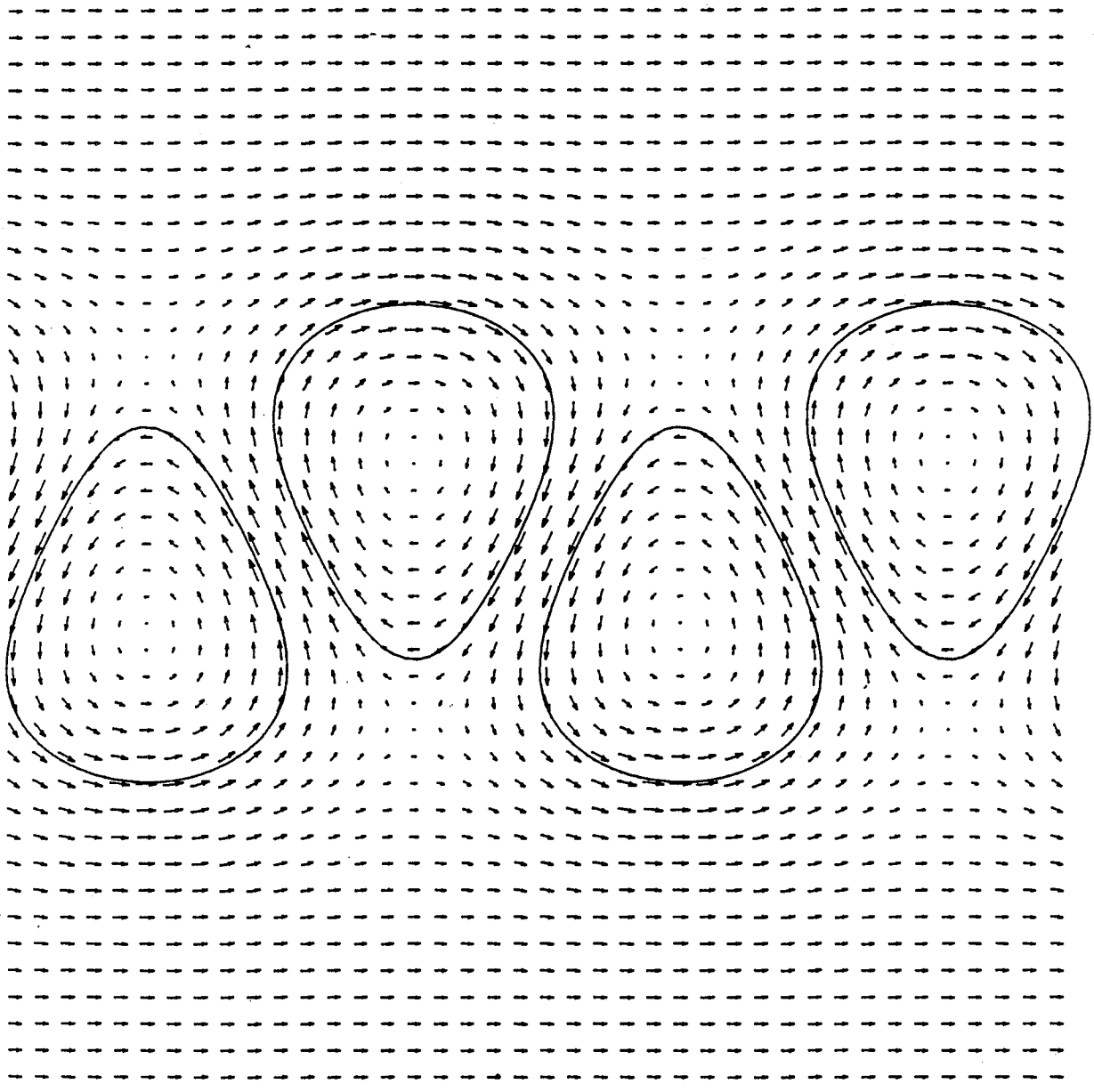

Figure 21. Plot of the vortex shapes and the velocity field for

$\kappa$=.3 $\alpha$=.2541

Arrow length is proportional to the speed of the fluid at midpoint.

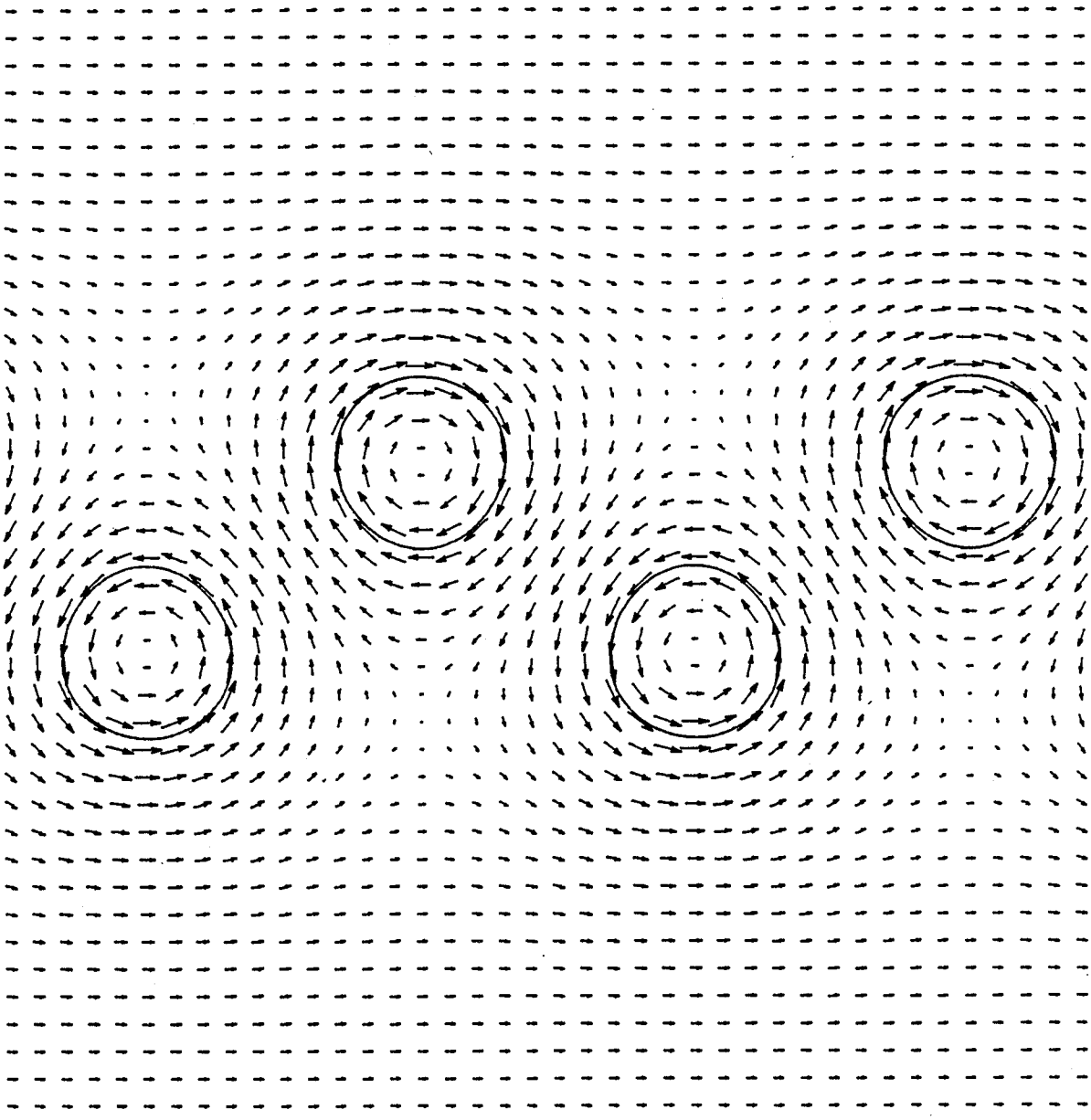

Figure 22. Plot of the vortex shapes and the velocity field for

$\kappa$=.35 $\alpha$=.07613

Arrow length is proportional to the speed of the fluid at midpoint.

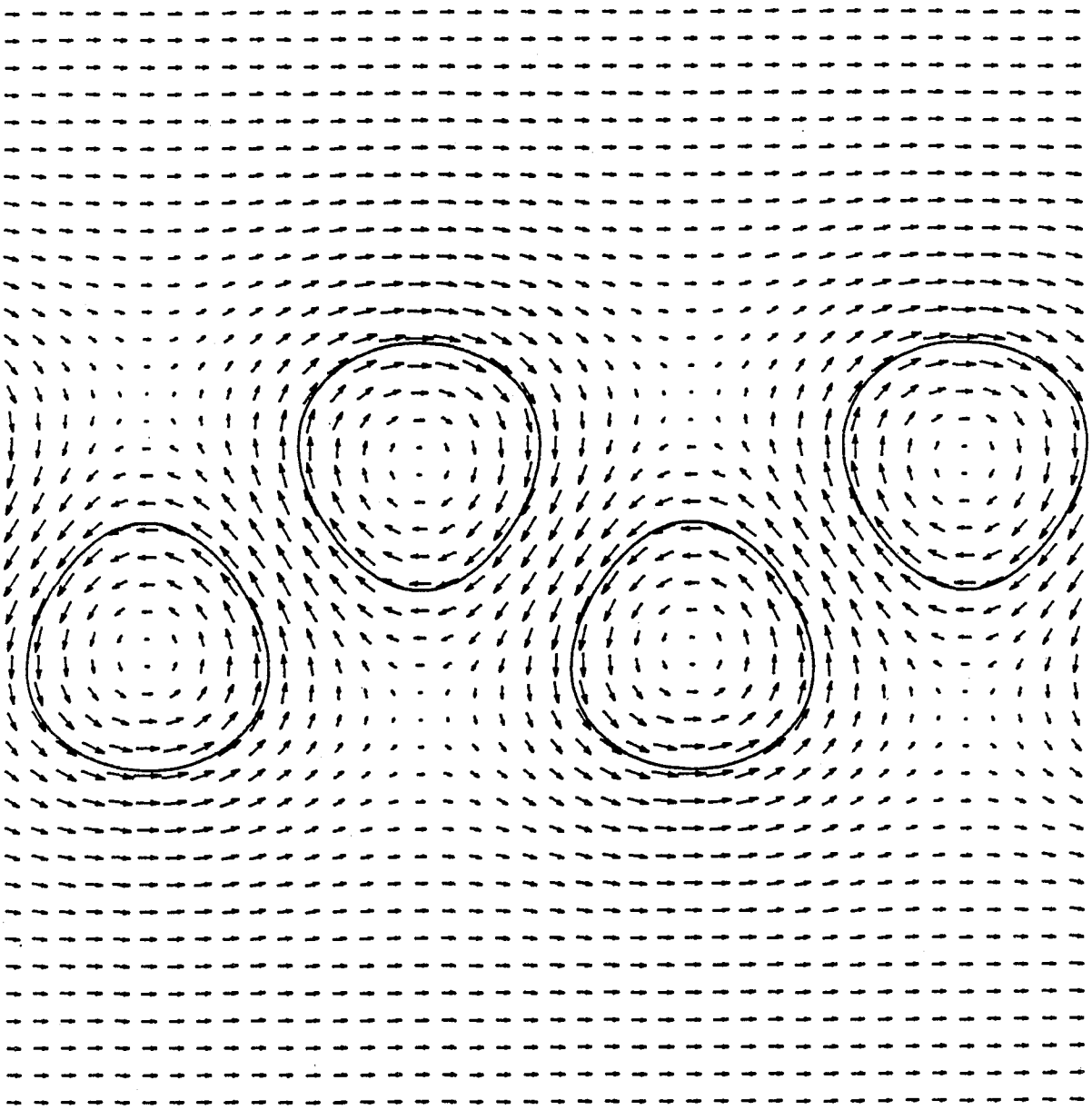

Figure 23. Plot of the vortex shapes and the velocity field for

$\kappa = .35$ $\alpha = .1543$

Arrow length is proportional to the speed of the fluid at midpoint.

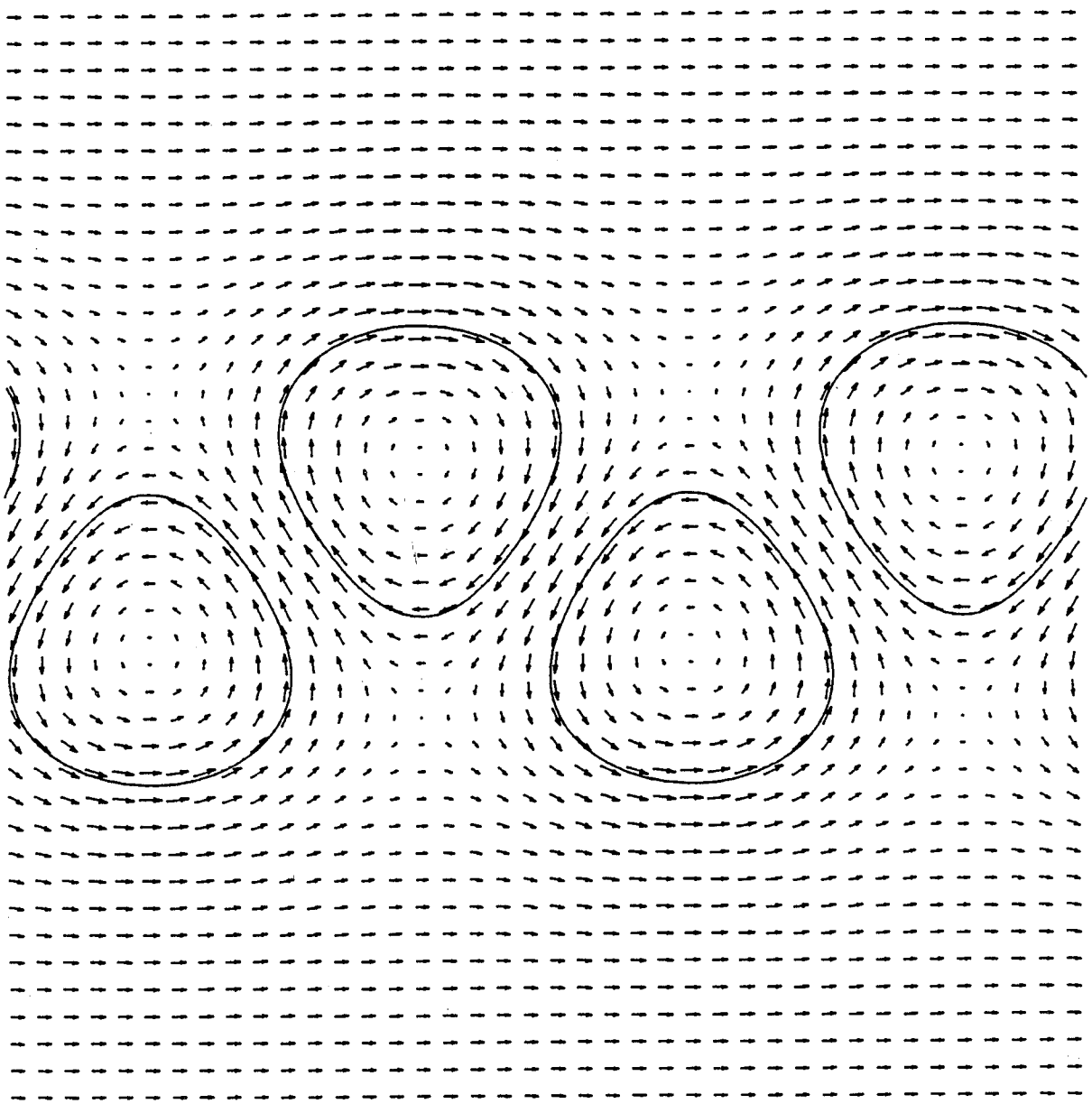

Figure 24. Plot of the vortex shapes and the velocity field for

$\kappa$=.35 $\alpha$=.2090

Arrow length is proportional to the speed of the fluid at midpoint.

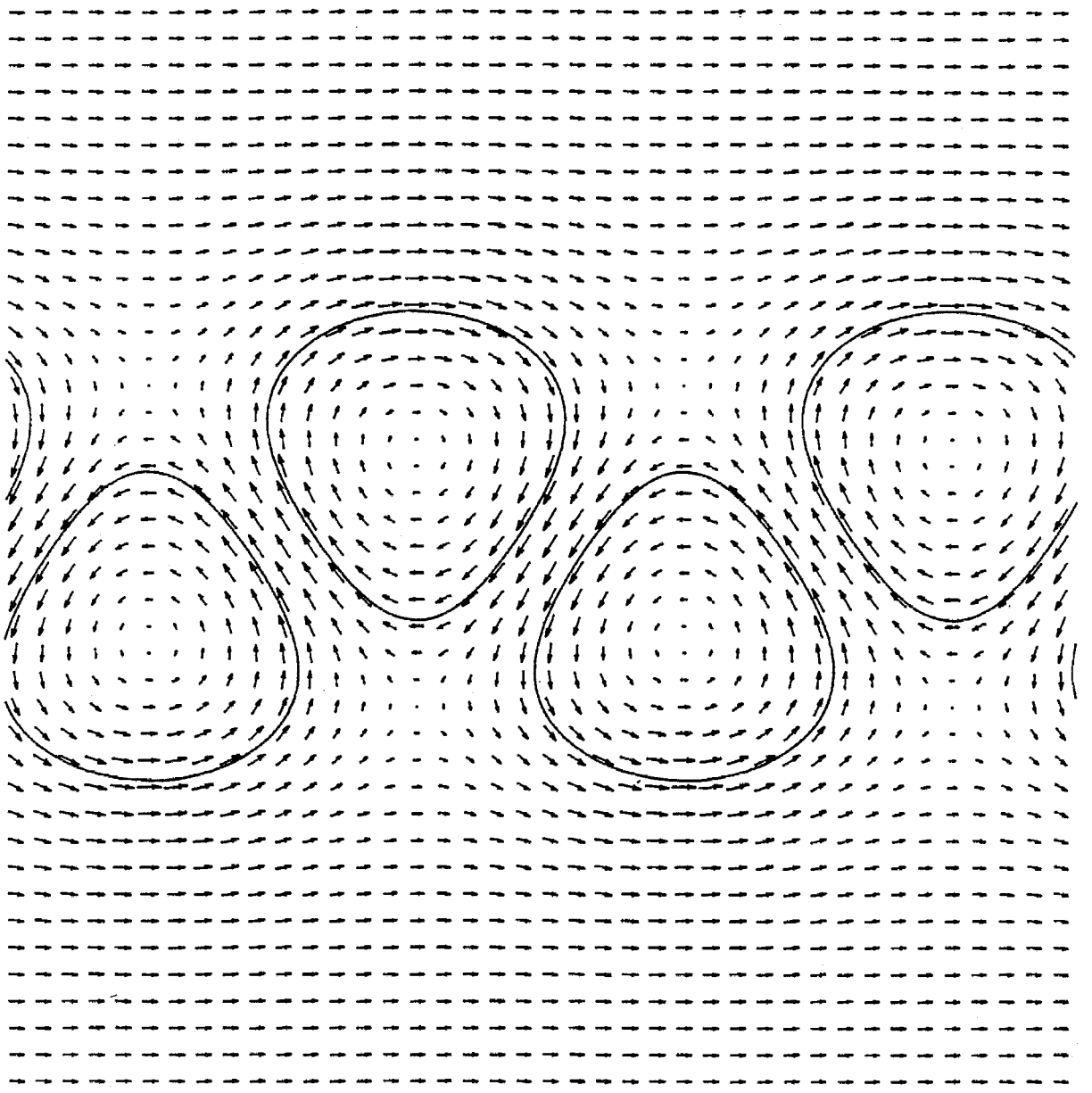

Figure 25. Plot of the vortex shapes and the velocity field for

$\kappa$=.35 $\alpha$=.2358

Arrow length is proportional to the speed of the fluid at midpoint.

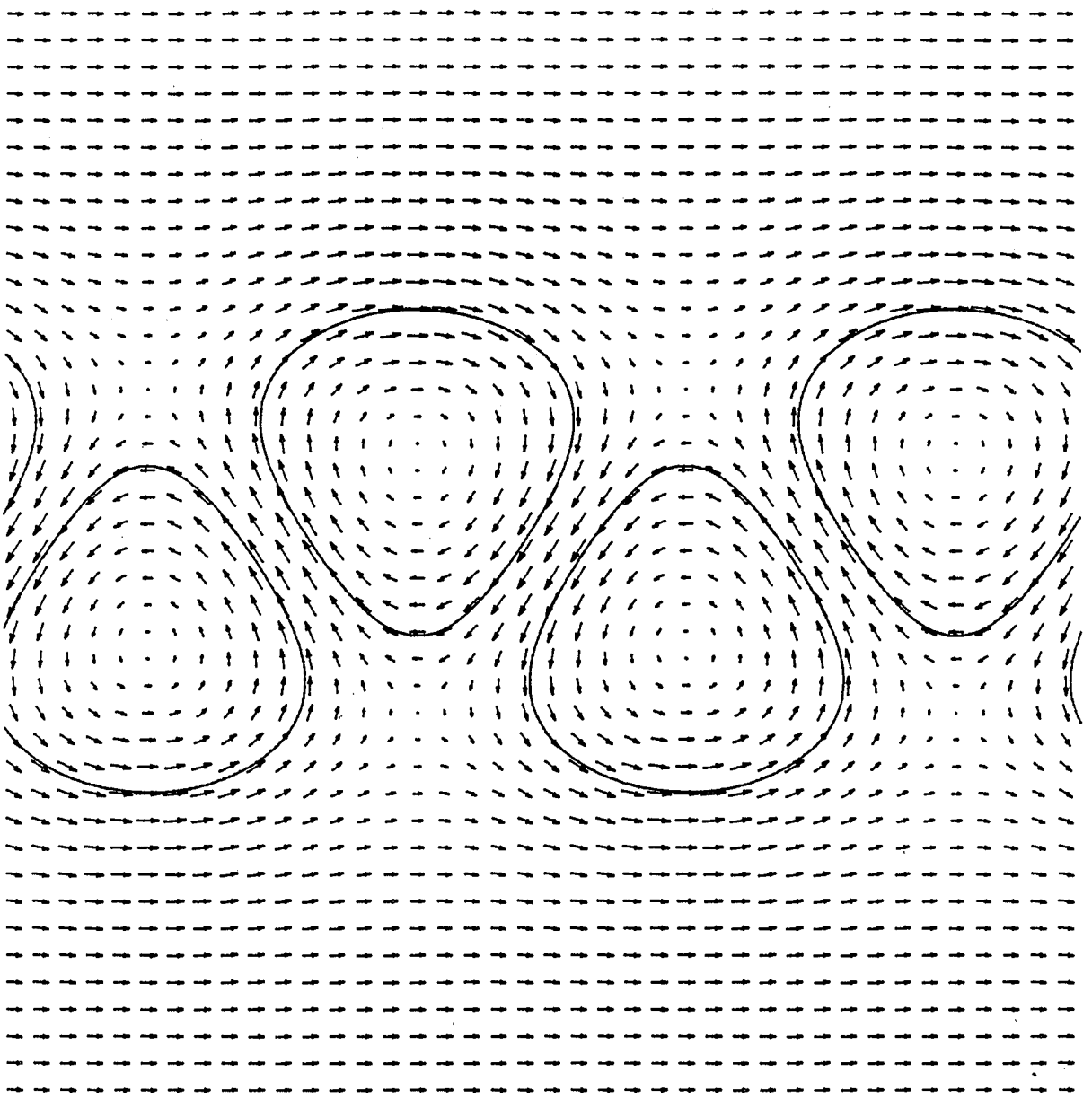

Figure 26. Plot of the vortex shapes and the velocity field for

$\kappa = .35$ $\alpha = .2551$

Arrow length is proportional to the speed of the fluid at midpoint.

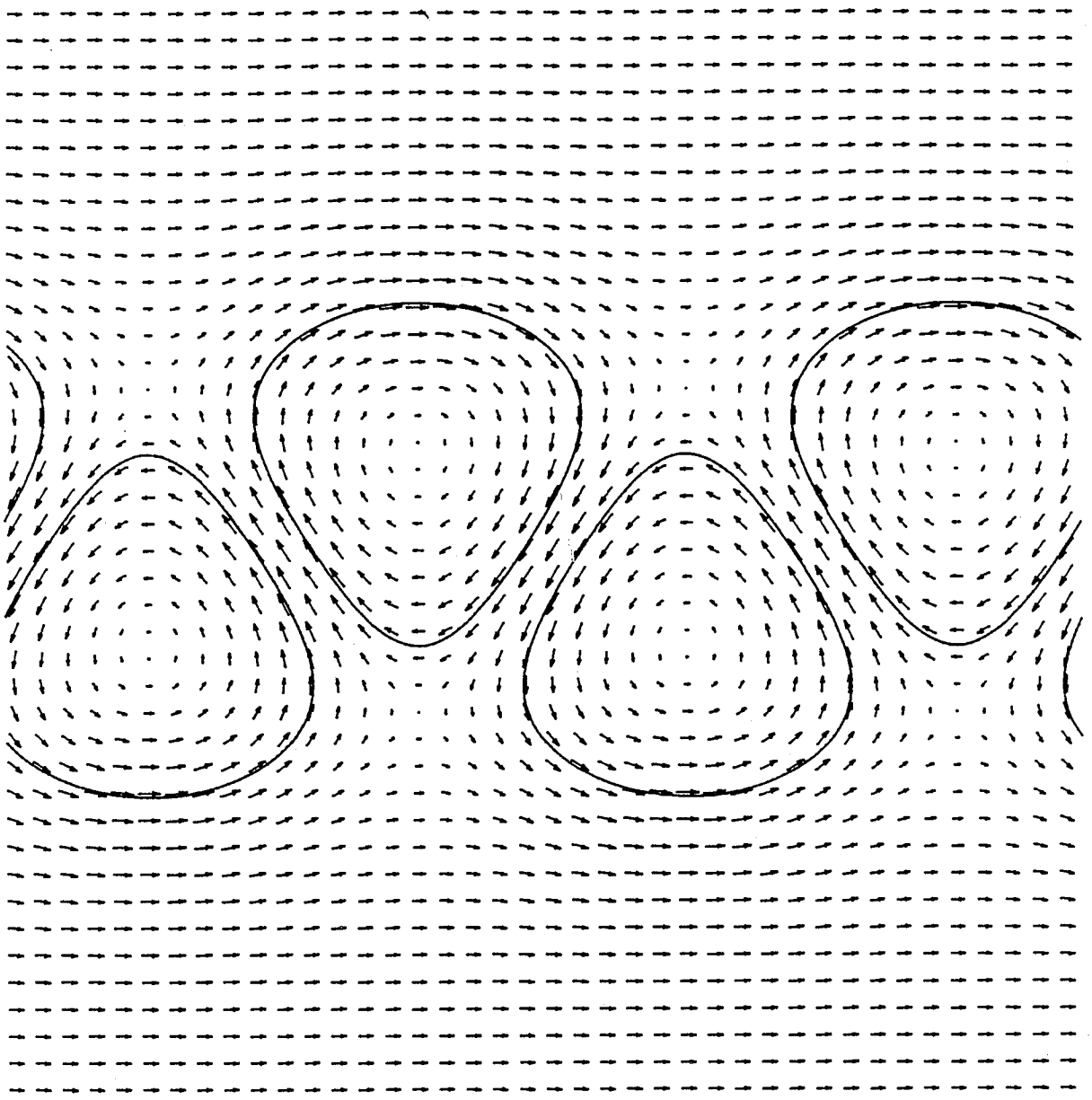

Figure 27. Plot of the vortex shapes and the velocity field for

$\kappa$=.35 $\alpha$=.2653

Arrow length is proportional to the speed of the fluid at midpoint.

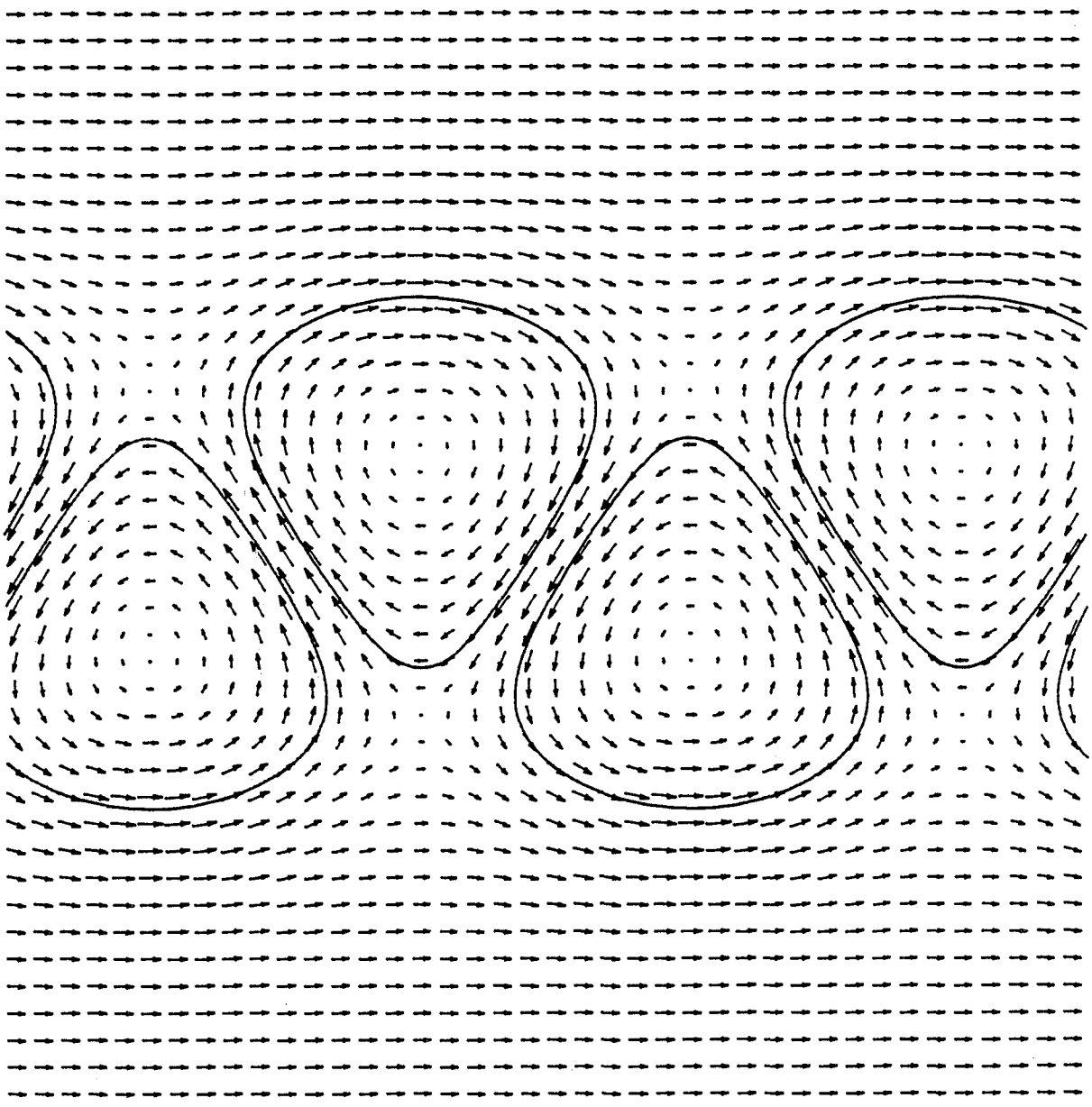

Figure 28. Plot of the vortex shapes and the velocity field for

$\kappa = .35$ $\alpha = .3100$

Arrow length is proportional to the speed of the fluid at midpoint.

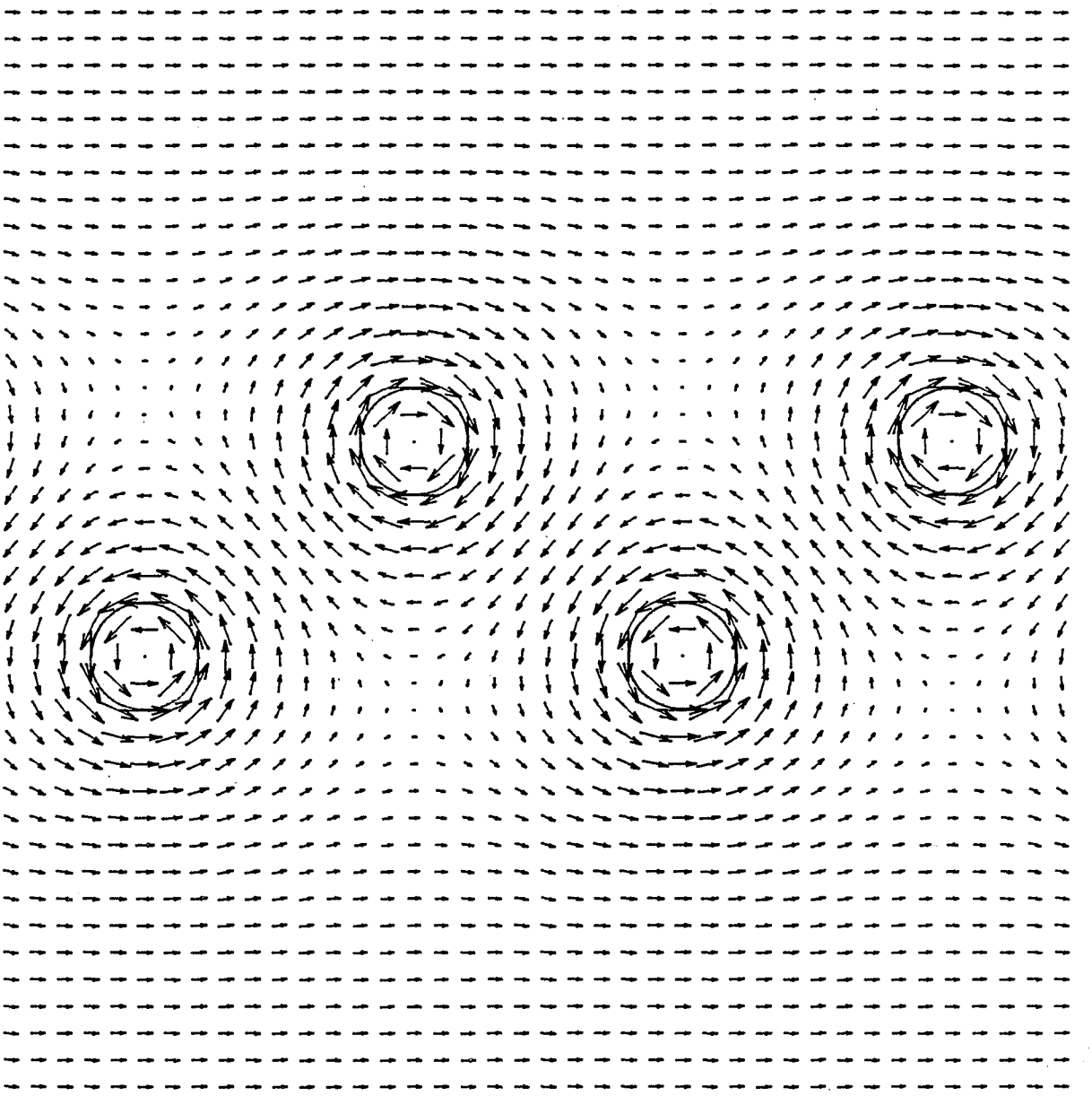

Figure 29. Plot of the vortex shapes and the velocity field for

$\kappa=.4$ $\alpha=.03105$

Arrow length is proportional to the speed of the fluid at midpoint.

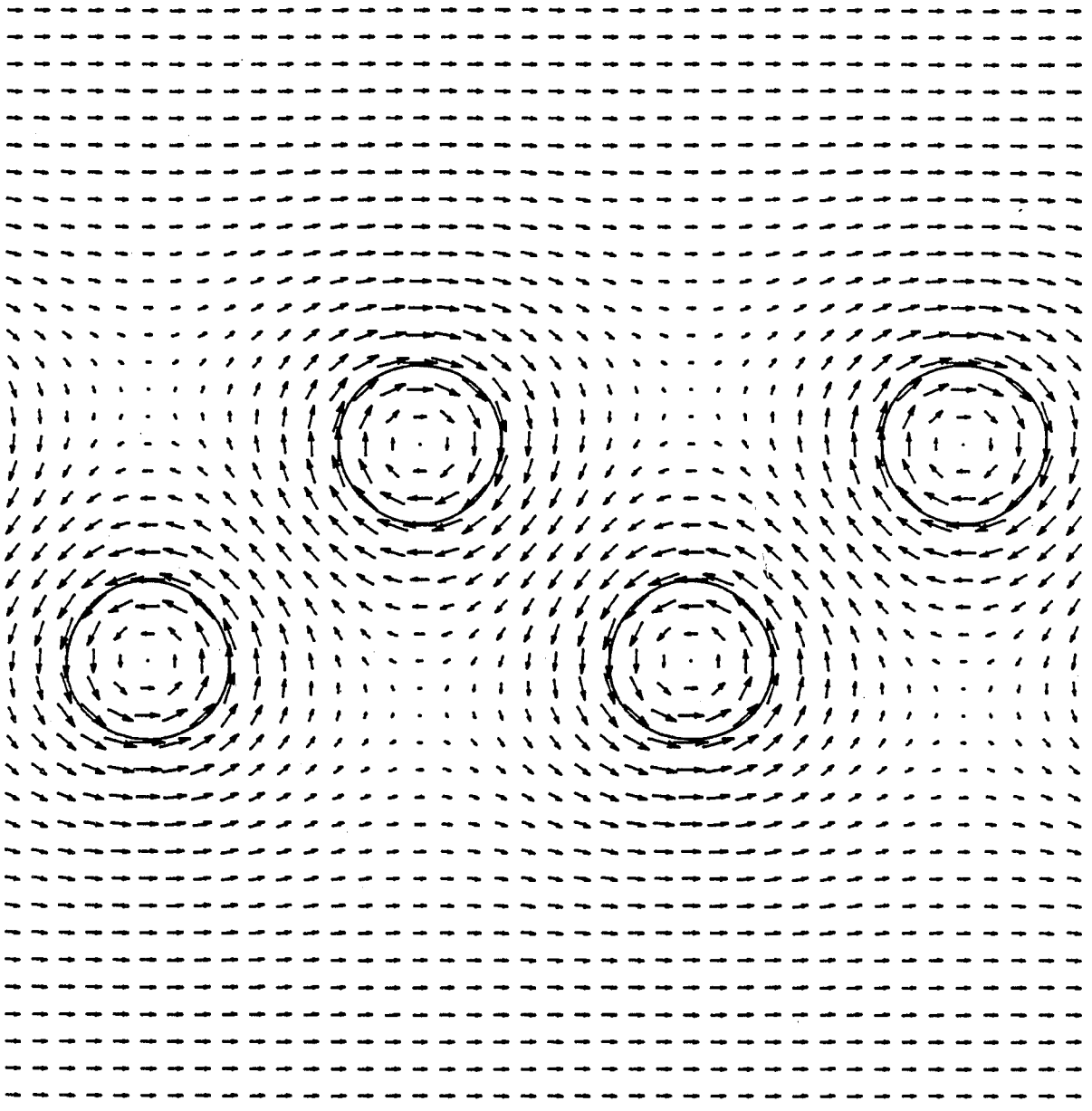

Figure 30. Plot of the vortex shapes and the velocity field for

$\kappa=.4$ $\alpha=.06869$

Arrow length is proportional to the speed of the fluid at midpoint.

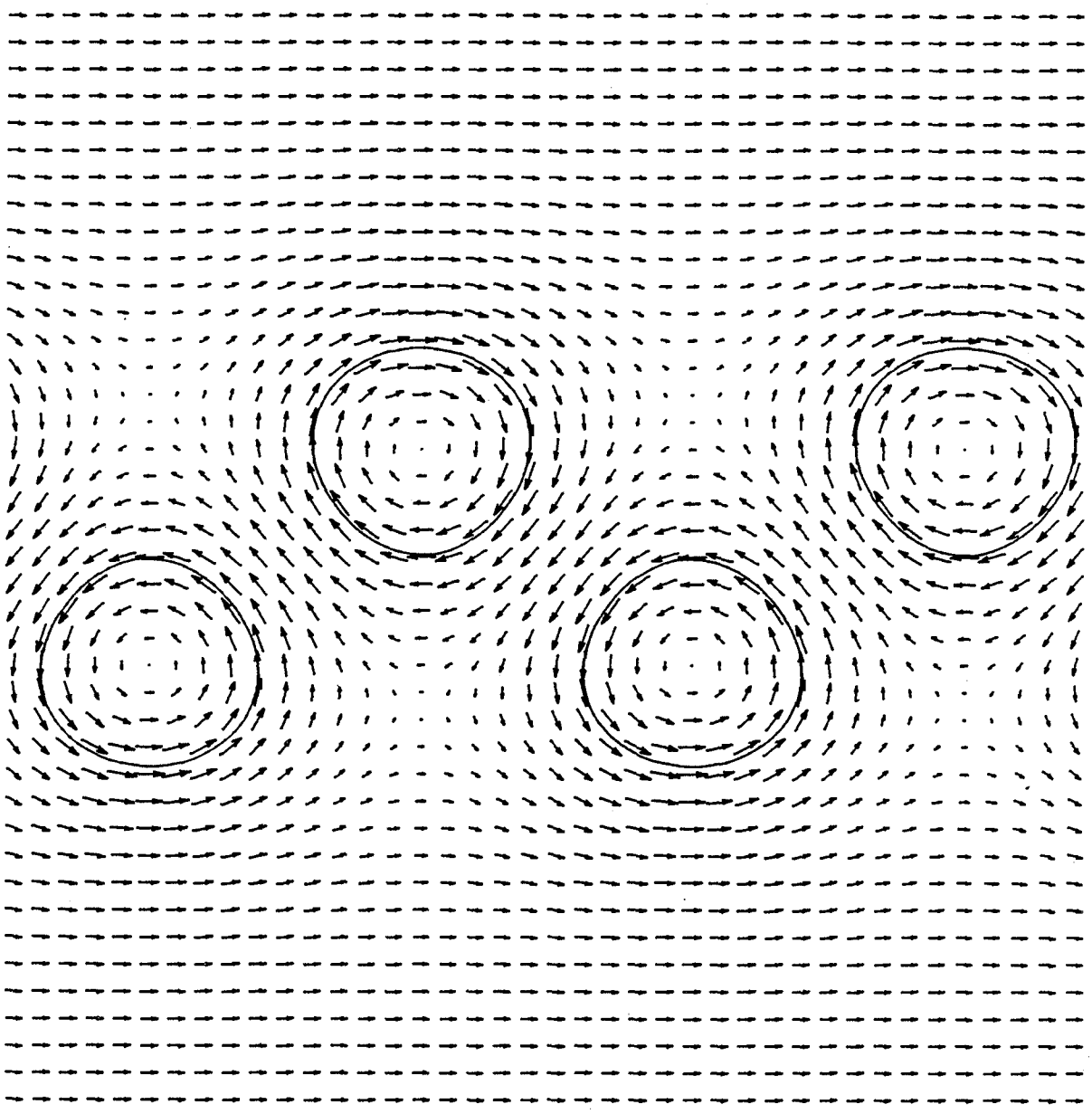

Figure 31. Plot of the vortex shapes and the velocity field for

$\kappa=.4$ $\alpha=.1188$

Arrow length is proportional to the speed of the fluid at midpoint.

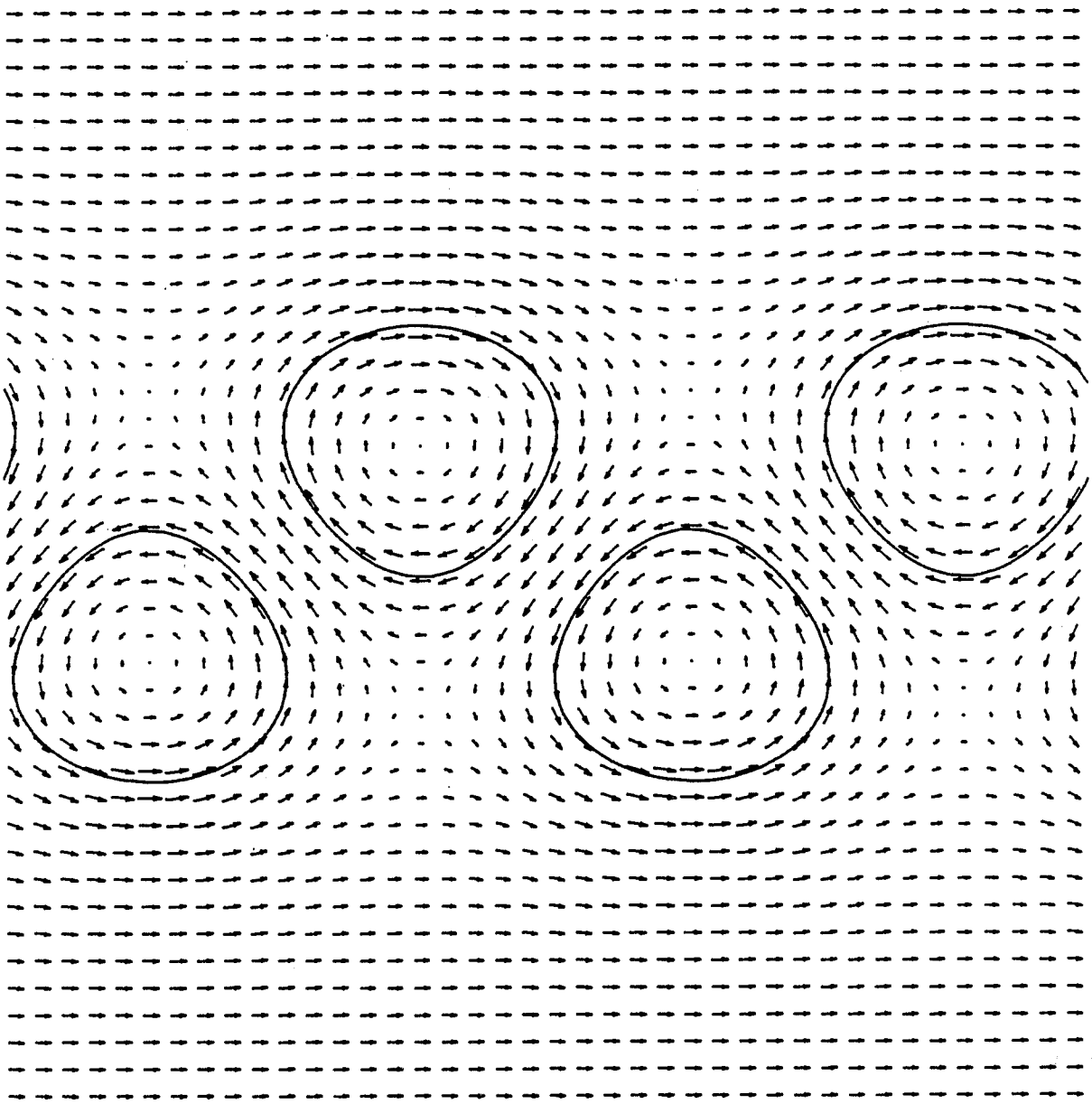

Figure 32. Plot of the vortex shapes and the velocity field for

$\kappa = .4$ $\alpha = .1777$

Arrow length is proportional to the speed of the fluid at midpoint.

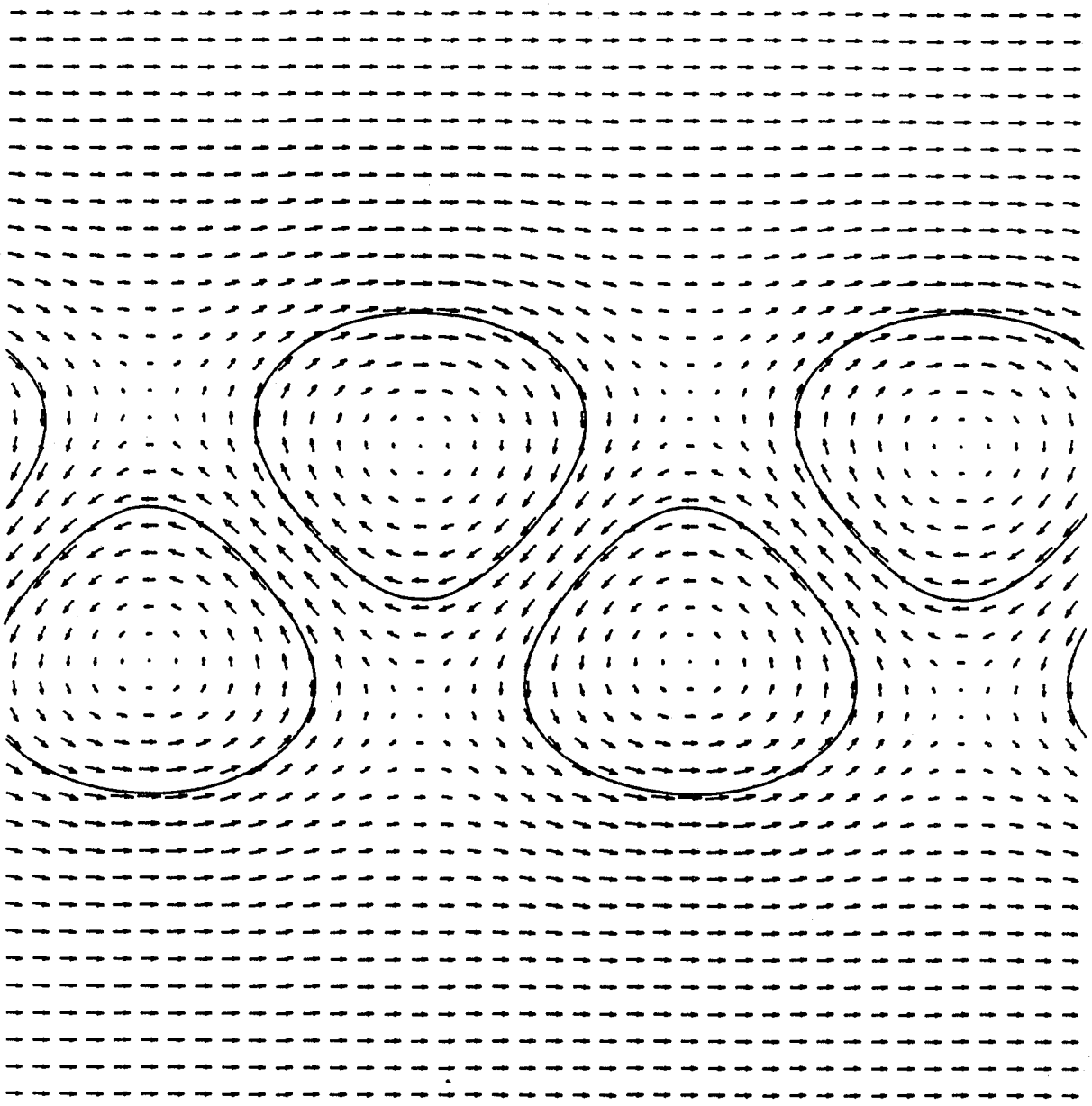

Figure 33. Plot of the vortex shapes and the velocity field for

$\kappa = .4$ $\alpha = .2388$

Arrow length is proportional to the speed of the fluid at midpoint.

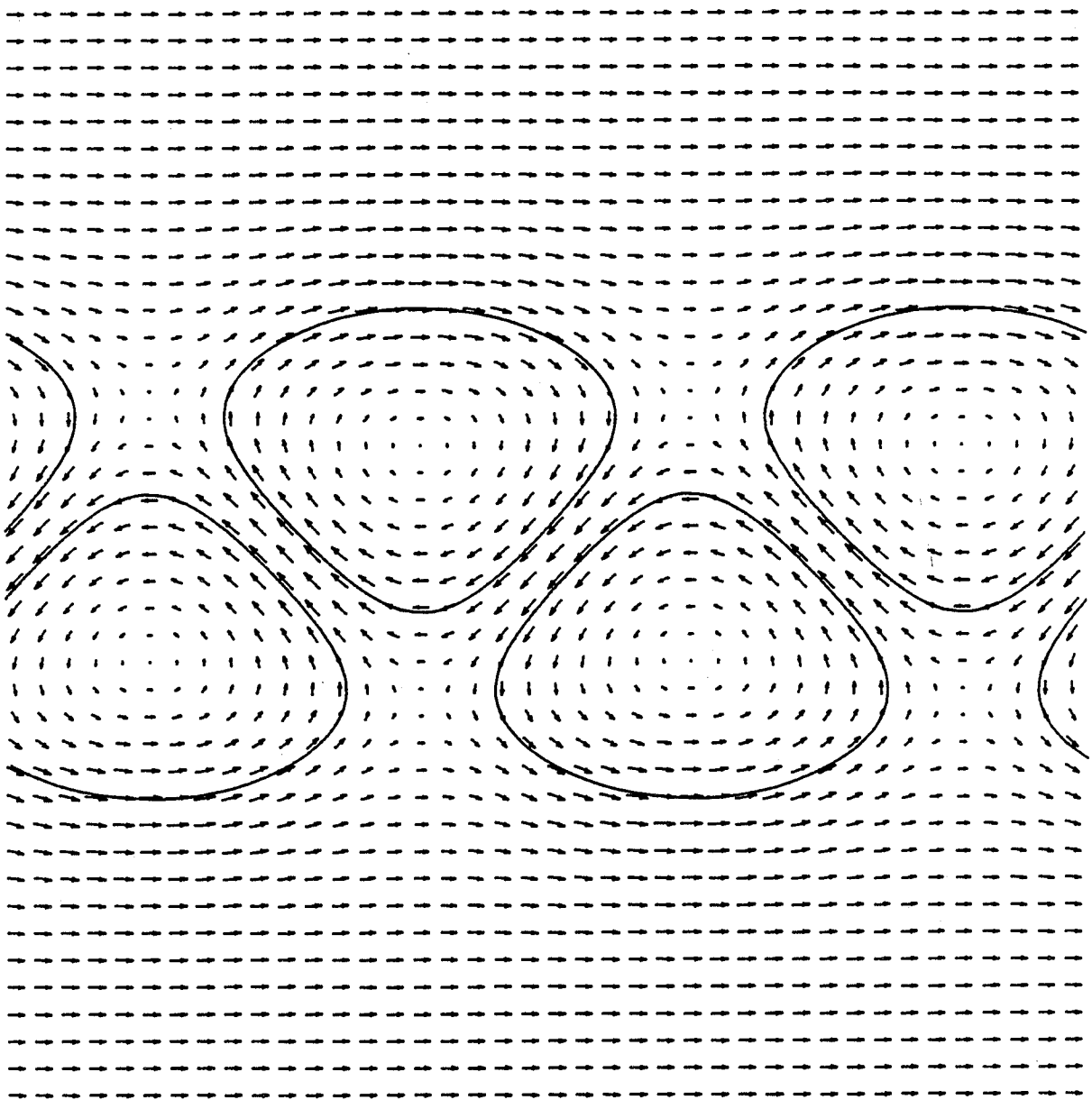

Figure 34. Plot of the vortex shapes and the velocity field for

$\kappa = .4$ $\alpha = .2888$

Arrow length is proportional to the speed of the fluid at midpoint.

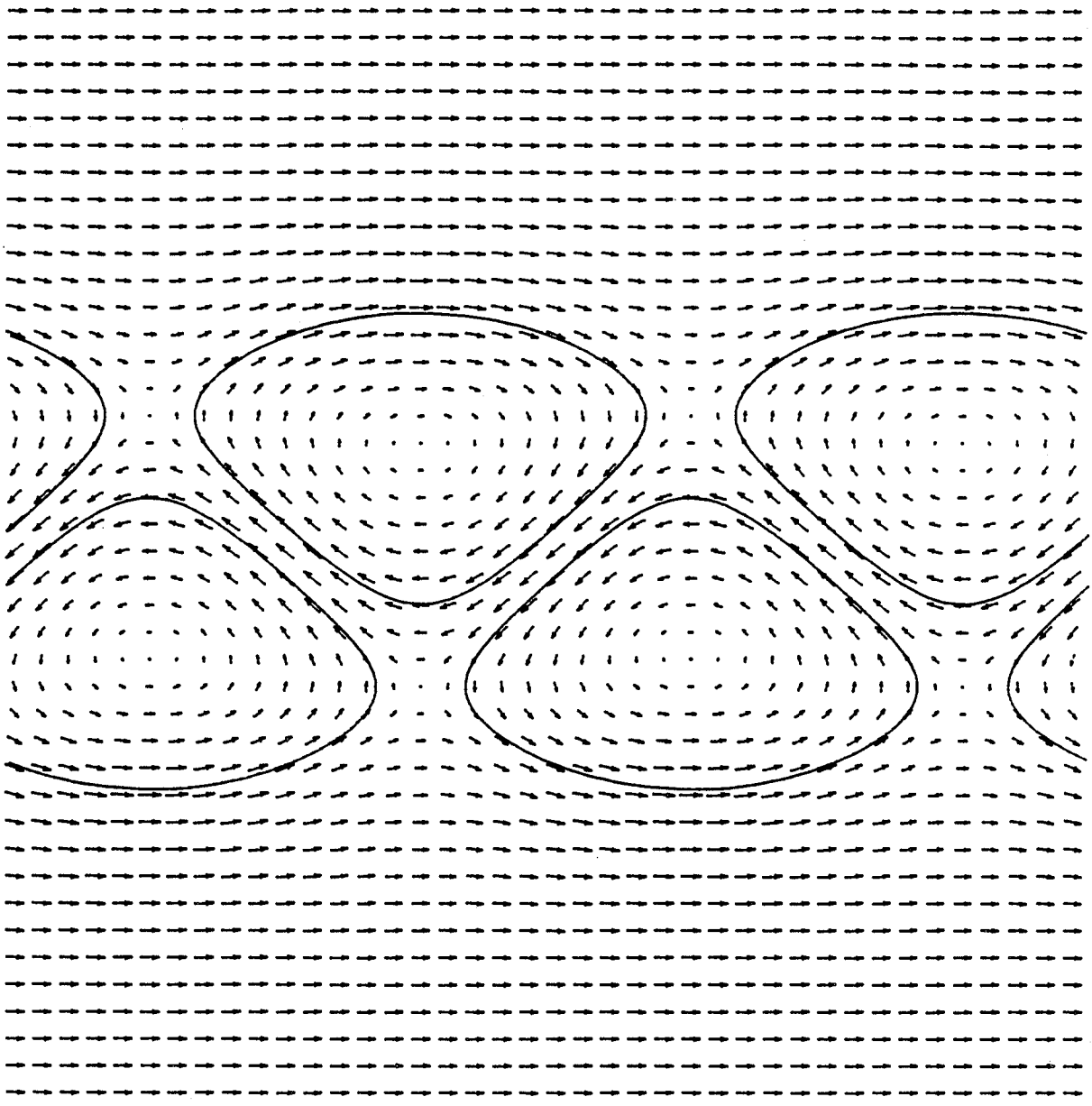

Figure 35. Plot of the vortex shapes and the velocity field for

$\kappa = .4$ $\alpha = .3080$

Arrow length is proportional to the speed of the fluid at midpoint.

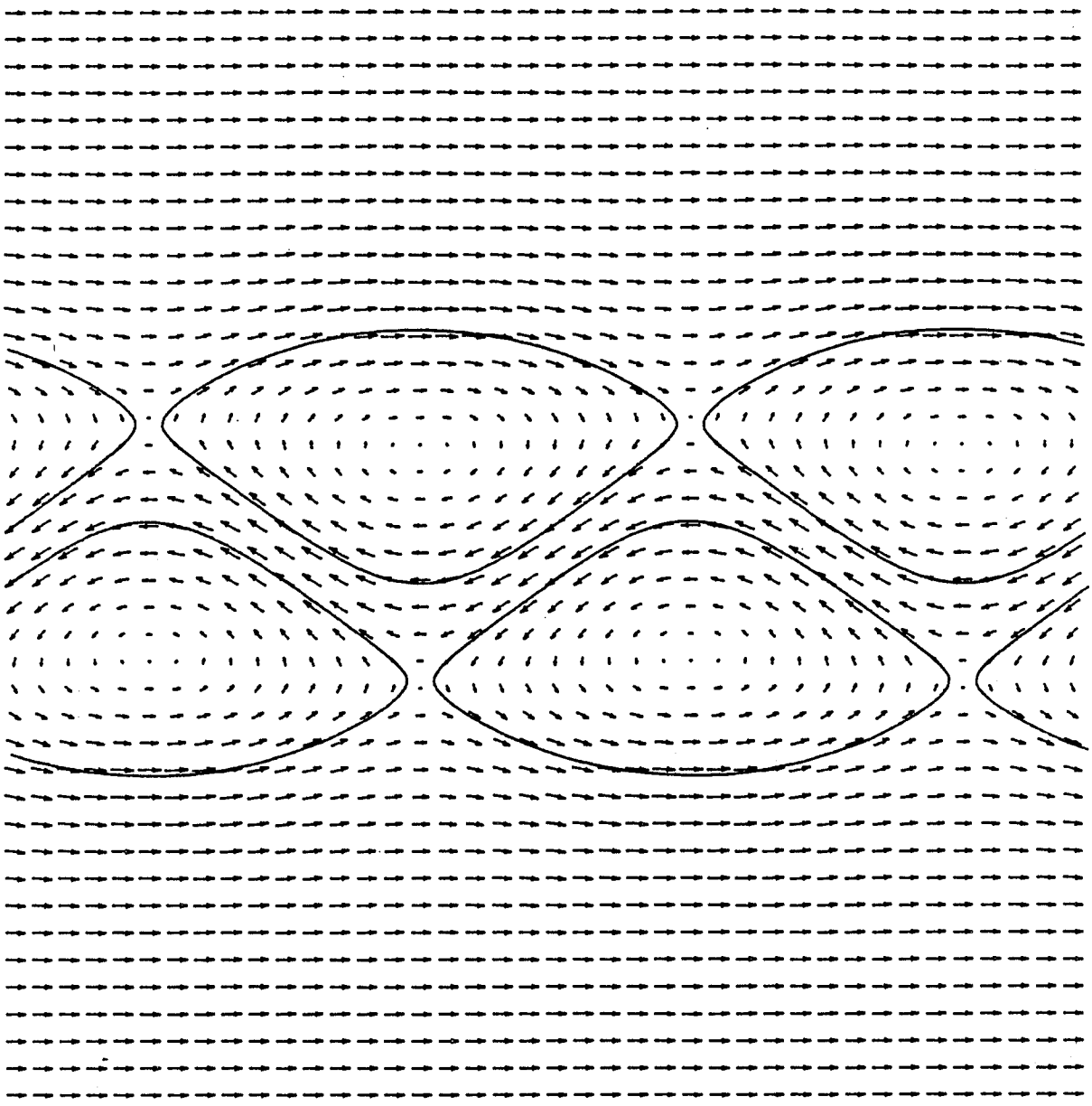

Figure 36. Plot of the vortex shapes and the velocity field for
$\kappa=.4$ $\alpha=.2933$ (smaller energy case)
Arrow length is proportional to the speed of the fluid at midpoint.

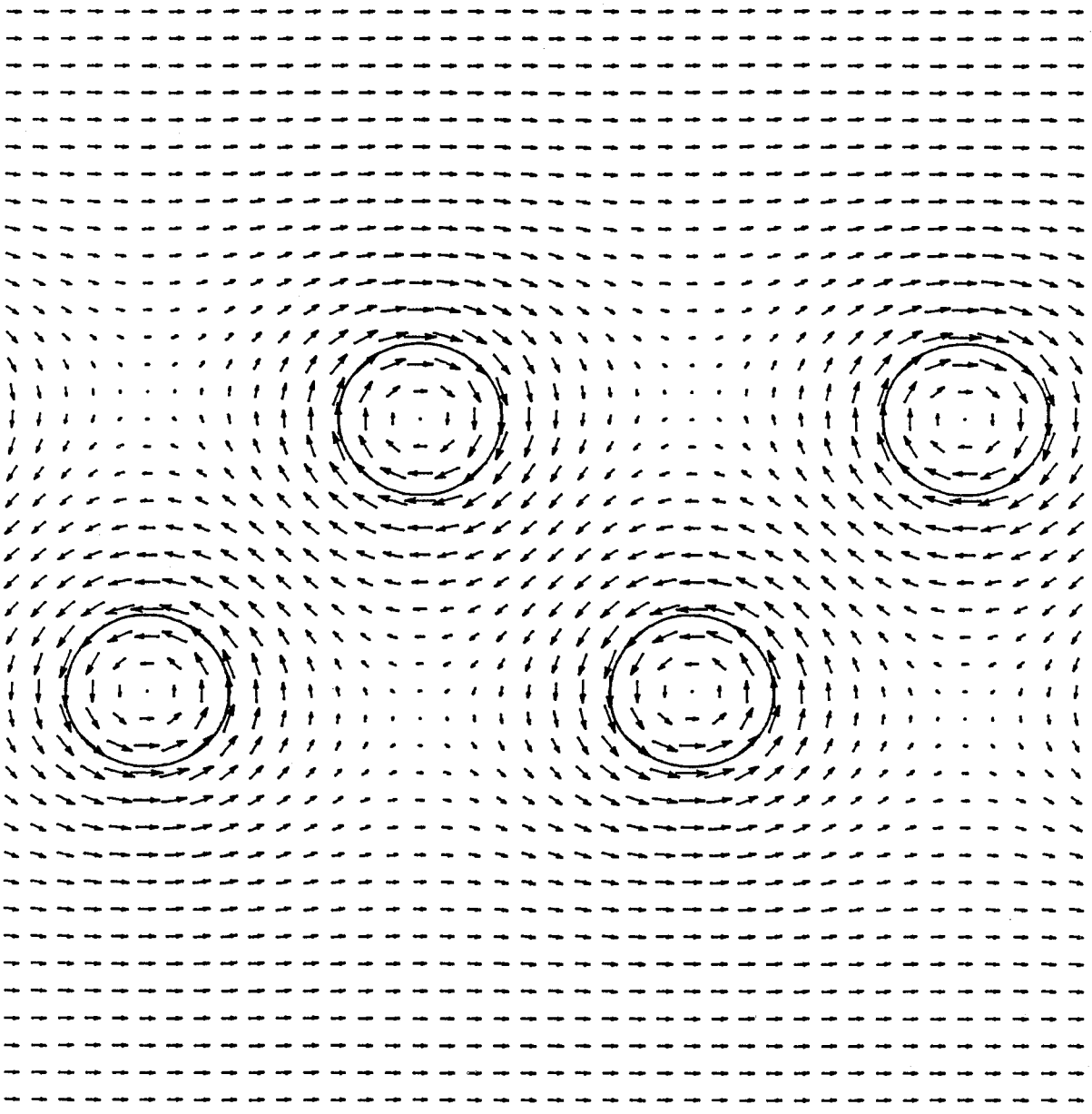

Figure 37. Plot of the vortex shapes and the velocity field for

$\kappa=.5$ $\alpha=.06549$

Arrow length is proportional to the speed of the fluid at midpoint.

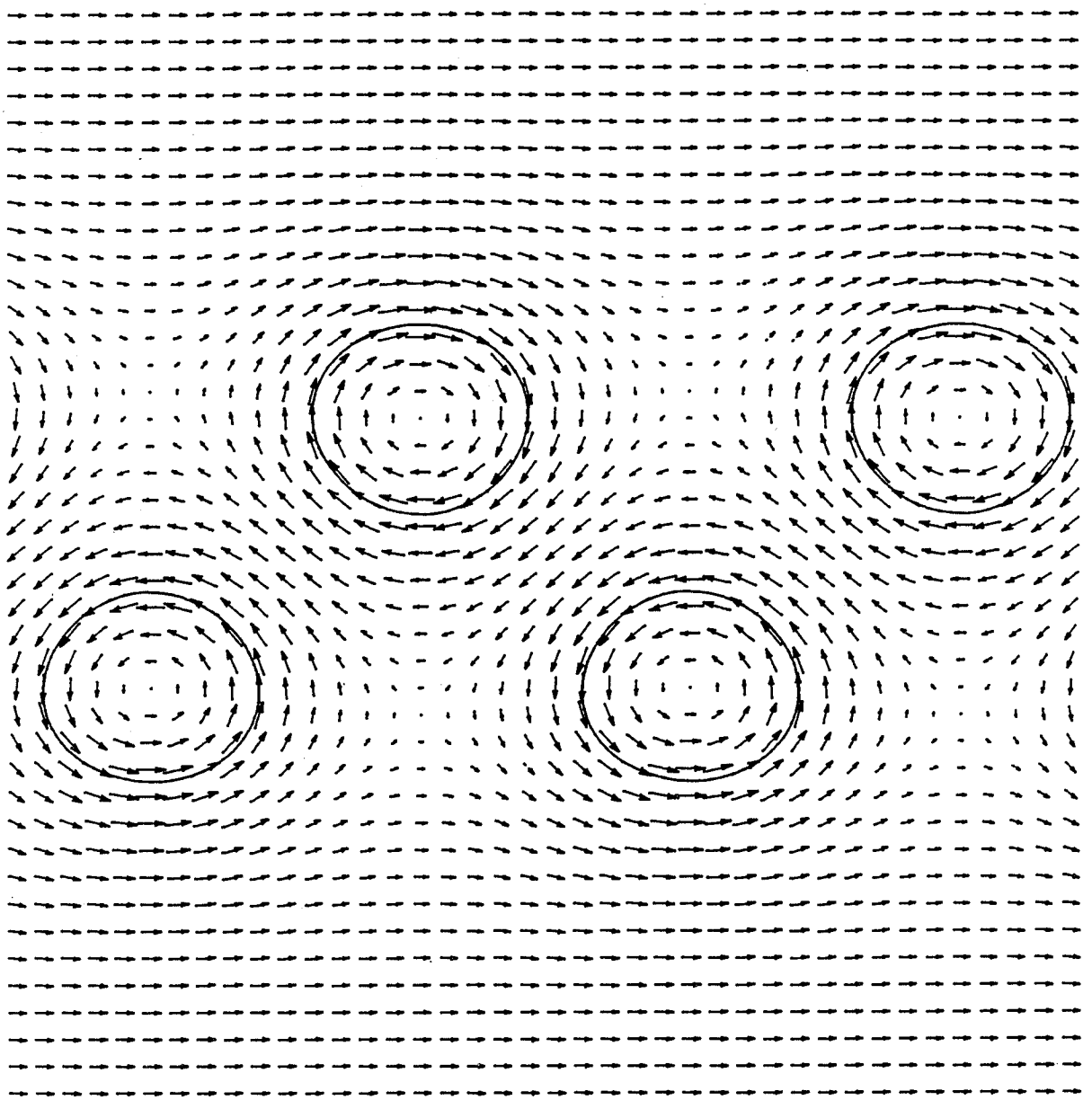

Figure 38. Plot of the vortex shapes and the velocity field for

$\kappa = .5$ $\alpha = .1096$

Arrow length is proportional to the speed of the fluid at midpoint.

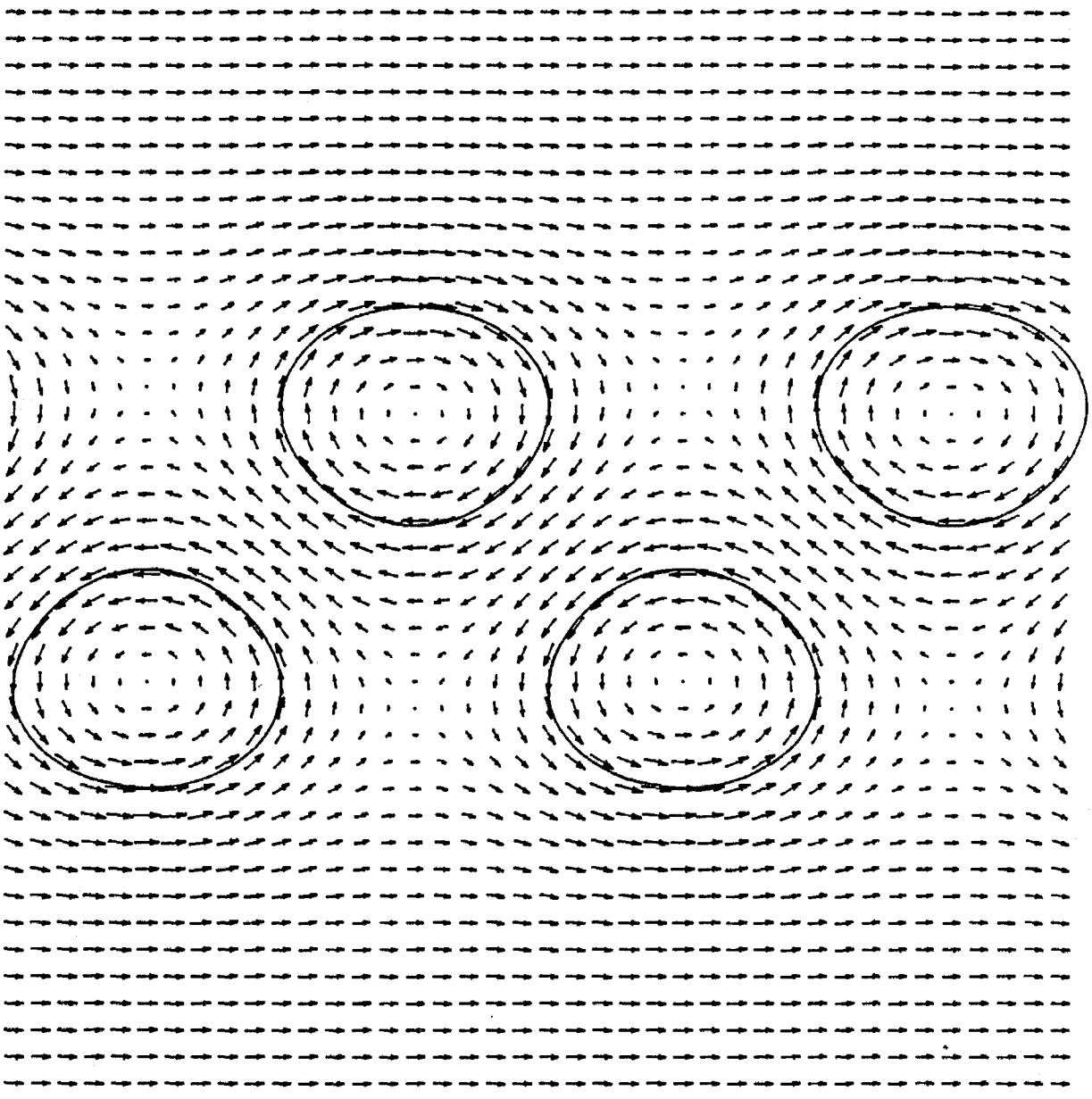

Figure 39. Plot of the vortex shapes and the velocity field for

$\kappa = .5$ $\alpha = .1578$

Arrow length is proportional to the speed of the fluid at midpoint.

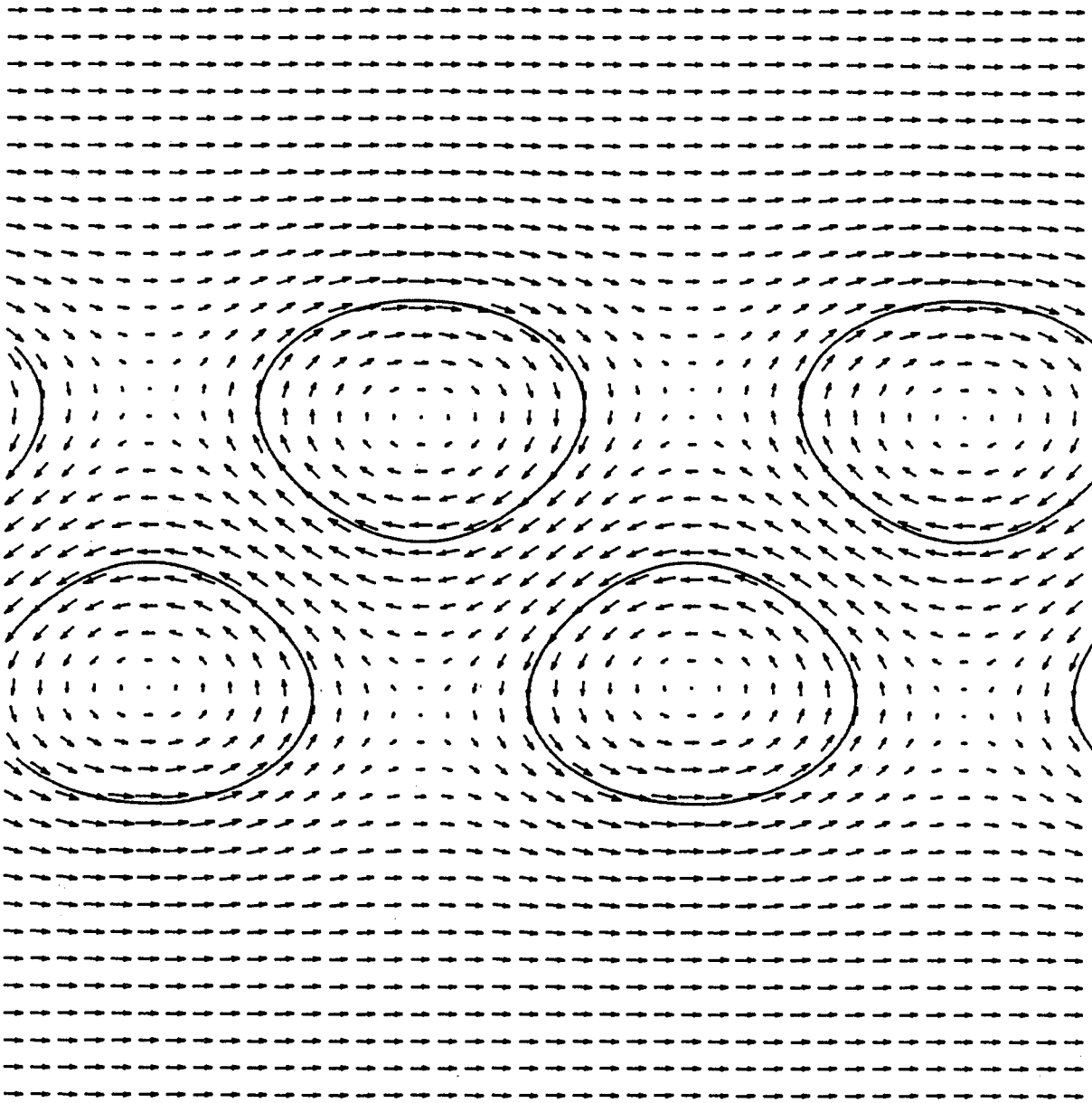

Figure 40. Plot of the vortex shapes and the velocity field for

$\kappa=.5$ $\alpha=.2037$

Arrow length is proportional to the speed of the fluid at midpoint.

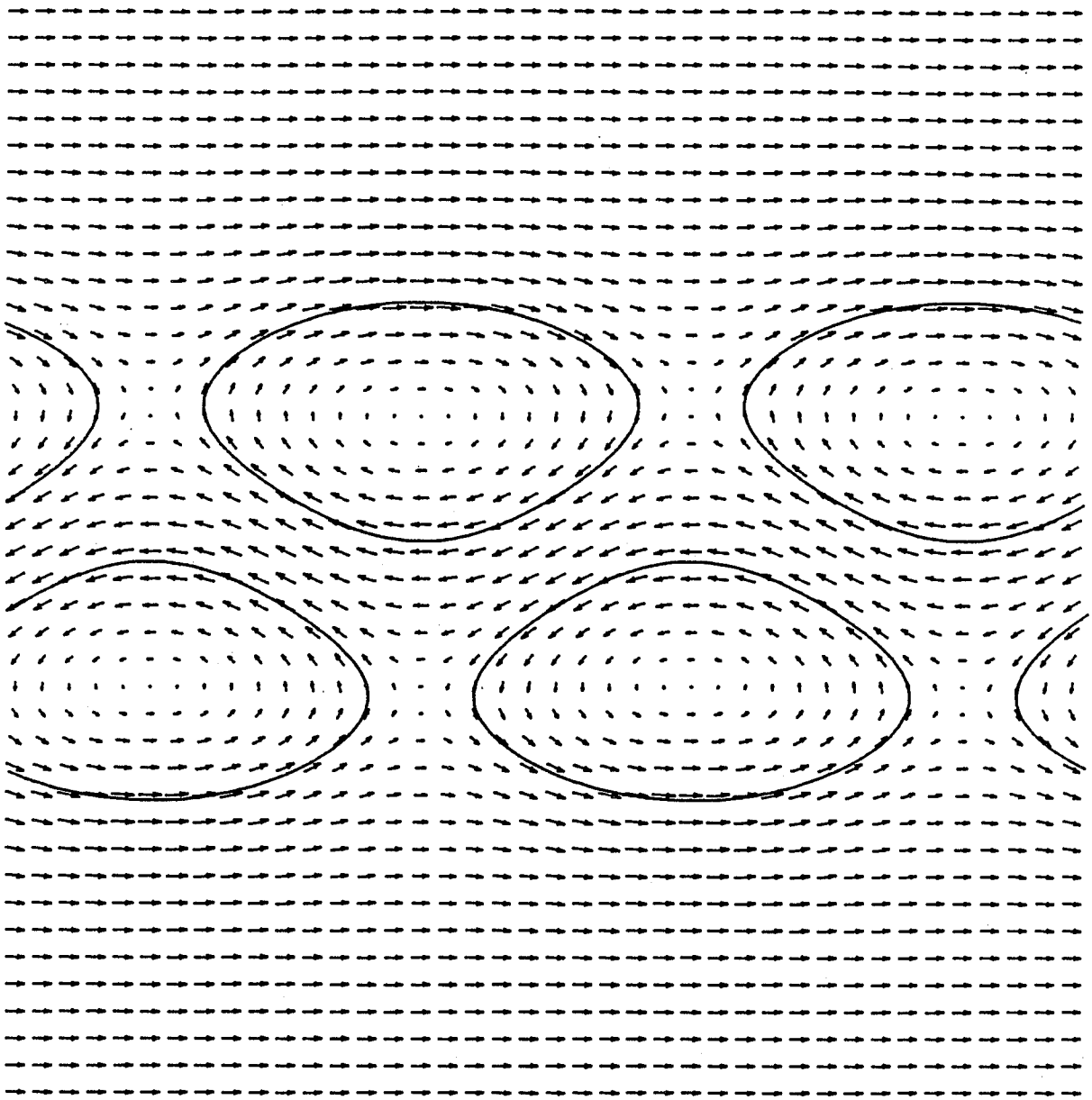

Figure 41. Plot of the vortex shapes and the velocity field for

$\kappa$=.5 $\alpha$=.2609

Arrow length is proportional to the speed of the fluid at midpoint.

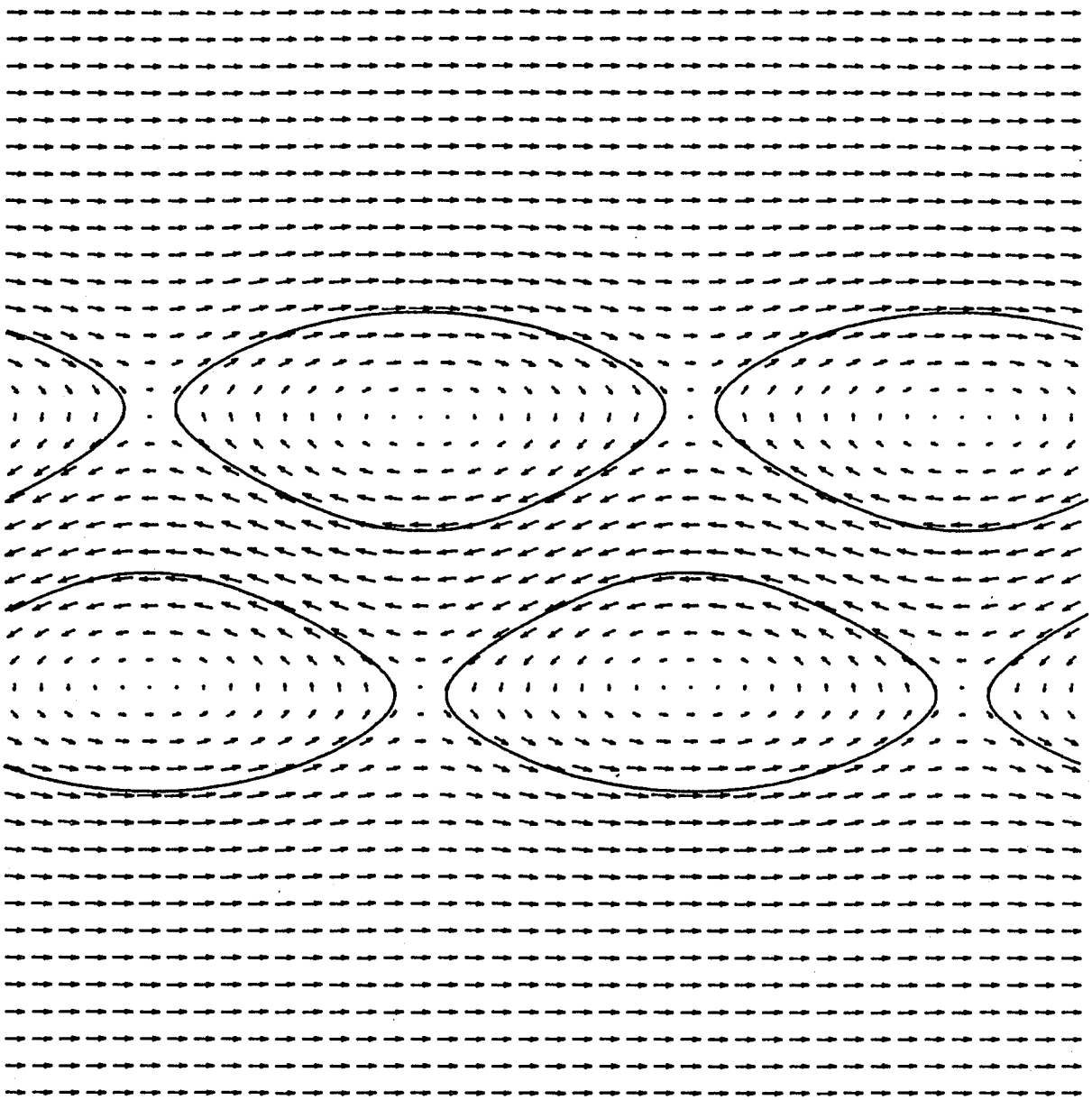

Figure 42. Plot of the vortex shapes and the velocity field for

$\kappa$=.5 $\alpha$=.2613

Arrow length is proportional to the speed of the fluid at midpoint.

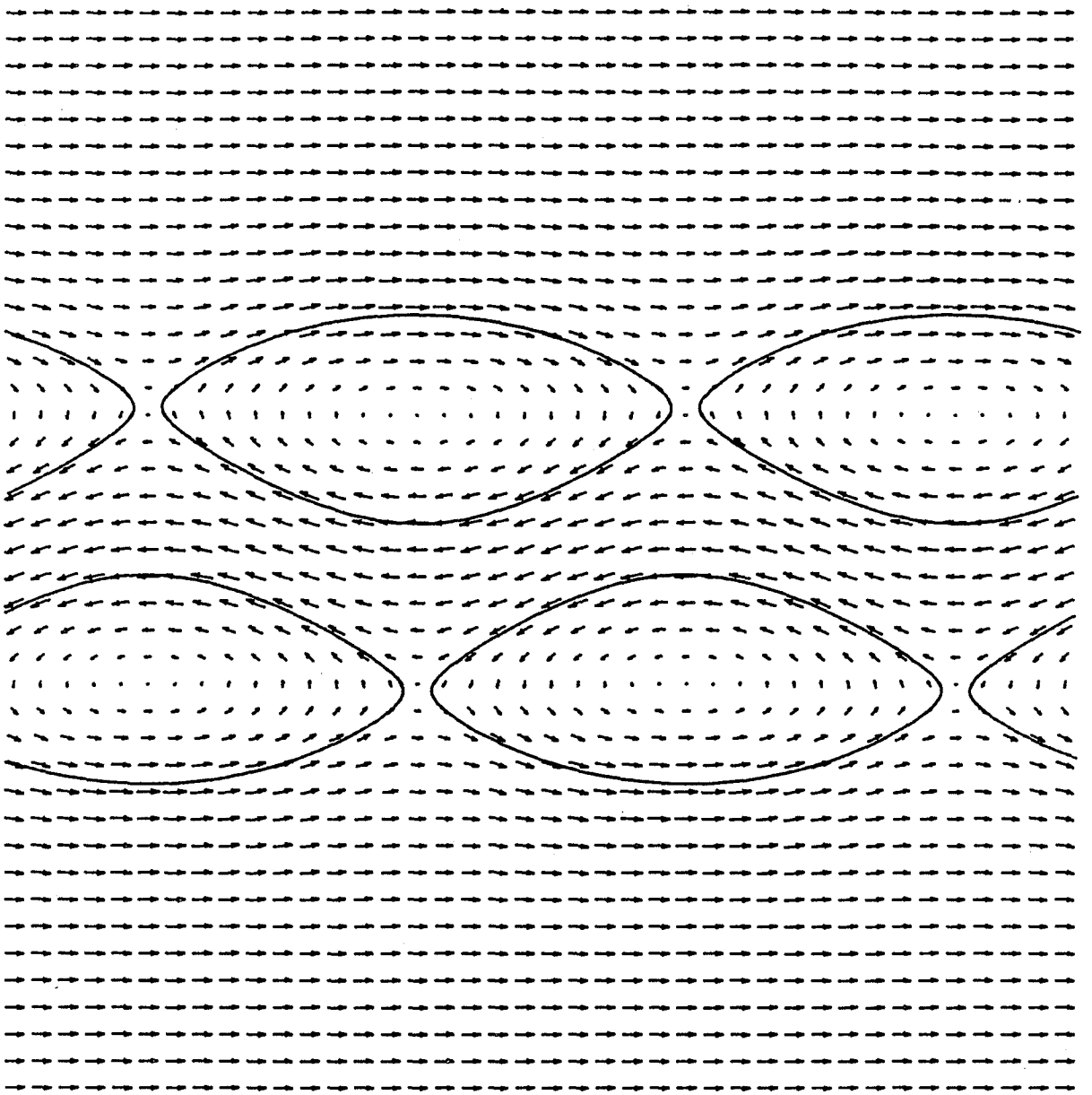

Figure 43. Plot of the vortex shapes and the velocity field for

$\kappa$=.5 $\alpha$=.2562 (smaller energy case)

Arrow length is proportional to the speed of the fluid at midpoint.

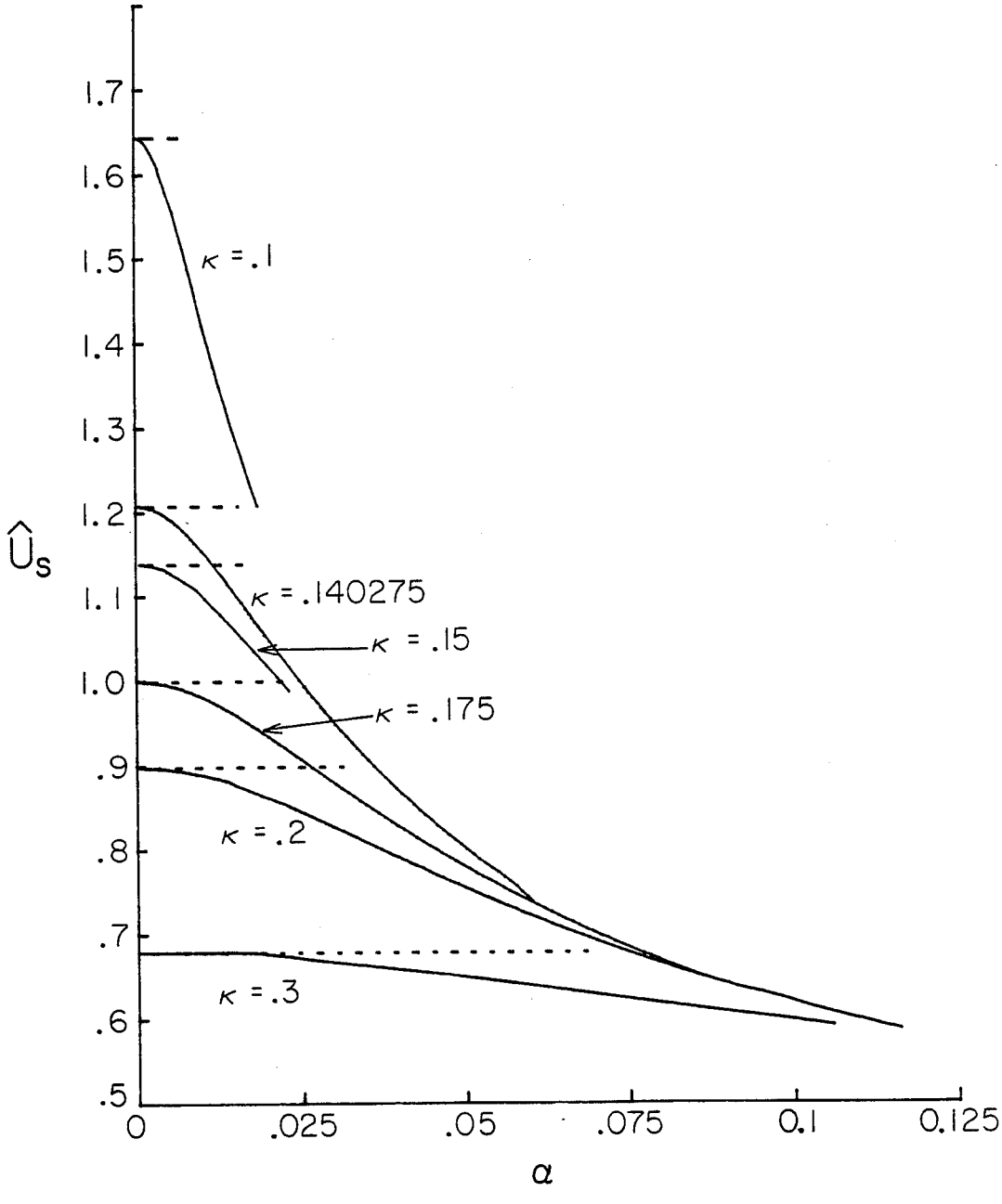


Figure 44. Values of the propagation speed $\hat{U}_s$ for the aligned vortex array ($\mu$=0). Solid lines denote the calculated values for the exact problem and dashed lines denote the circular vortex approximation.

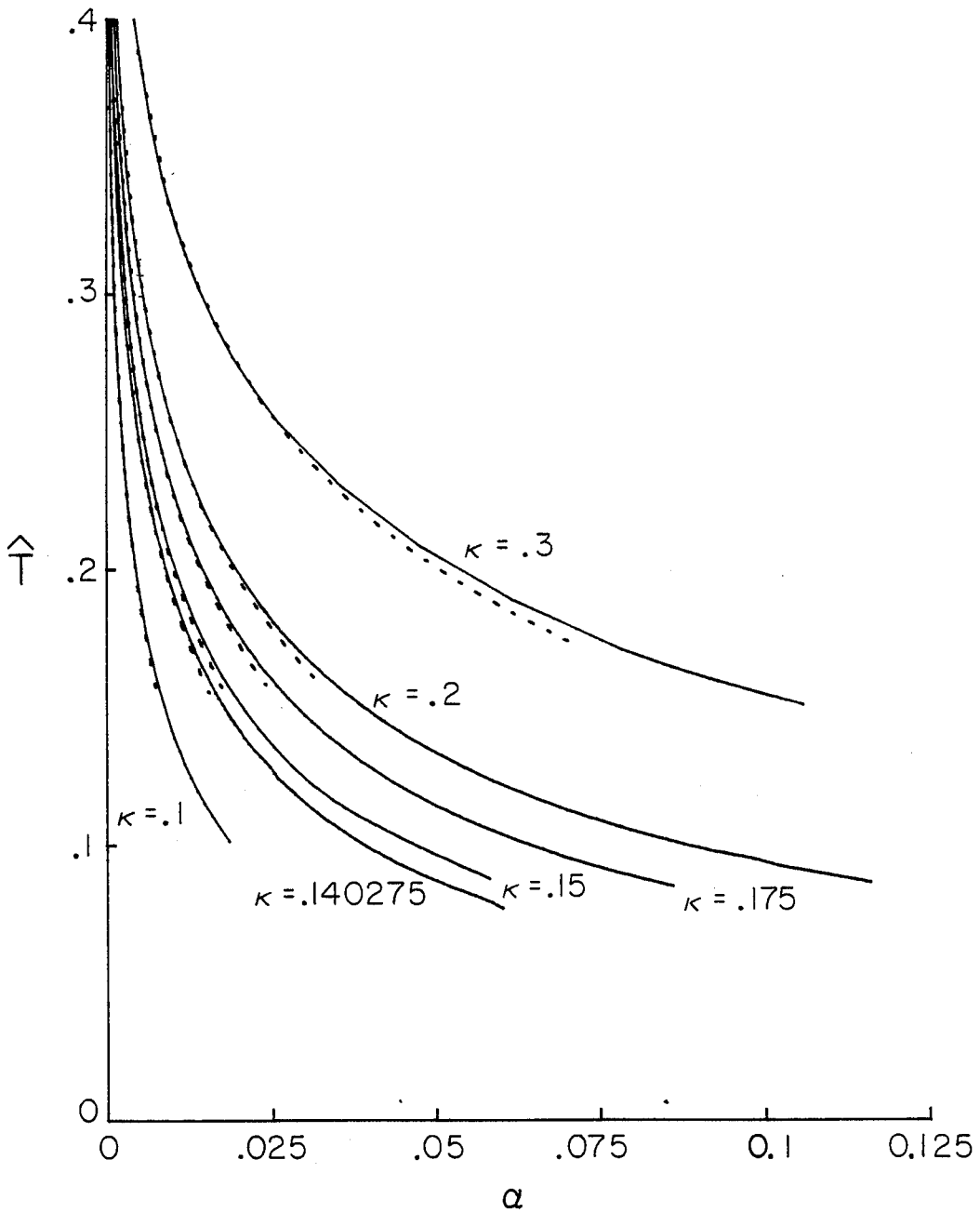


Figure 45. Values of the kinetic energy $\hat{T}$ for the aligned vortex array ($\mu$=0). Solid lines denote the calculated values for the exact problem and dashed lines denote the circular vortex approximation.

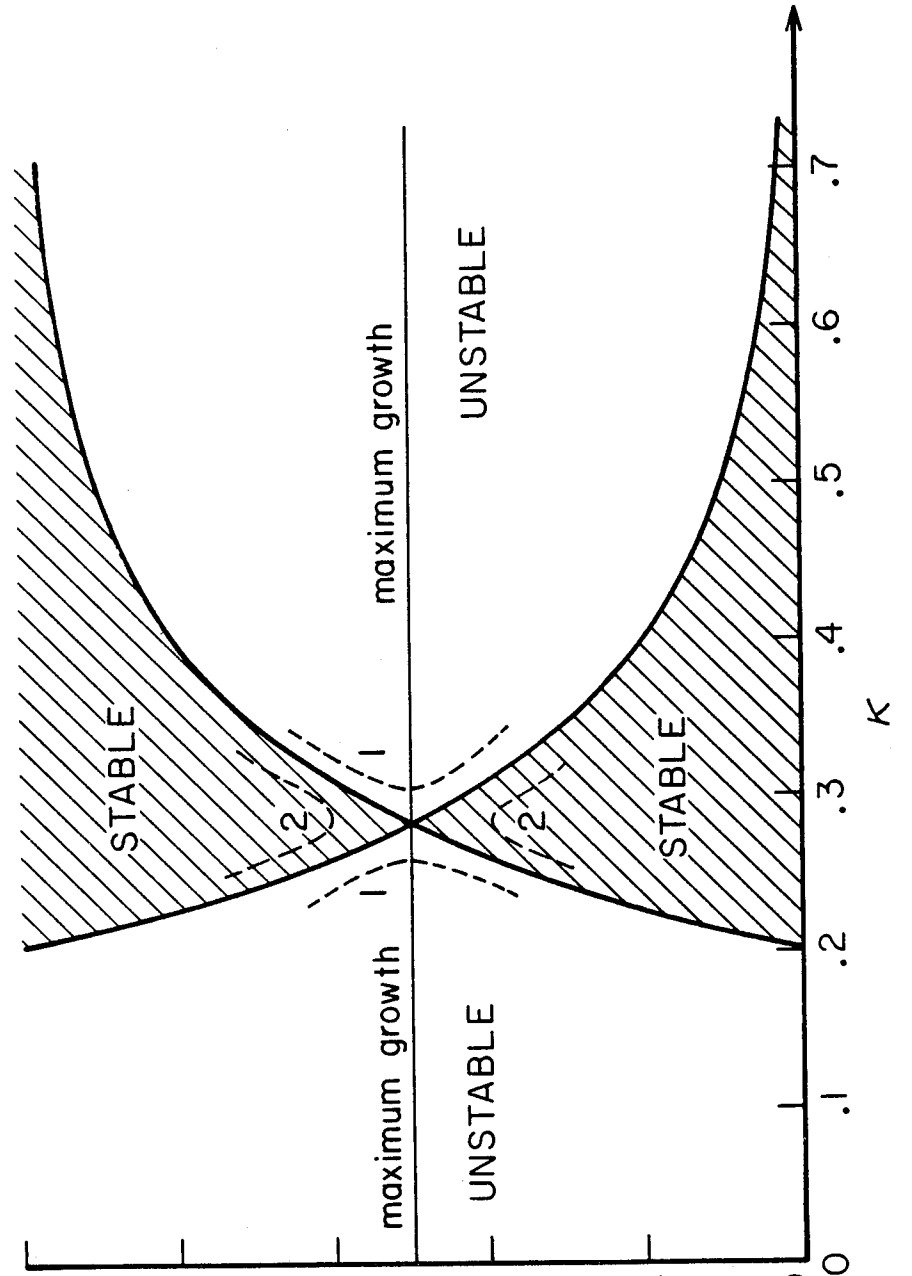


Figure 46. The stability boundary in the periodicity p versus spacing ratio K plane for point vortex configurations. The growth rates are symmetric about p=0.5 which also gives the maximum rate of growth for all K. Curves 1 and 2 qualitatively show the two possible perturbed boundaries for small area. The calculations indicate that curve 1 is the true result.

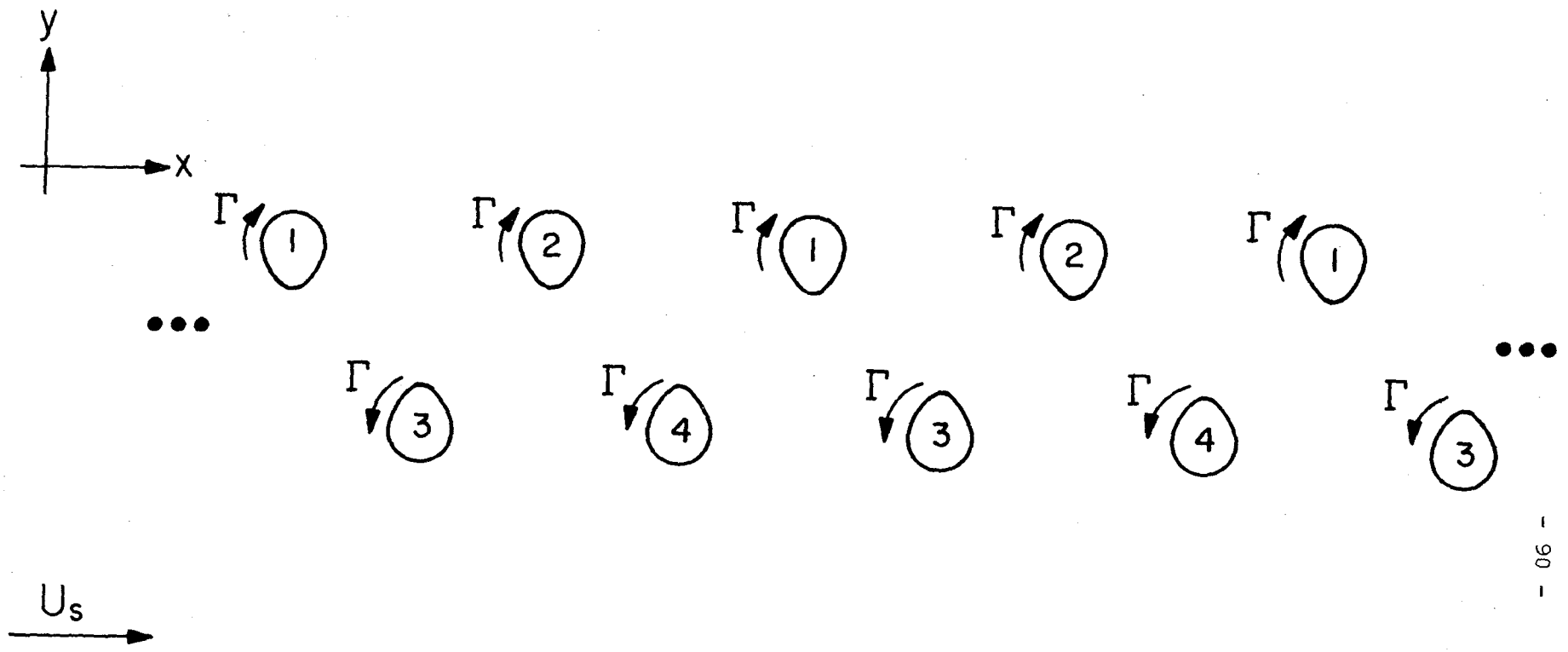


Figure 47. Diagram of the vortex street configuration showing the four independent perturbations.

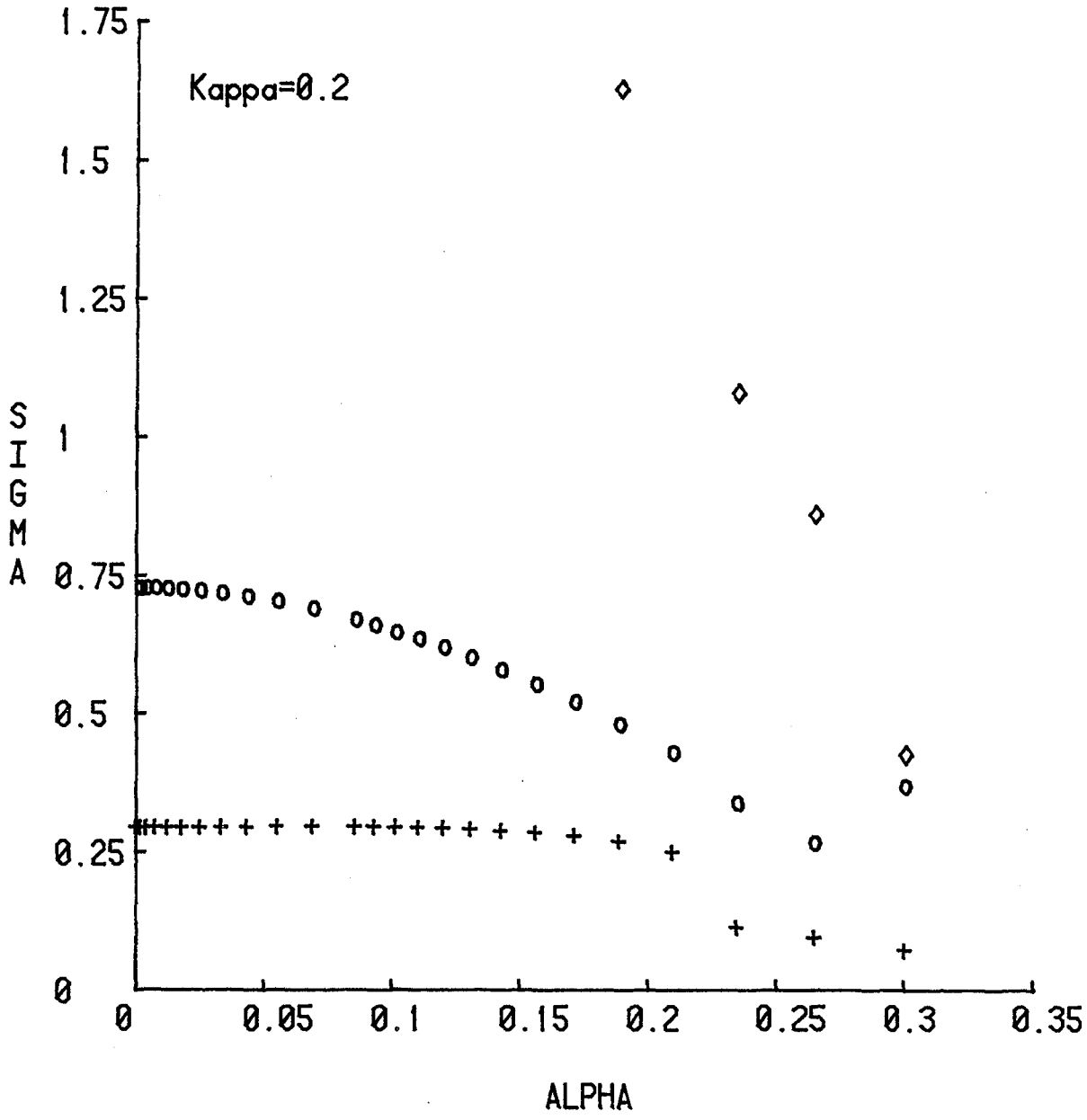


Figure 48. Calculated non-dimensional eigenvalues ($\sigma \cdot l^2/\Gamma$) from the linear stability analysis.

\+ denotes real part (growth rate)
o denotes corresponding imaginary part (frequency)
◊ denotes neutral eigenvalue of lowest frequency

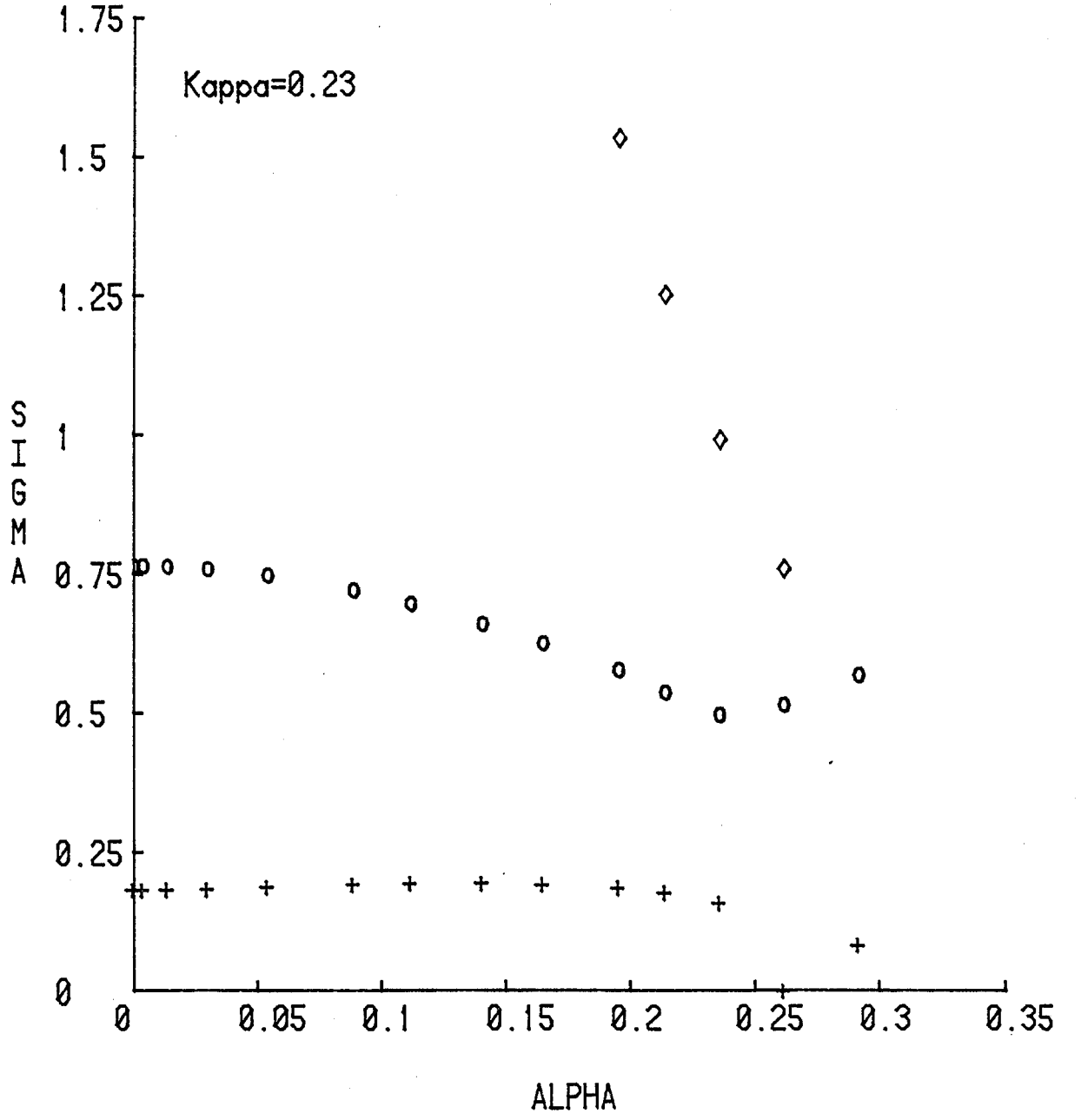


Figure 49. Calculated non-dimensional eigenvalues ($\sigma \cdot 1^2/\Gamma$) from the linear stability analysis.

+ denotes real part (growth rate)
o denotes corresponding imaginary part (frequency)
◇ denotes neutral eigenvalue of lowest frequency, showing degeneracy at change of stability

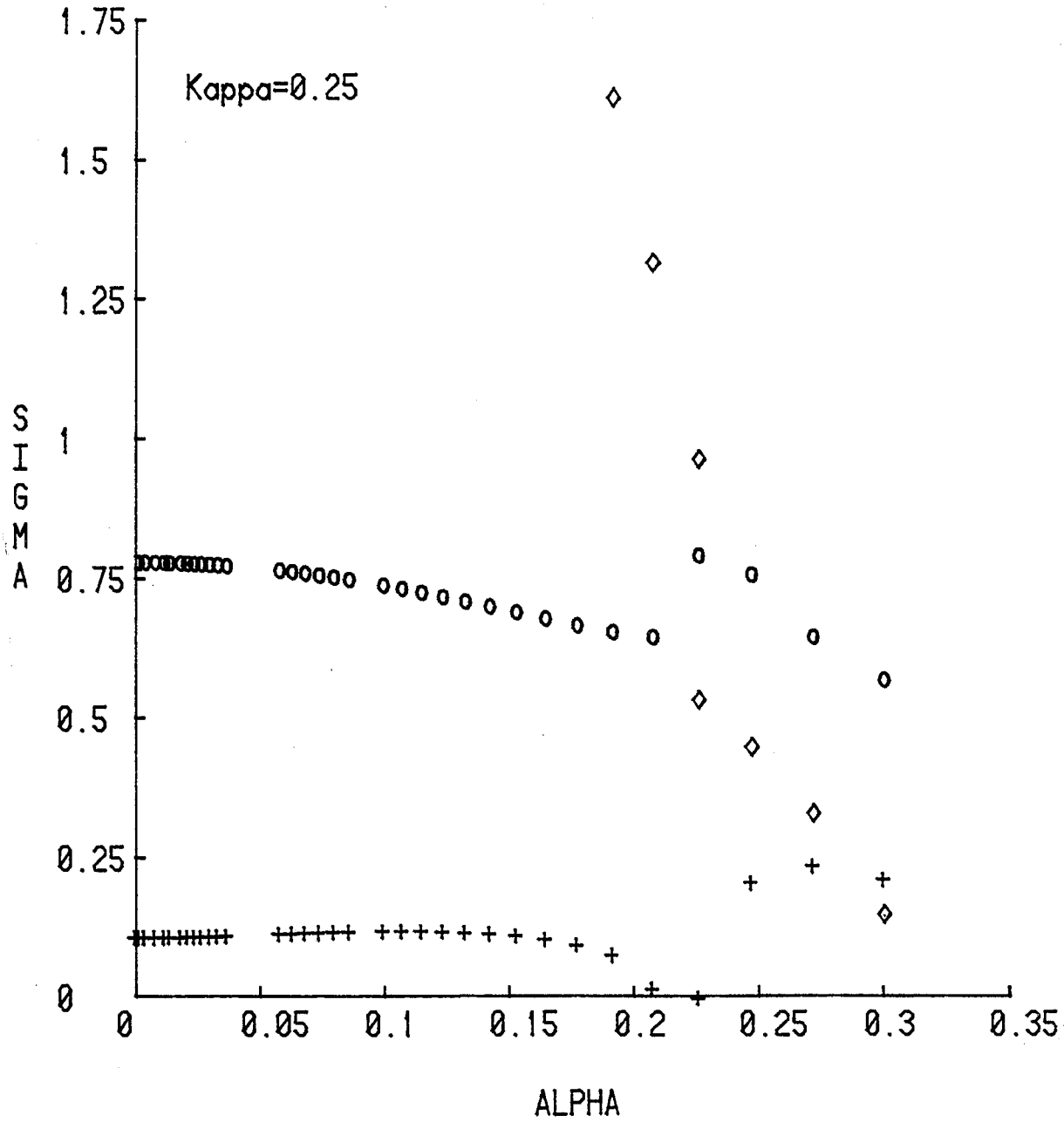


Figure 50. Calculated non-dimensional eigenvalues ($\sigma \cdot 1^2/\Gamma$) from the linear stability analysis.

\+ denotes real part (growth rate)
o denotes corresponding imaginary part (frequency)
◆ denotes neutral eigenvalue of lowest frequency, showing degeneracy at change of stability

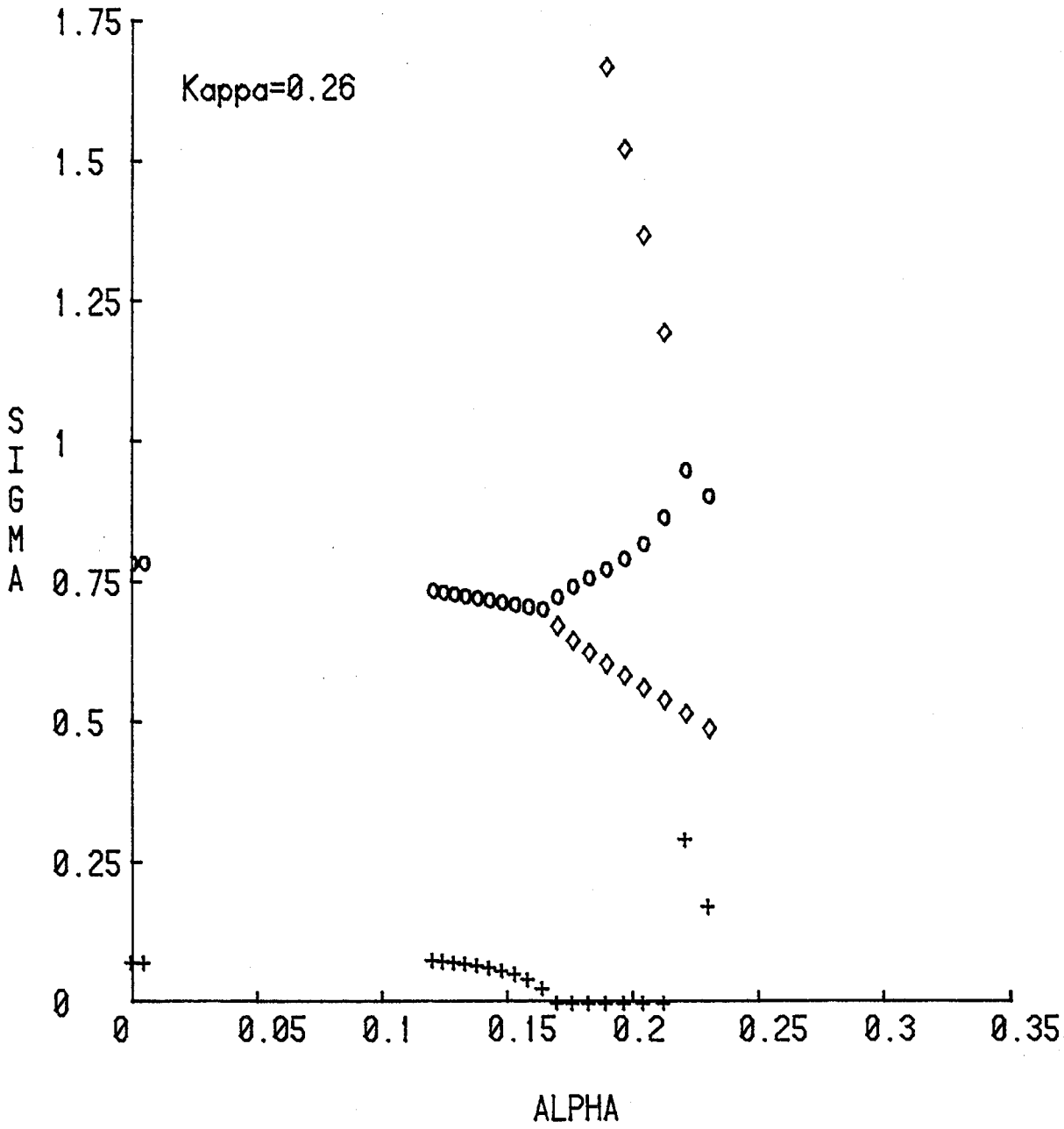


Figure 51. Calculated non-dimensional eigenvalues ($\sigma \cdot l^2/\Gamma$) from the linear stability analysis.

+ denotes real part (growth rate)
o denotes corresponding imaginary part (frequency)
◇ denotes neutral eigenvalue of lowest frequency, showing degeneracy at change of stability

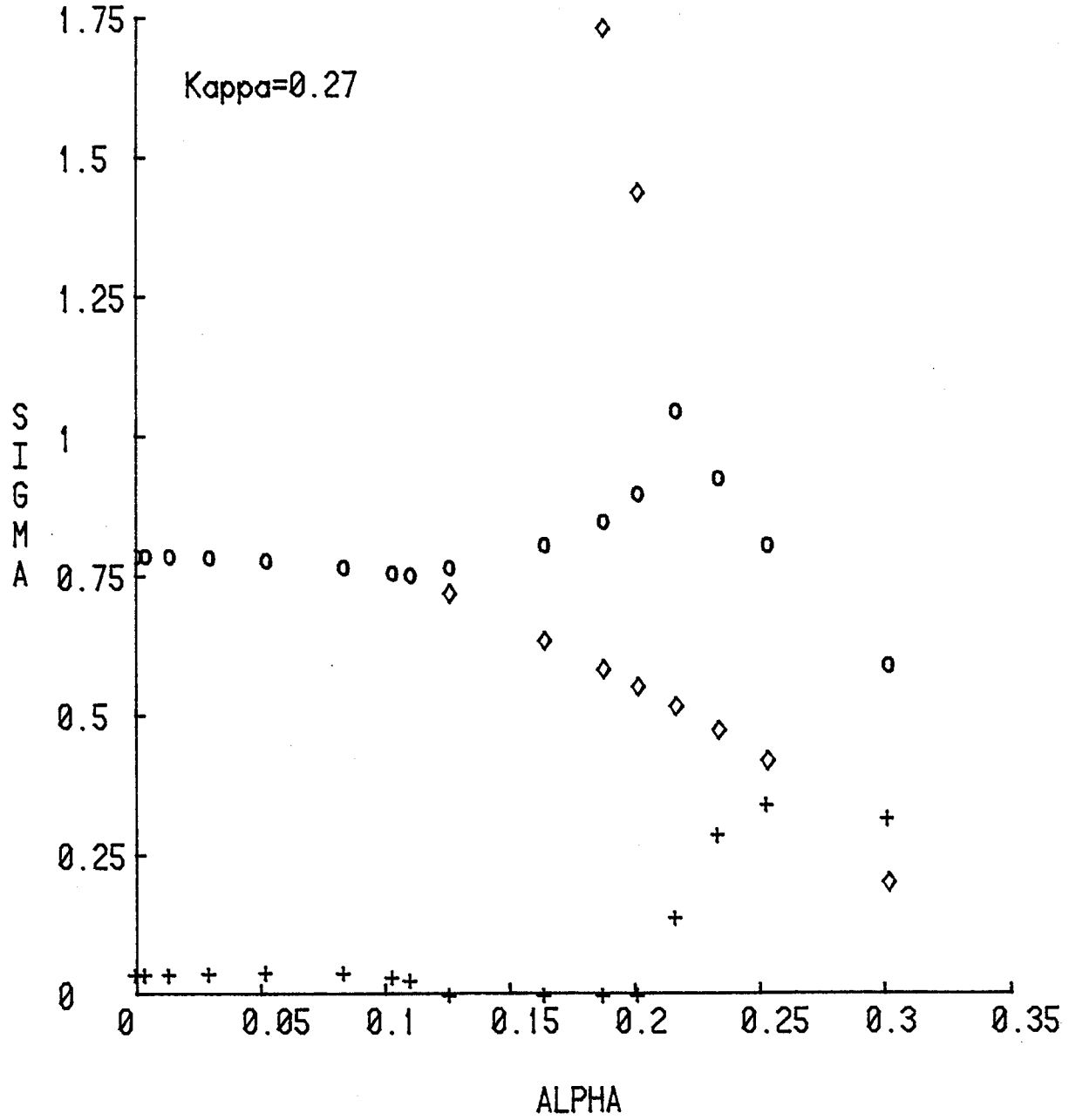


Figure 52. Calculated non-dimensional eigenvalues ($\sigma \cdot l^2/\Gamma$) from the linear stability analysis.

+ denotes real part (growth rate)
o denotes corresponding imaginary part (frequency)
◇ denotes neutral eigenvalue of lowest frequency, showing degeneracy at change of stability

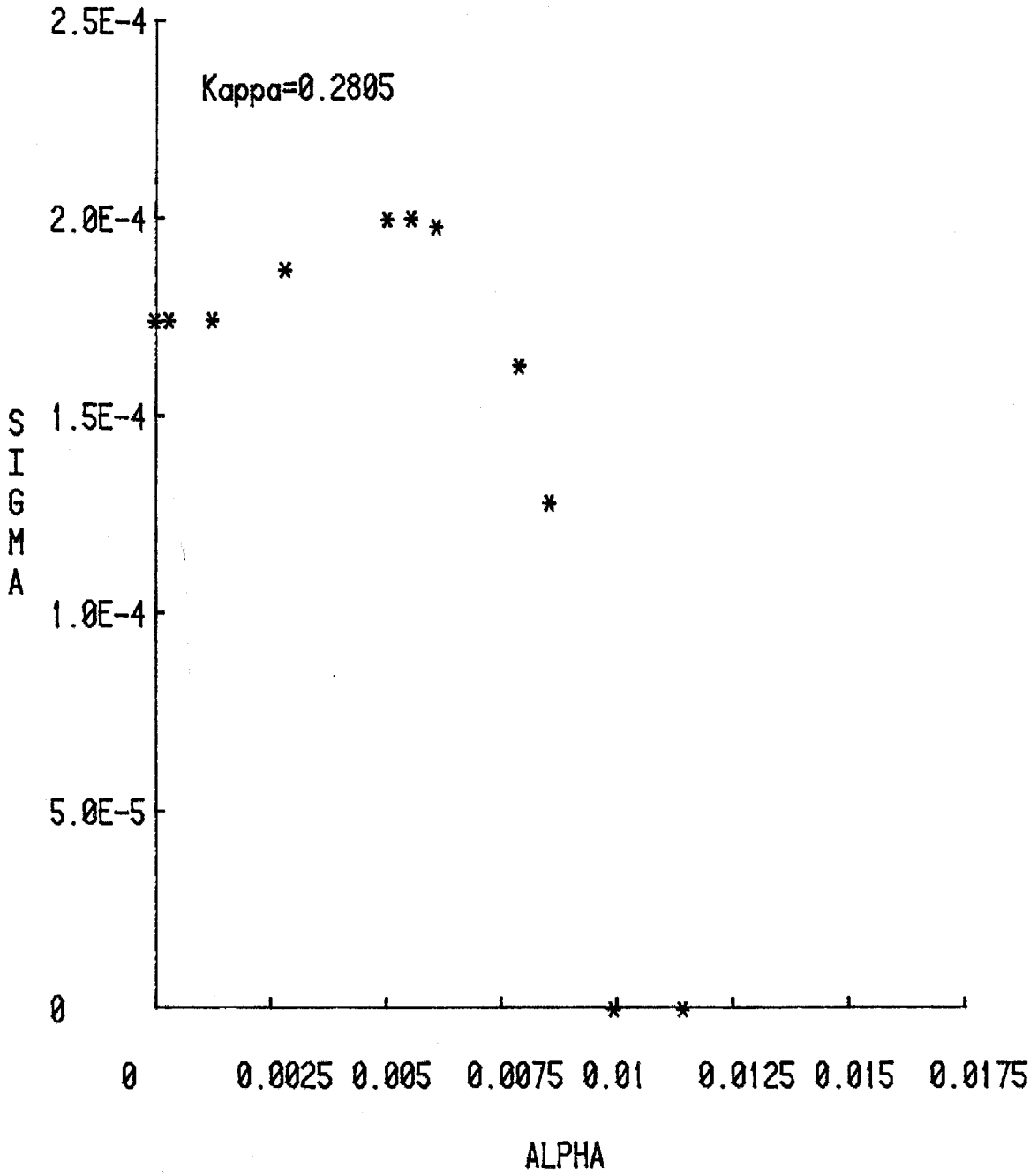


Figure 53. Calculated non-dimensional real part (growth rate) of the eigenvalues ($\sigma \cdot l^2/\Gamma$) from the linear stability analysis.

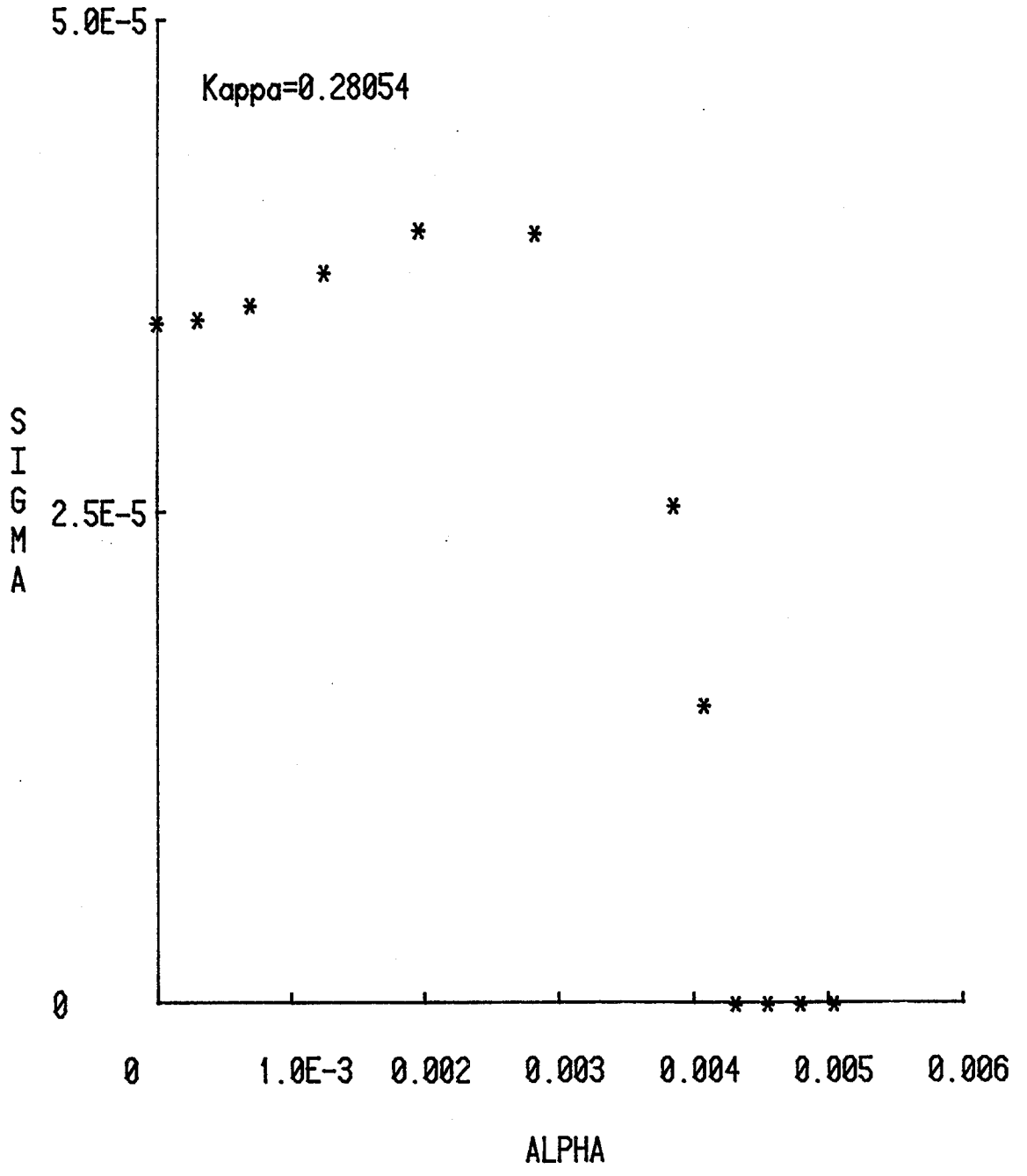


Figure 54. Calculated non-dimensional real part (growth rate) of the eigenvalues ($\sigma \cdot l^2/\Gamma$) from the linear stability analysis.

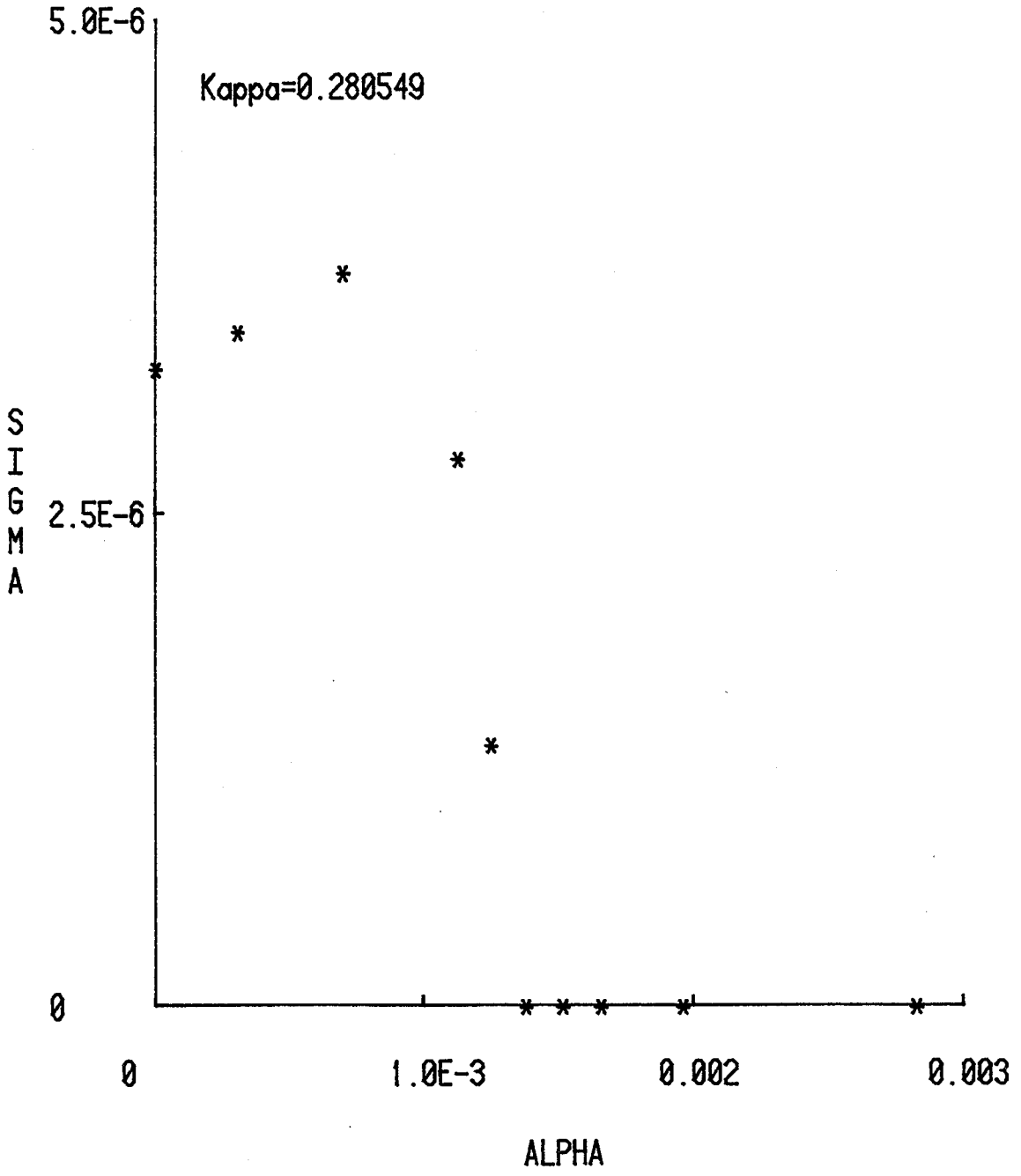


Figure 55. Calculated non-dimensional real part (growth rate) of the eigenvalues ($\sigma \cdot l^2/\Gamma$) from the linear stability analysis.

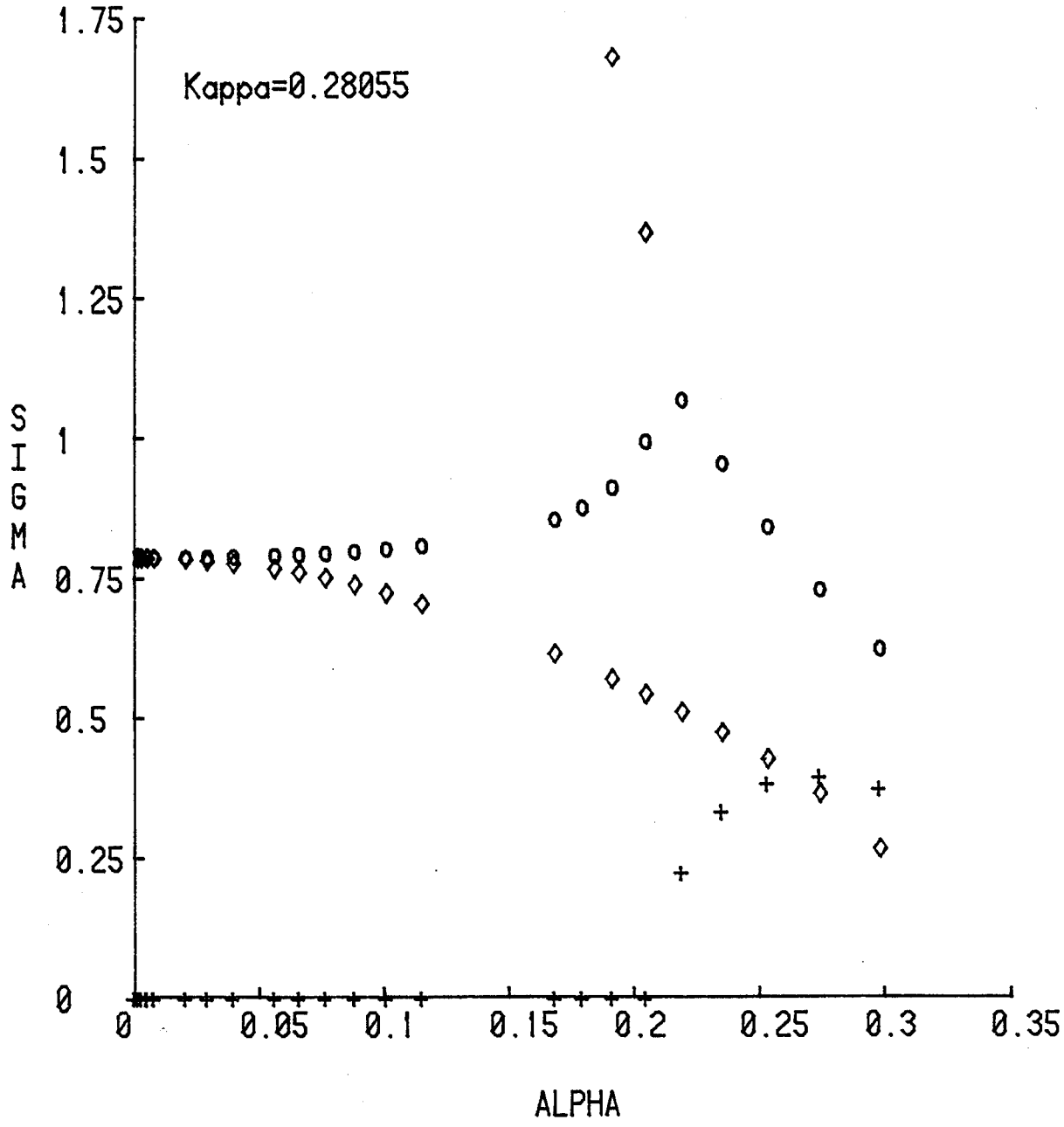


Figure 56. Calculated non-dimensional eigenvalues ($\sigma \cdot 1^2/\Gamma$) from the linear stability analysis.

+ denotes real part (growth rate)
o denotes corresponding imaginary part (frequency)
◇ denotes neutral eigenvalue of lowest frequency, showing degeneracy at change of stability

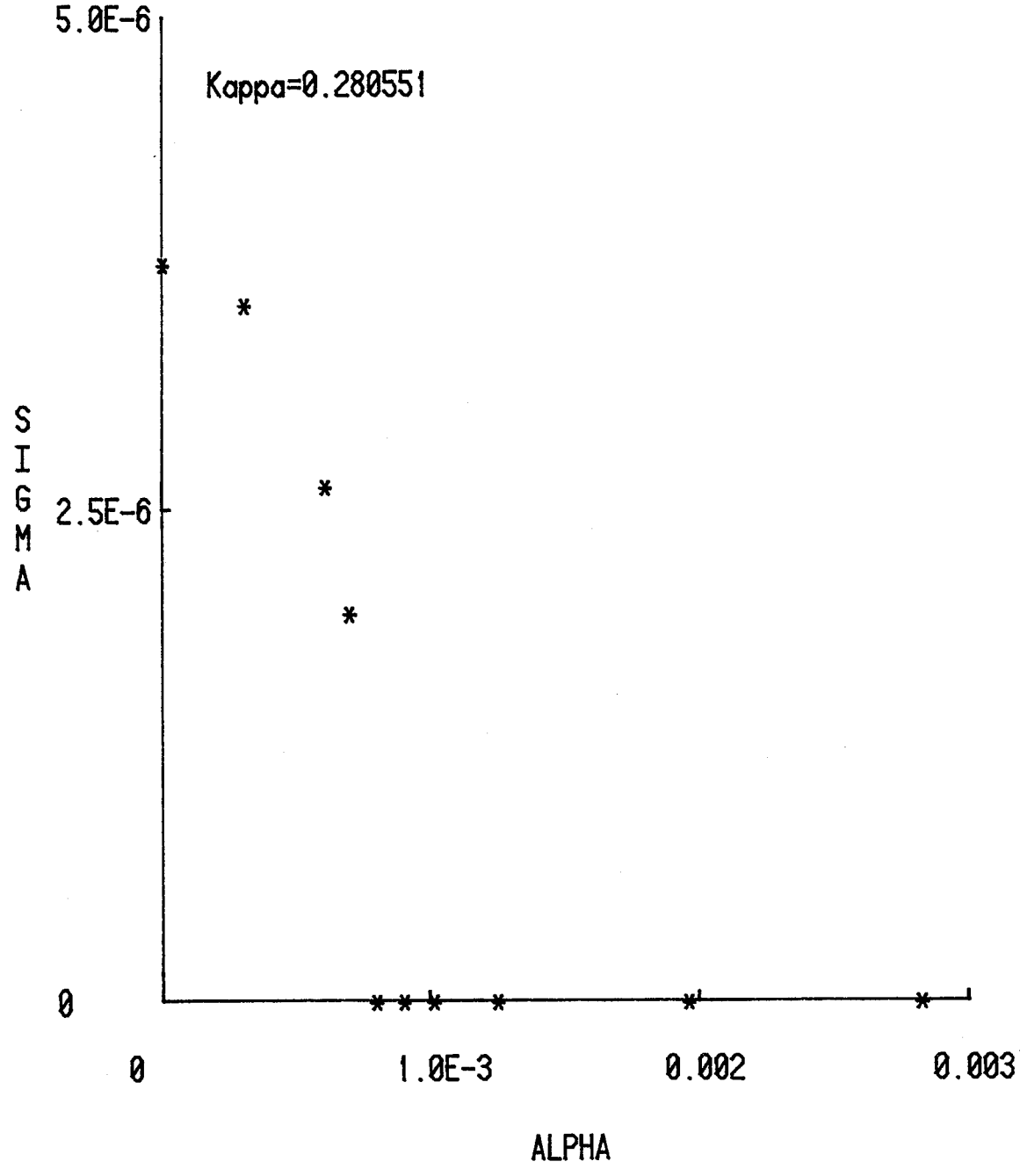


Figure 57. Calculated non-dimensional real part (growth rate) of the eigenvalues ($\sigma \cdot 1^2/\Gamma$) from the linear stability analysis.

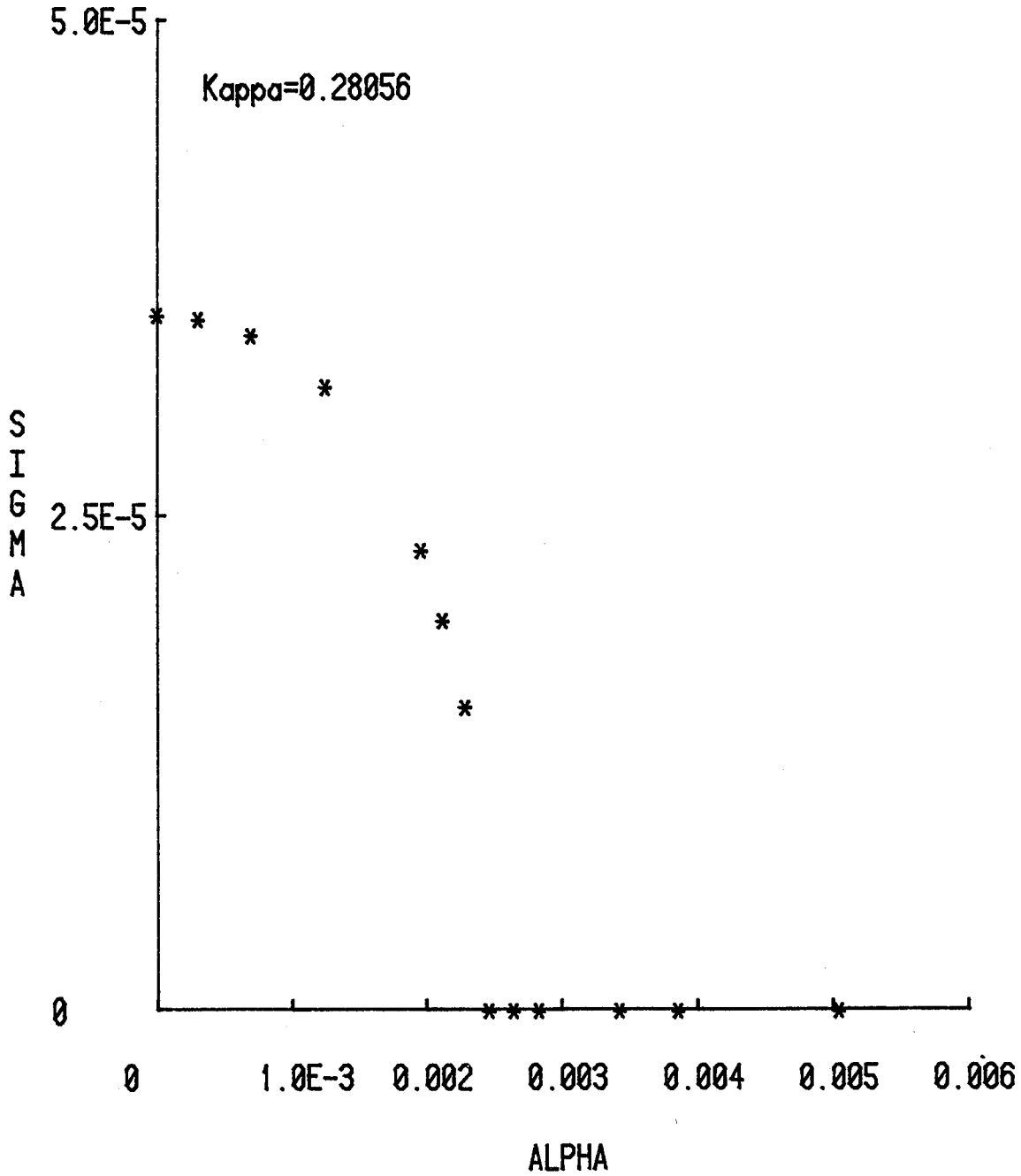


Figure 58. Calculated non-dimensional real part (growth rate) of the eigenvalues ($\sigma \cdot 1^2/\Gamma$) from the linear stability analysis.

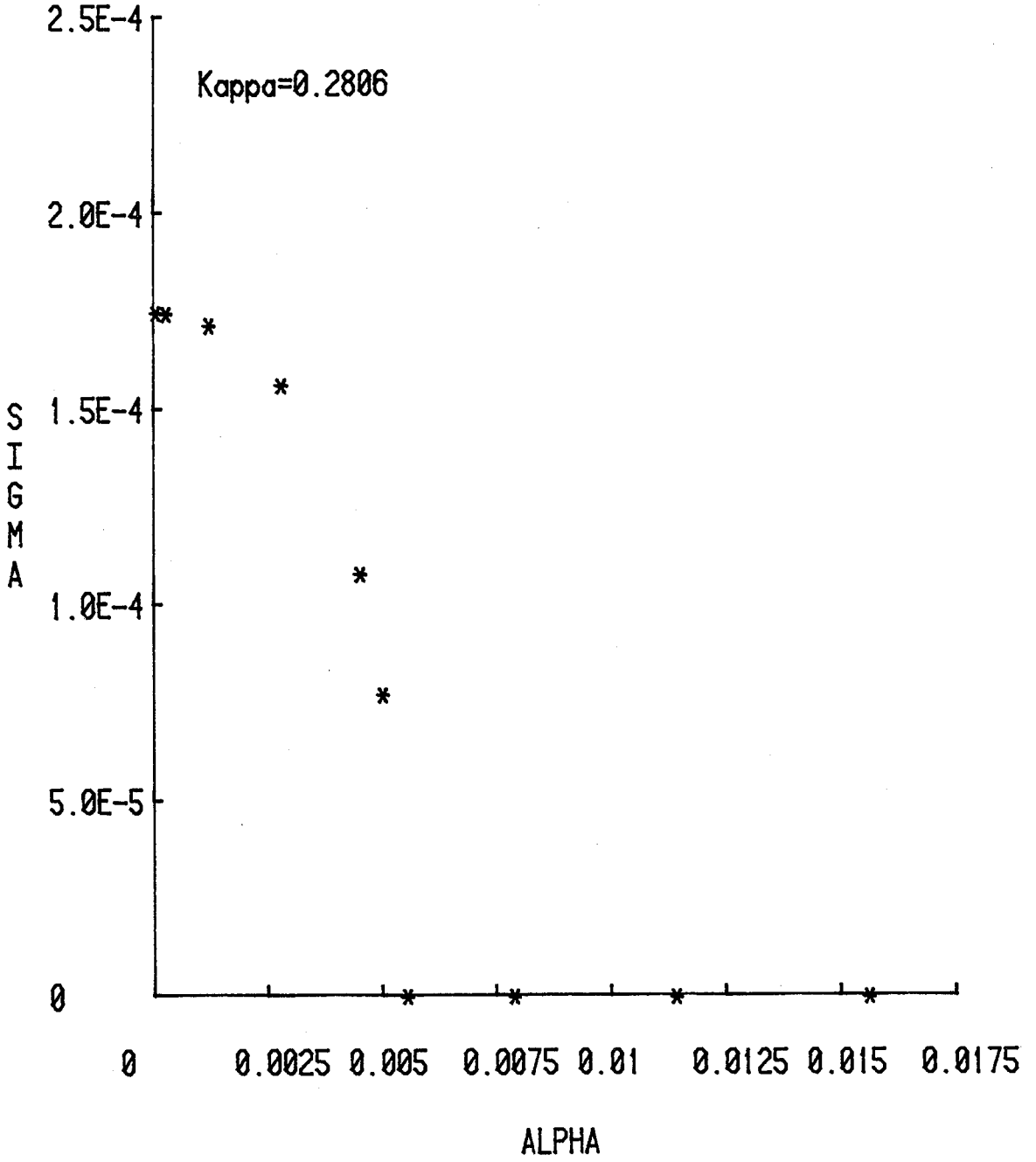


Figure 59. Calculated non-dimensional real part (growth rate) of the eigenvalues ($\sigma \cdot 1^2/\Gamma$) from the linear stability analysis.

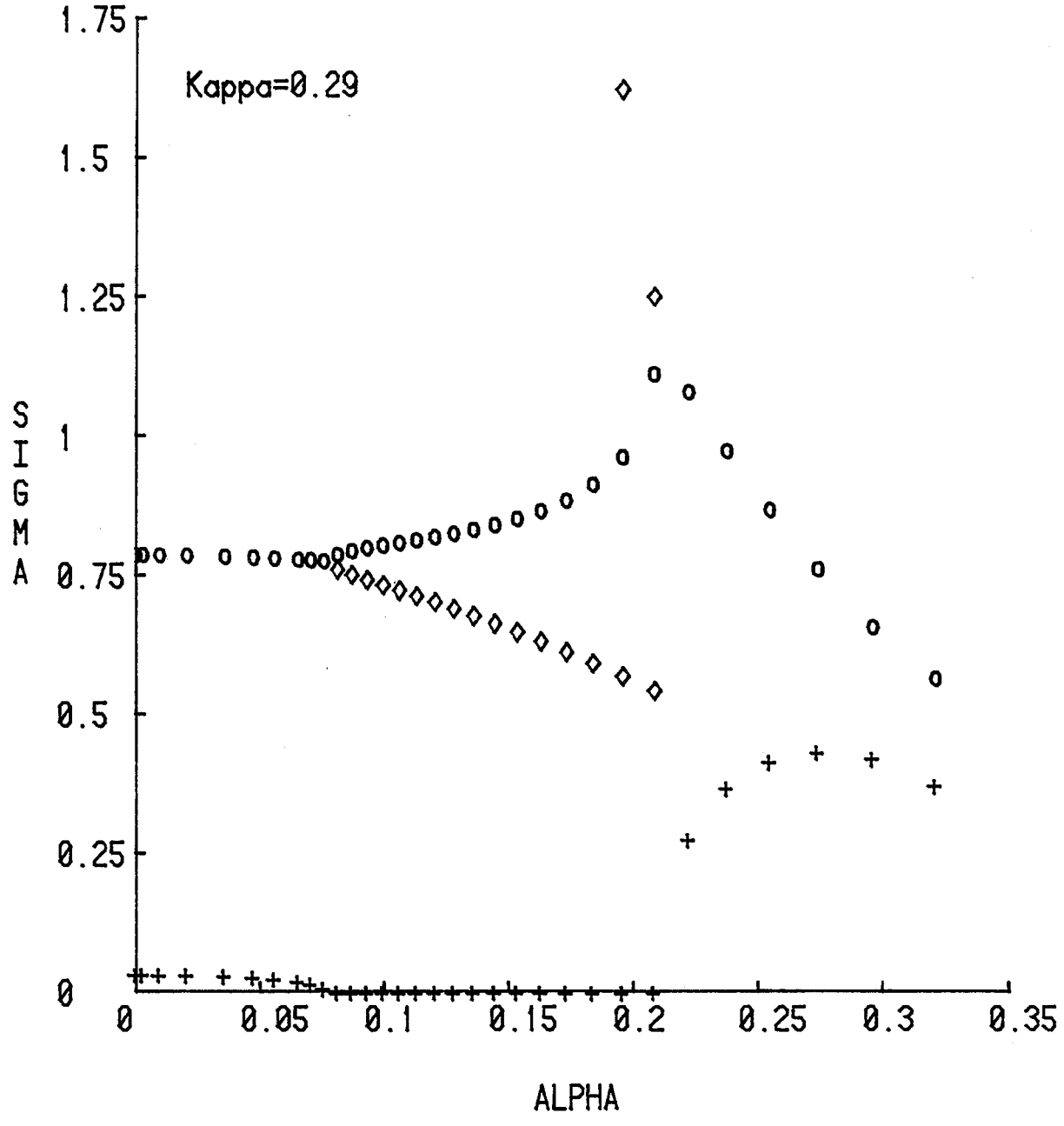


Figure 60. Calculated non-dimensional eigenvalues ($\sigma \cdot 1^2/\Gamma$) from the linear stability analysis.

\+ denotes real part (growth rate)
o denotes corresponding imaginary part (frequency)
◇ denotes neutral eigenvalue of lowest frequency, showing degeneracy at change of stability

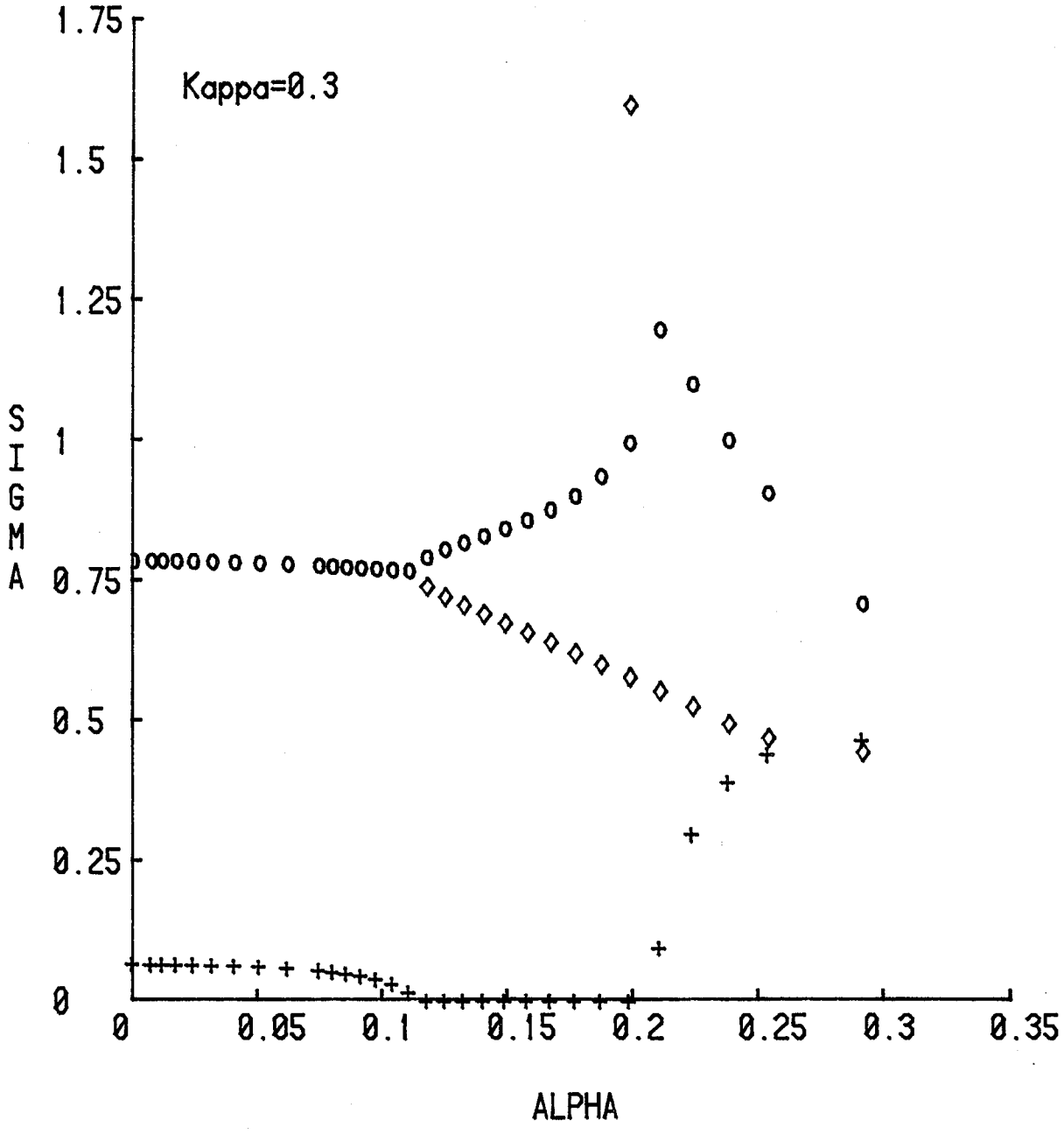


Figure 61. Calculated non-dimensional eigenvalues ($\sigma \cdot 1^2/\Gamma$) from the linear stability analysis.

+ denotes real part (growth rate)
o denotes corresponding imaginary part (frequency)
◇ denotes neutral eigenvalue of lowest frequency, showing degeneracy at change of stability

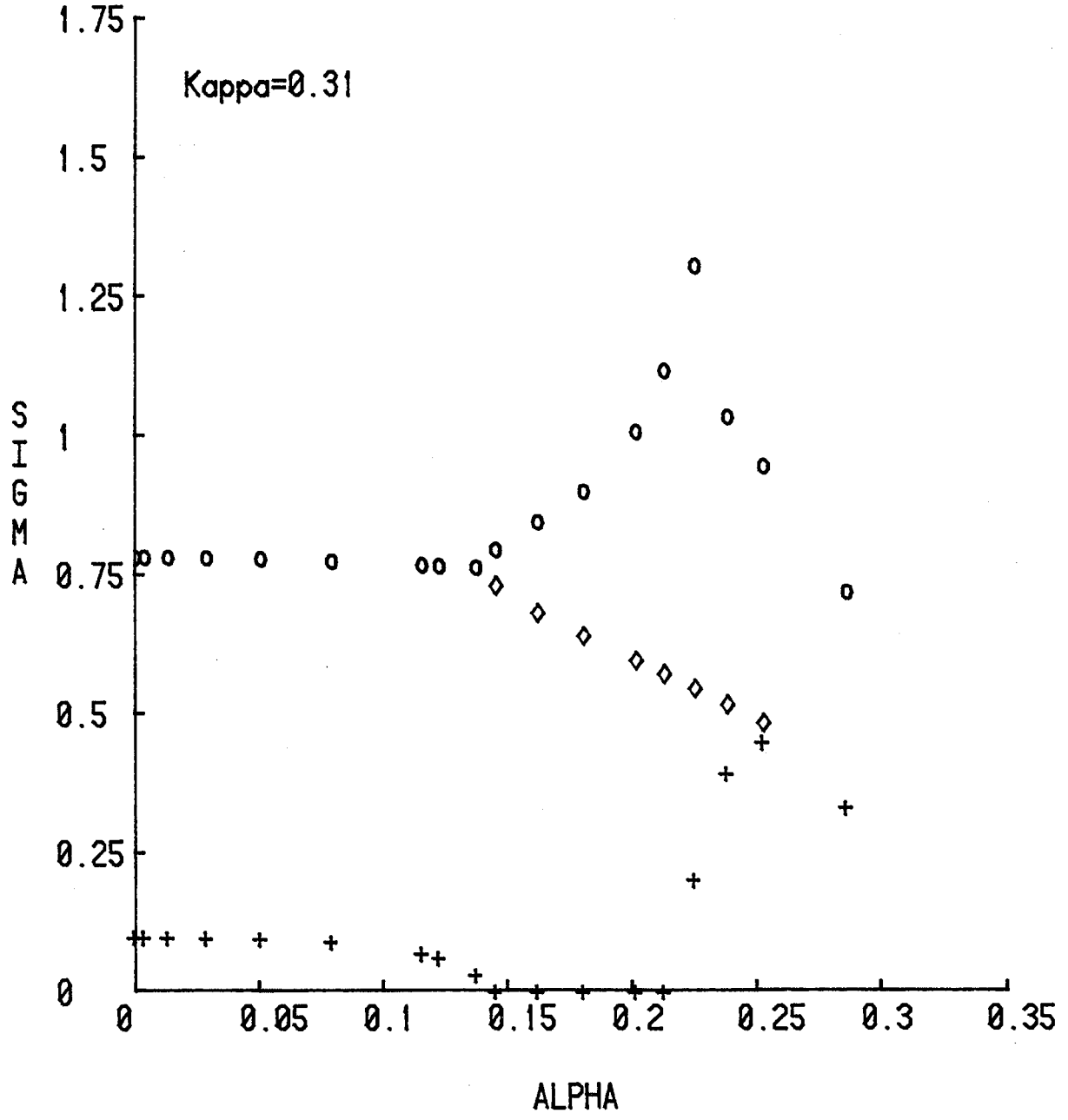


Figure 62. Calculated non-dimensional eigenvalues ($\sigma \cdot l^2/\Gamma$) from the linear stability analysis.

+ denotes real part (growth rate)
o denotes corresponding imaginary part (frequency)
◇ denotes neutral eigenvalue of lowest frequency, showing degeneracy at change of stability

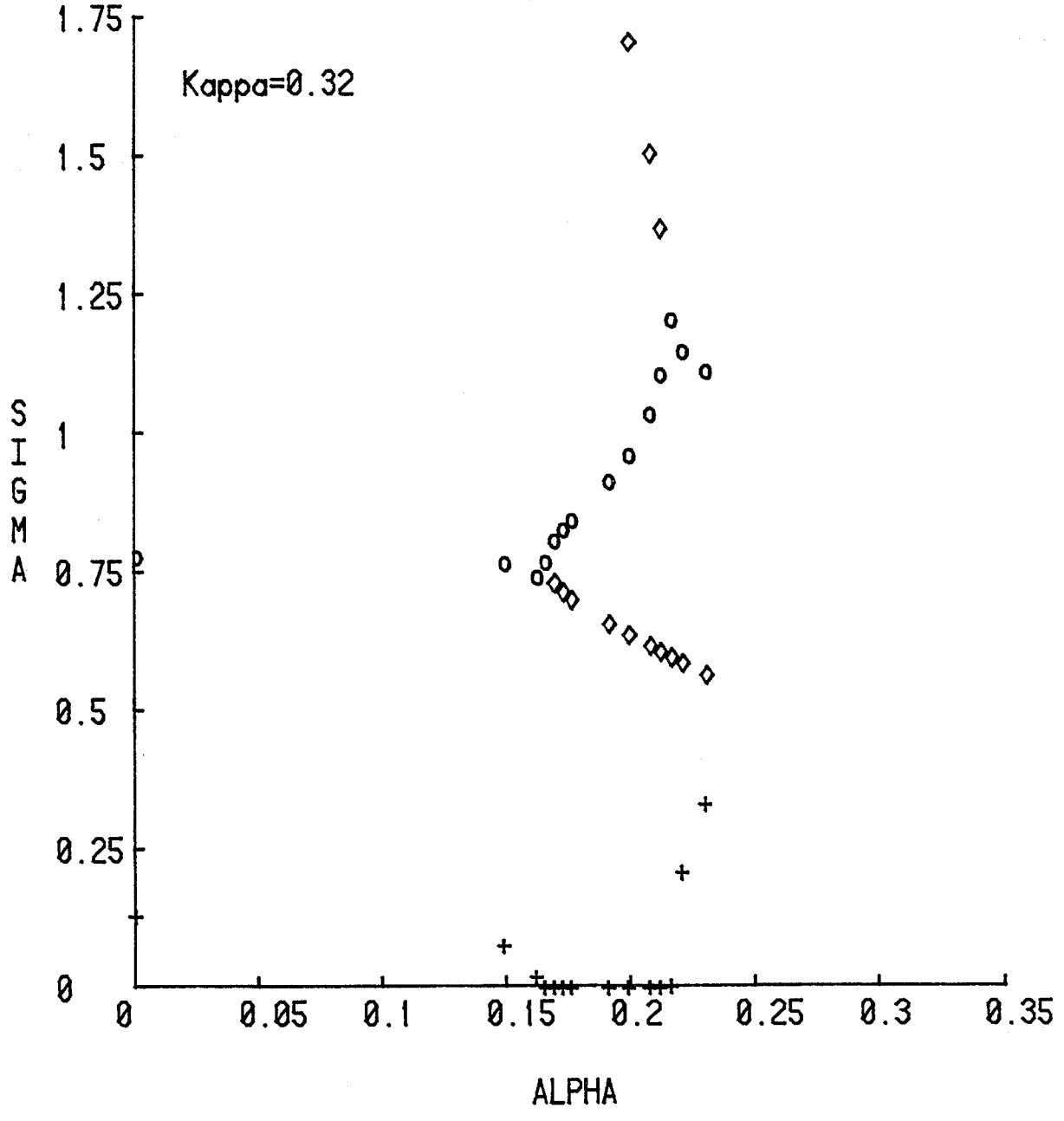


Figure 63. Calculated non-dimensional eigenvalues ($\sigma \cdot 1^2/\Gamma$) from the linear stability analysis.

+ denotes real part (growth rate)
o denotes corresponding imaginary part (frequency)
◇ denotes neutral eigenvalue of lowest frequency, showing degeneracy at change of stability

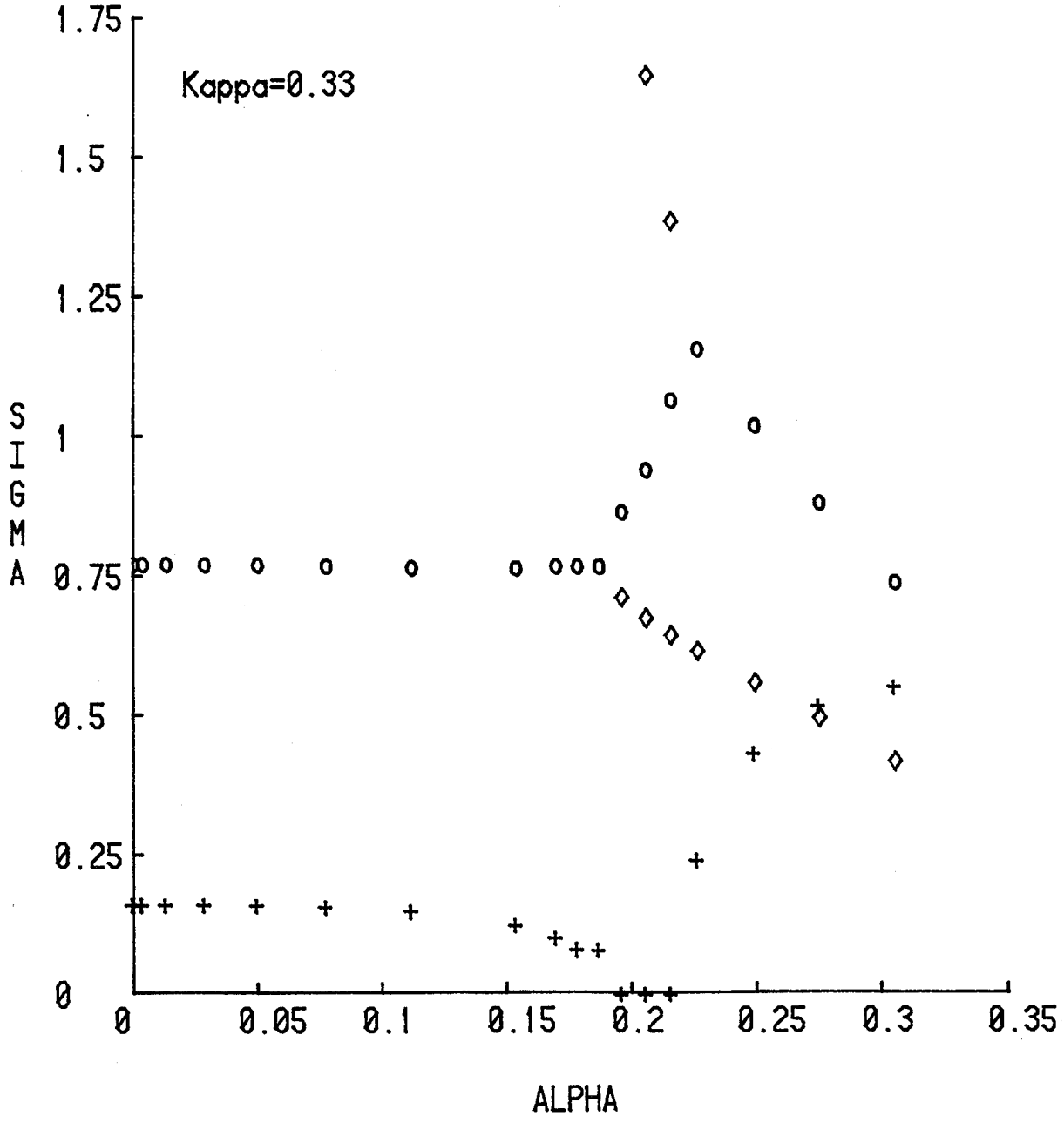


Figure 64. Calculated non-dimensional eigenvalues ($\sigma \cdot l^2/\Gamma$) from the linear stability analysis.

+ denotes real part (growth rate)
o denotes corresponding imaginary part (frequency)
◇ denotes neutral eigenvalue of lowest frequency, showing degeneracy at change of stability

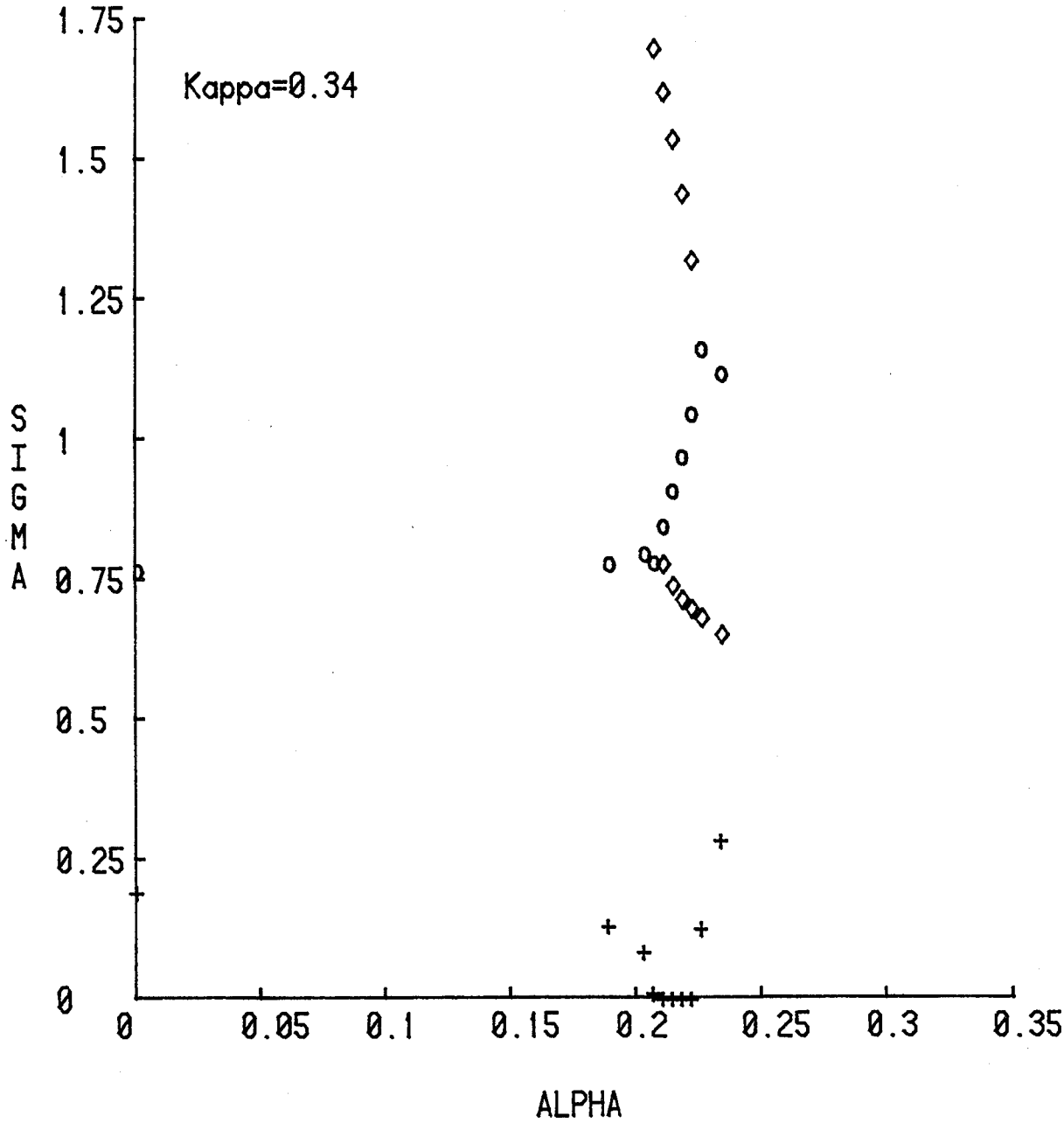


Figure 65. Calculated non-dimensional eigenvalues ($\sigma \cdot l^2/\Gamma$) from the linear stability analysis.

+ denotes real part (growth rate)
o denotes corresponding imaginary part (frequency)
◊ denotes neutral eigenvalue of lowest frequency, showing degeneracy at change of stability

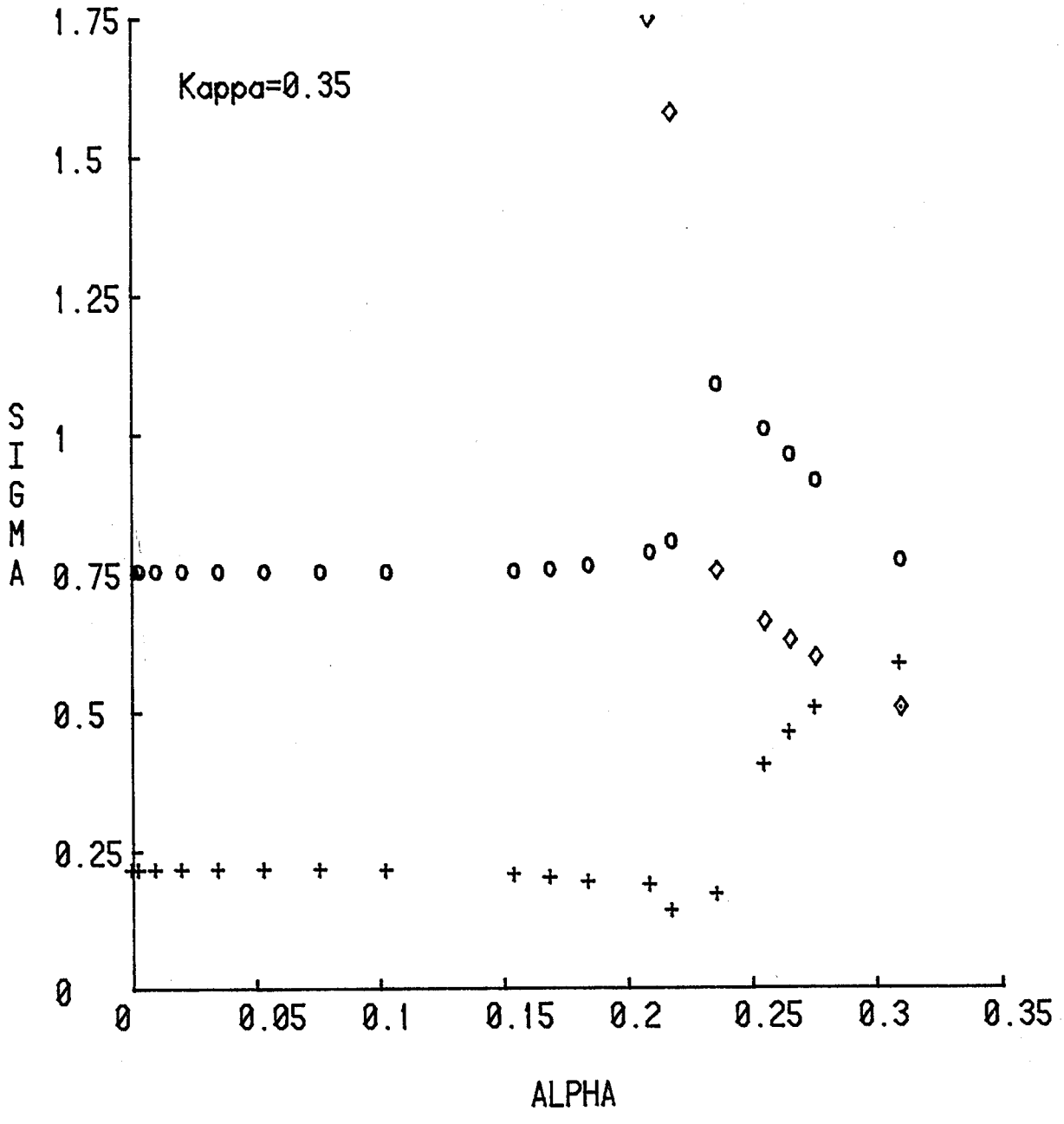


Figure 66. Calculated non-dimensional eigenvalues ($\sigma \cdot l^2/\Gamma$) from the linear stability analysis.

\+ denotes real part (growth rate)
o denotes corresponding imaginary part (frequency)
◇ denotes neutral eigenvalue of lowest frequency

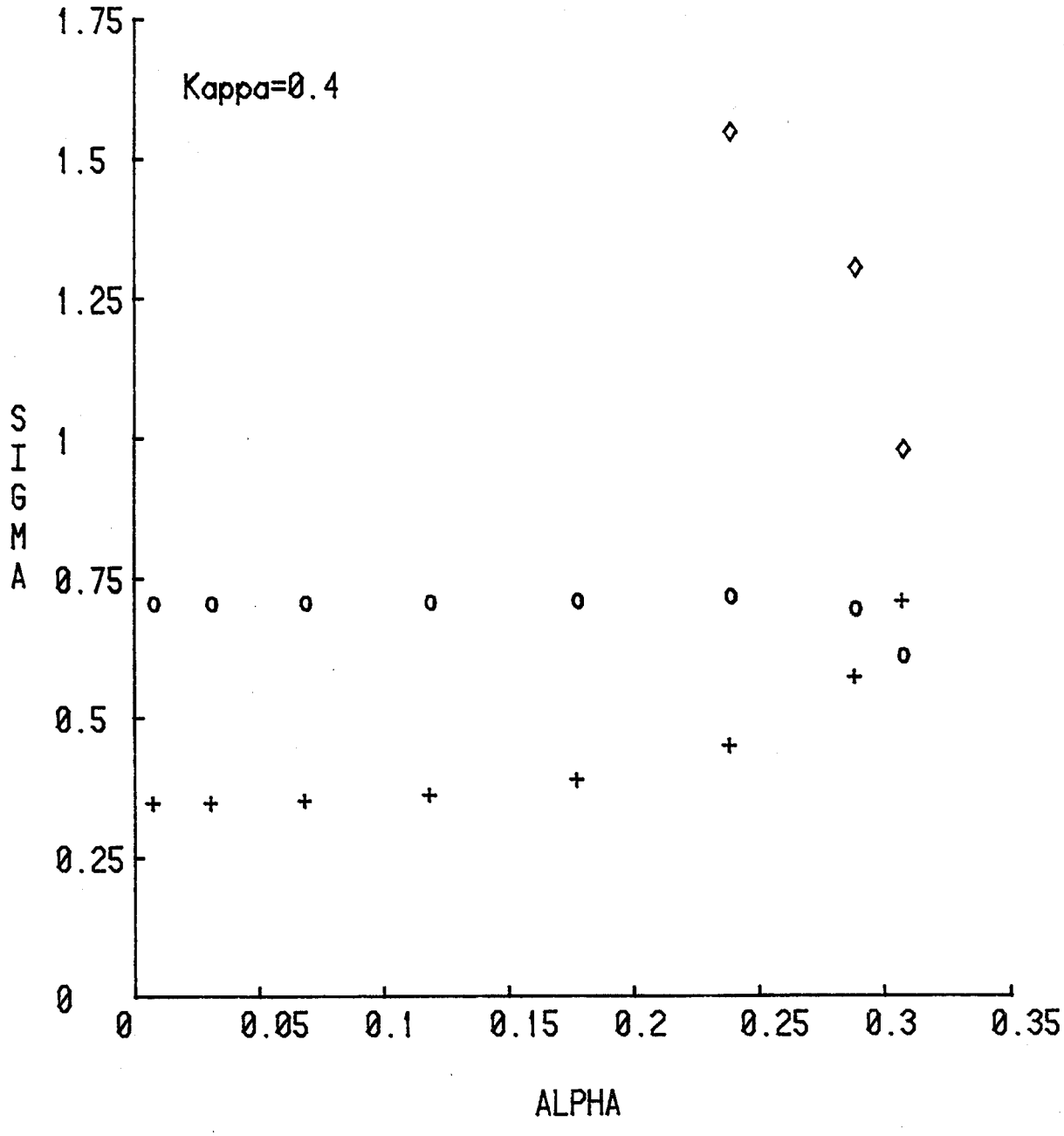


Figure 67. Calculated non-dimensional eigenvalues ($\sigma \cdot l^2/\Gamma$) from the linear stability analysis.

+ denotes real part (growth rate)
o denotes corresponding imaginary part (frequency)
◇ denotes neutral eigenvalue of lowest frequency

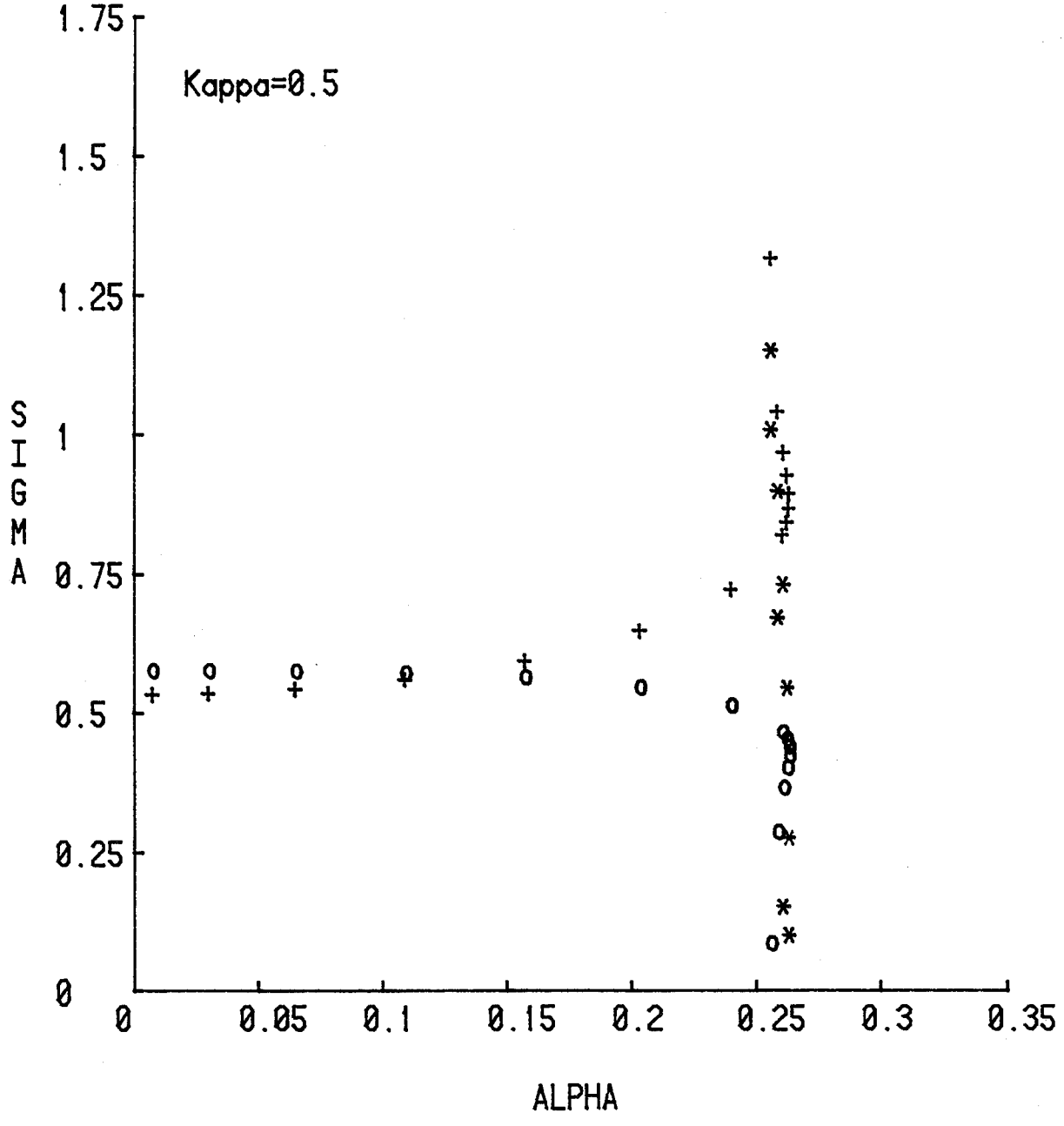


Figure 68. Calculated non-dimensional eigenvalues ($\sigma \cdot l^2/\Gamma$) from the linear stability analysis.

\+ denotes real part (growth rate)
o denotes corresponding imaginary part (frequency)
* denotes the real eigenvalues for the smaller energy state in the non-unique region (see text)

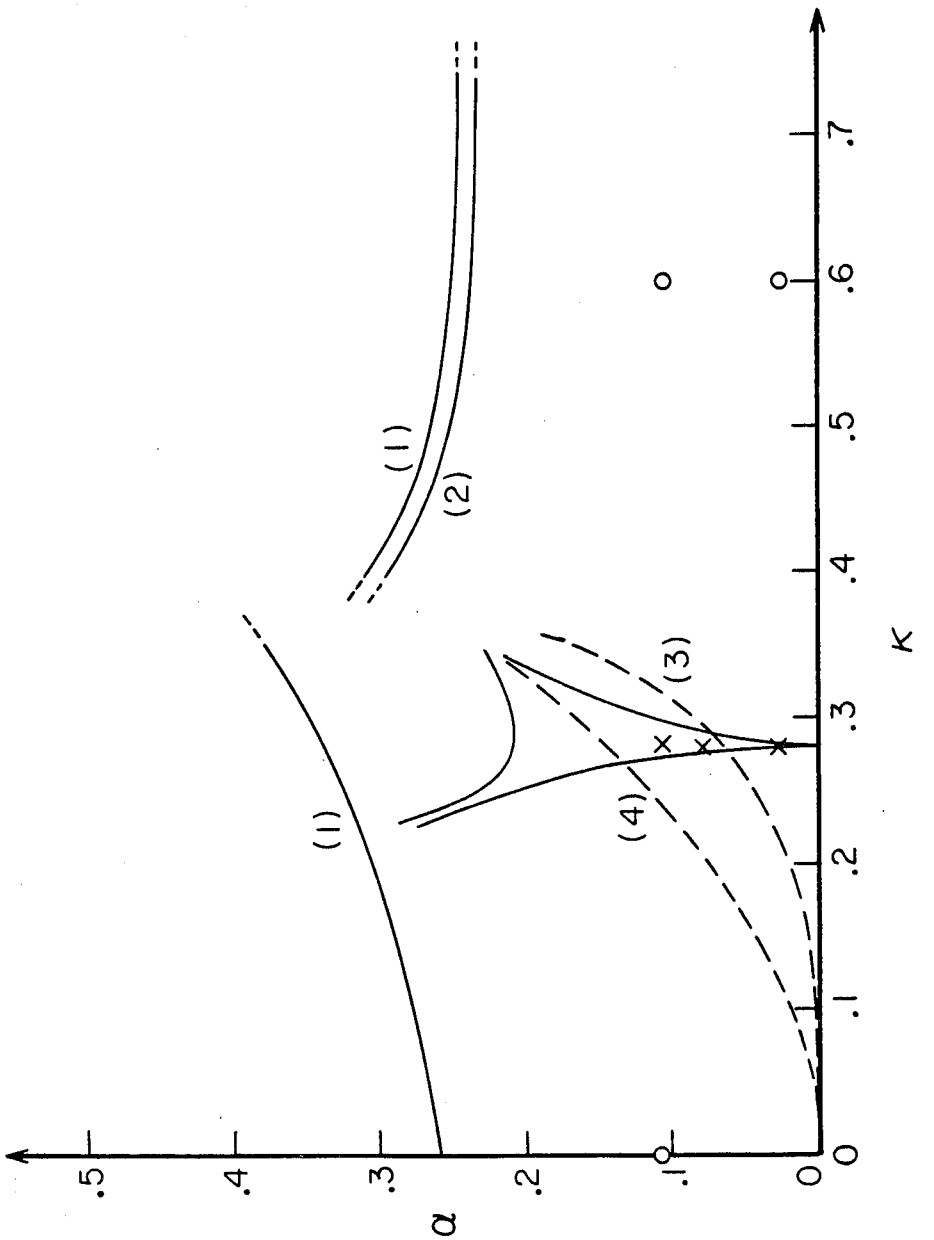


Figure 69. A plot of the area $\alpha$ versus spacing ratio $\kappa$ plane. Curve 1 denotes the maximum area for a given spacing ratio. The segment corresponding to smaller $\kappa$ should be regarded as a lower bound for the maximum area. Above curve 2, there are two solutions for a given pair $(\kappa,\alpha)$. The nearly enclosed v-shaped central region has neutral linear stability; configurations outside this region are linearly unstable. Dashed curve 3 (see §10) shows the line $E_2=E_3$, below and to the right $E_2>E_3$. Dashed curve 4 shows the largest area for which configuration (2) exists. The symbols × mark stable and o mark unstable states according to Christiansen and Zabusky (1973).

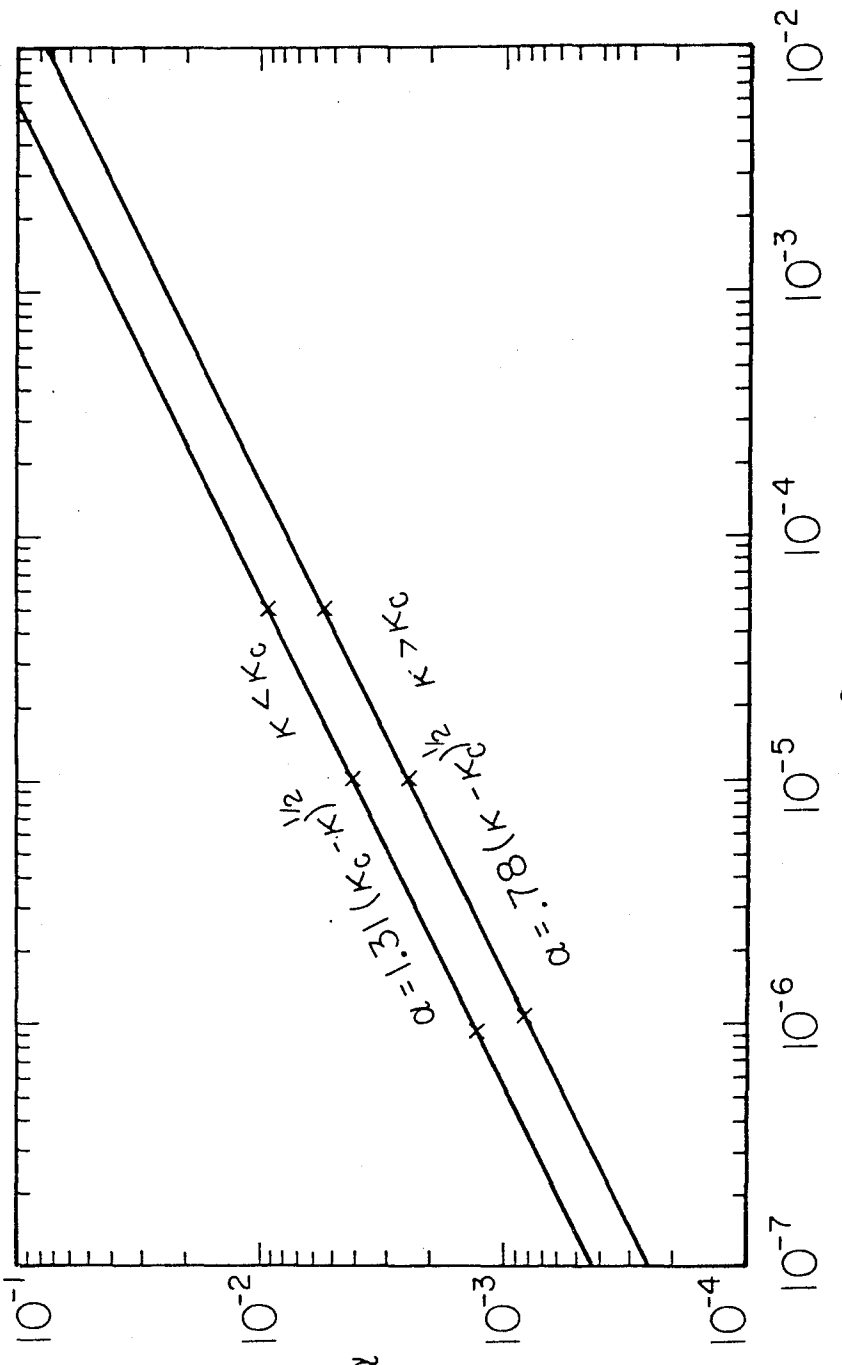


Figure 70. Logarithmic plot of the critical area $\alpha$ at which stabilization occurs versus the distance in $K$ away from $K_c \equiv 0.280549926...$

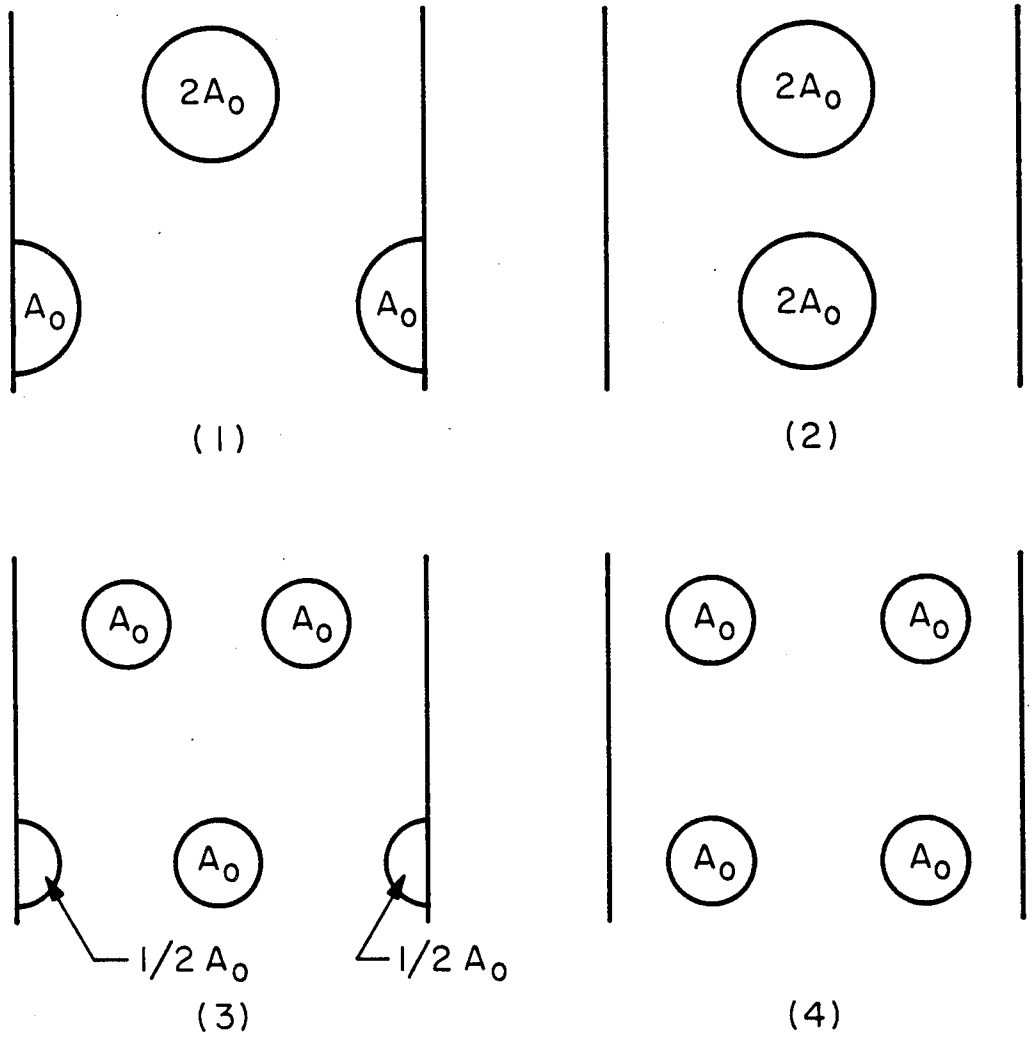


Figure 71. The four vortex configurations for the energy criterion for stability.